IDENTIFICATION OF NOVEL POTENTIAL CANCER THERAPIES BY SYNTHETIC LETHAL SCREENING

by

Peter Ryan McDonald

B.Sc. Biology, Geneva College, 2002

Submitted to the Graduate Faculty of the

School of Medicine in partial fulfillment

of the requirements for the degree of

Doctor of Philosophy

University of Pittsburgh

2008

UNIVERSITY OF PITTSBURGH

SCHOOL OF MEDICINE

This dissertation was presented

by

Peter Ryan McDonald

It was defended on

June 9, 2008

and approved by

Don DeFranco, Ph.D.
Professor, Department of
Pharmacology & Chemical Biology
Committee Chair

Thomas E. Smithgall, Ph.D.
Professor, Department of
Molecular Genetics and Biochemistry
Committee Member

Yu Jiang, Ph.D.
Associate Professor, Department of
Pharmacology & Chemical Biology
Committee Member

Qiming Jane Wang, Ph.D.
Assistant Professor, Department of
Pharmacology & Chemical Biology
Committee Member

John S. Lazo, Ph.D.
Allegheny Foundation Professor,
Department of Pharmacology & Chemical Biology
Dissertation Advisor

IDENTIFICATION OF NOVEL POTENTIAL CANCER THERAPIES BY SYNTHETIC LETHAL SCREENING

Peter Ryan McDonald

University of Pittsburgh, 2008

There is an urgent need for novel effective drug regimens for the treatment of cancer. Current chemotherapy suffers from a slim therapeutic index, with significant toxicity from effective drug doses or tumor recurrence at low drug doses. Identifying synergistic interactions between drugs is a difficult process. To accelerate the discovery of potential drug combinations, I have developed a druggable genome siRNA synthetic lethal screen capable of rapidly identifying novel drug targets that would sensitize cancer cells to sublethal concentrations of microtubule destabilizing agents. I employed a high-throughput cell-based 16,560-siRNA screen to isolate a high-confidence list of genes that, when silenced, enhanced glioblastoma multiforme cancer cell chemosensitivity. Two gene products that were the major focus of my work were midline2 and the neurokinin receptor NK1R. Silencing of midline2, a PP2A-microtubule tether, sensitized cells to two microtubule destabilizing agents, vinblastine and disorazole C_1, suggesting a mechanistic dependency of the phosphatidylinositol 3-kinase pathway on microtubule functionality. Combinations of phosphatidylinositol 3-kinase inhibitors with disorazole C_1 and several vinca alkaloids confirmed this hypothesis. To verify microtubule destabilizing agent sensitization by NK1R silencing, I demonstrated a significant collaboration of neurokinin receptor NK1R antagonists with low concentrations of vinca alkaloids. These assay results and subsequent novel combination strategies demonstrate the tremendous ability of this synthetic

lethal screen to predict potent collaborations between different classes of drugs, as well as identifying molecular constituents mediating those interactions.

TABLE OF CONTENTS

LIST OF TABLES

LIST OF FIGURES

ACKNOWLEDGEMENTS

I wish to express my deepest appreciation to my advisor, John Lazo, for his guidance and support over the past five years. His mentoring has greatly enhanced my writing and presentation skills, and he helped me build strong collaborations with other laboratories to further our research capabilities. He provided me with incredible opportunities to develop rare and valuable skills, and provided a tremendous atmosphere of freedom to enhance my learning and maturing as a scientist. I will truly miss working with him.

I would like to thank Drs. Don DeFranco, Thomas Smithgall, Jane Wang, and Yu Jiang for their interest in my projects, their time, and their advice while serving as members of my dissertation committee.

I would like to thank the Lazo lab, both past and present, for many years of help and support, as well as the many great memories and fun times we had. I thank Drs. Elizabeth Sharlow, Andreas Vogt, and Paul Johnston for their mentoring and constructive criticisms, not only for my research but also for my scientific development. Their knowledge and experience helped me with many of the hurdles of cell based assays and screening, and their career advice has been very helpful. I thank Caleb, CC, John, Brian T., Steve, Steph, and Harold for always being willing to spare time to help me. I thank Celeste Reese for always listening, and helping me stay excited about my research. Thanks to the graduate students, I truly enjoyed the

camaraderie and support I received from Alex, Pallavi, Robb, Pierre, Carolyn, and Yan. They made it fun to come to the lab every day.

Thanks to Cindy Duffy and Jennifer Walker for their incredible support and help in navigating through the many years of graduate school. I also thank the staff of the University of Pittsburgh Drug Discovery Institute and the Department of Pharmacology and Chemical Biology, especially Jim Kaczyinski, Rhonda Toth, Sharon Webb, Jen Wong, Pat Smith, and Jeanette McDew. They have always been more than willing to answer all of my questions.

I am indebted to my family and my wife's family for their love, support, and prayers from afar. My brothers Jonathan and Michael were very influential in my life, and I have learned many life lessons from them. I also want to thank my parents, Paul and Jocele, for their guidance and strength, for teaching me persistence, and teaching me that "I can do all things through Christ who gives me strength".

Finally, special thanks to my wife and best friend, Rachel, and my daughter, Abigail. Rachel shared in my struggles and successes, and her encouragement and love carried me through the entire Ph.D. Abby provided encouragement in her own way, excitedly crawling to me after work, and giving me a big smile when I was discouraged. I could not have made it through the final few months without their loving support.

Soli Deo gloria.

ABBREVIATIONS

AP-1	Activator protein 1
CDDP	Cisplatin
CI	Combination index
CYP	Cytochrome P450
DisC1	Disorazole C_1
DMSO	Dimethylsulfoxide
DNA	Deoxyribonucleic acid
Dox	Doxorubicin
ERK	Extracellular signal regulated kinase
GAPDH	Glyceraldehyde-3-phosphate dehydrogenase
GBM	Glioblastoma multiforme
GPCR	G-protein coupled receptor
GTA	Greater than additive
IPA	Ingenuity Pathway Analysis
JNK	c-Jun n-terminal kinase
L7	L-733,060, non-peptide NK1R antagonist, (2S,3S)-3-[(3,5-bis(Trifluoromethyl)phenyl)methoxy] -2-phenylpiperidine hydrochloride
LY	LY-294,002, specific cell permeable PI3K inhibitor, 2-(4-Morpholinyl)-8-phenyl-1(4H)-benzopyran-4-one hydrochloride
MAP	Microtubule-associated protein
MAPK	Mitogen-activated protein kinase
MDA	Microtubule destabilizing agent
MEK	MAP or ERK kinase
MID1/2	Midline 1/2
mTOR	Mammalian target of rapamycin
NK1	Neuorkinin 1 tachykinin
NK1R	Neurokinin 1 tachykinin receptor
PTX	Paclitaxel
PBS	Phosphate-buffered saline
PI3K	Phosphatidylinositol 3-kinase
PP2A	Protein phosphatase 2A
RNA	Ribonucleic acid
SCLC	Small cell lung cancer
siRNA	Small interfering RNA
TACR1	Tachykinin 1

VBL	Vinblastine
VCR	Vincristine
VEL	Vinorelbine
WIN	WIN-51,708, non-peptide NK1R antagonist, 17-β-Hydroxy-17-α-ethynyl-5-α-androstano[3,2-β]pyrimido [1,2-α]benzimidazole

1.0 INTRODUCTION

1.1 THE CHEMOTHERAPEUTIC WINDOW.

Cancer chemotherapy had its origins one century ago, with the establishment of Paul Ehrlich's side-chain/receptor theory, where he first proposed the concept of targeted therapy against human diseases [1]. Cancer chemotherapy became practical in the early 1940s thanks to the breakthrough research of Louis Goodman and Alfred Gilman, using nitrogen mustard for cancer treatment [2]. Since then, cancer therapeutics has transformed into a multi-billion dollar industry [3]. In an attempt to stimulate oncology research, President Nixon enacted the National Cancer Act in 1971, declaring a "war on cancer". Nonetheless, despite decades of research, we have made little progress in changing cancer mortality statistics, with cancer still accounting for about 25% of all deaths [4, 5].

A major difficulty in treating cancer is dose-limiting and poor quality-of-life side effects, which limits the amount of chemotherapy that can be administered. The level of chemotherapeutic selectivity in distinguishing cancer cells from normal cells is referred to as the therapeutic window, a drug concentration range between the effective dose and a toxic dose. Combination chemotherapy increases efficacy by widening the therapeutic window. The need for new agents or combinations are highlighted by chemoresistant and radioresistant tumors,

such as glioblastoma multiforme (GBM), which have an especially slim chemotherapeutic window. GBM, the most common and aggressive type of primary brain, is a grade 4 astrocytoma in particular with strong resistance to chemotherapy and radiation therapy, and is associated with a median overall survival of approximately 1 year [6-8].

1.2 CANCER DRUG DISCOVERY CHALLENGES.

Identifying novel, potent therapies for cancer is hindered by numerous factors inherent to cancer drug research, such as chemoresistance and tumor heterogeneity. The ability of particular tumors to resist chemotherapy may be due to expression of multidrug efflux transporters, including members of the ATP-binding cassette family such as ABCB1 and ABCC1. These efflux pumps protect tumor cells from many chemotherapeutic compounds, especially hydrophobic amphipathic compounds, by interacting with the compounds and pumping them out of the cell [9]. Tumor heterogeneity poses a hurdle to drug discovery as well, as it is difficult to target specific upregulated or altered proteins in the face of wide molecular variability among tumors and the diversity of the cells within the tumor [10]. These factors greatly complicate target based drug discovery.

1.2.1 Target-based drug discovery.

Target-based drug discovery focuses on a key alteration with a specific phenotype, but it is difficult to pick a drug target that is indespensible for cancer cells but not normal cells. The cellular necessity of a drug target to cancer versus normal cells dictates the width of the

therapeutic window, as inhibiting a crucial cancer-specific target may jeopardize the viability of normal cells. The ideal drug target would be essential to tumors, yet non-essential to normal cells [10]. Perhaps the best example of this is the Ableson kinase (ABL), which is non-essential to normal cells, but essential chronic myeloid leukemia (CML) cells, where ABL is activated. This makes ABL a cancer specific target, and provides high efficacy of the inhibitor imatinib by killing CML cells with minimal side effects at effective doses, providing a wide therapeutic window [11].

Following the lead of imatinib, perhaps the atrocious rate of attrition for cancer drugs could be abated by focusing cancer research around better drug targets. Currently, most cancer drugs require years of development before clinical trials, and suffer a clinical success rate of less than 5% [12, 13]. Researchers attempt to improve the likelihood of success by selecting small molecules that emulate the features of already used orally active drugs. The characteristics of orally active drugs that receive FDA approval have been described by algorithms such as the 'rule of five', five guidelines describing criteria that affect the solubility and permeability of a compound [14-16].

1.2.2 The druggable genome.

Much like the application of the "rule of five" to small molecules, researchers have attempted to annotate the human genome into those genes making protein products that historically have been identified as targets for drugs used for most human diseases. These have been defined as the "druggable genome" comprising between 3,000-10,000 genes that encode for proteins that are

potential drug targets [15]. These proteins were selected based on their potential binding capacity with small molecules with appropriate chemical properties or functional importance in disease processes, and include protein classes such as kinases, G-protein coupled receptors (GPCRs), phosphatases, proteases, and channels (Figure 1) [15]. An example of a druggable genome of 3,050 genes was presented by Andrew Hopkins in 2005, but more inclusive druggable genomes may include as many as 10,000 genes that loosely fit the definition of druggable. By focusing on the druggable genome one should increase the likelihood for success of finding good drug targets for human diseases in a drug discovery paradigm.

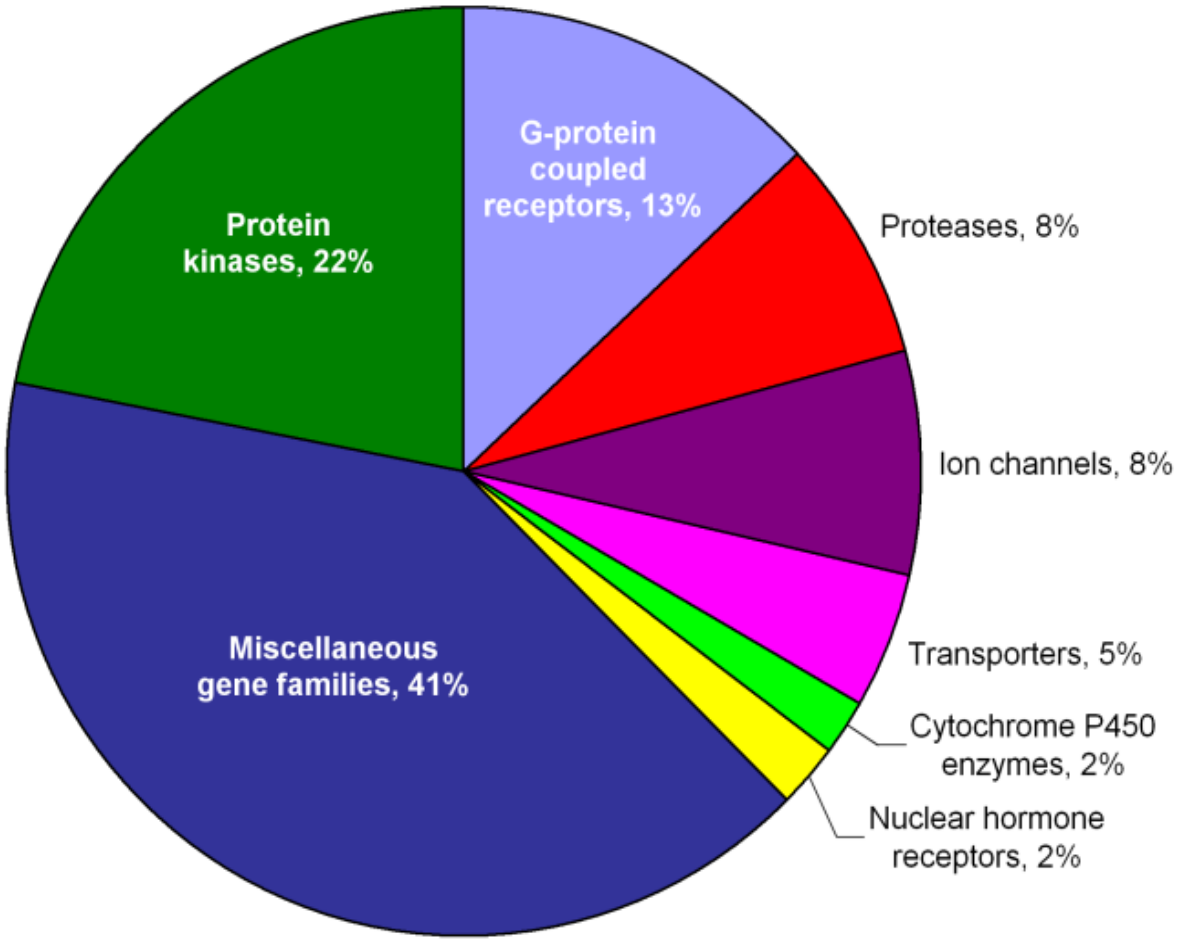

Figure 1. Gene distribution of the 3,050 genes in the 'druggable genome'.

Gene distribution of the 3,050 genes in the 'druggable genome' as described by Hopkins et al. Inspired by Hopkins, A. L. and C. R. Groom "The druggable genome." (2002) and Russ, A. P. and S. Lampel “The druggable genome: an update.” 2005 [15, 17].

1.3 COMBINATION CHEMOTHERAPY.

Combination chemotherapy is a useful approach to circumvent some of the problems of cancer treatment because the combination of two or more drugs with different mechanisms of action enable synergistic cancer cell death while maintaining a range of toxicity tolerated by the patient for each individual drug [18]. Combination therapies are used in treatment of all cancers, theoretically addressing the multiple gene mutations in cancers [19-22].

Combination chemotherapy has tremendous capability for reducing toxicity through requiring lower concentrations of multiple drugs, but identifying targets for combination and finding the right agents to combine is a difficult process. One strategy for identifying new drug combinations would be the use of a synthetic lethality screen. Two genes are synthetic lethal if the inhibition or mutation of one or the other does not kill the cell, while the inhibition of both is fatal to the cell [23]. This is very useful in the context of anticancer therapy, for inhibition of a gene that is synthetic lethal with a cancer mutation should only kill cancer cells, but not normal cells that lack the mutation. Cancer specific synthetic lethal genes make a very attractive pair of targets for combination chemotherapy.

1.4 SYNTHETIC LETHAL siRNA SCREENING.

Small interfering RNA (siRNA) libraries can simplify the search for drug targets that are synthetic lethal, due to its precise silencing mechanism, by preventing expression of a specific gene by the siRNA molecule. In the cell, siRNAs inhibit gene expression post-transcriptionally

by sequence-specific mRNA transcript degradation. siRNAs carry out this activity by assembling into RNA-induced silencing complexes (RISCs) together with endoribonucleases. The siRNA sequence guides the RISCs to messenger RNA molecules with sequence complementary, where the RISCs cleave the messenger RNA, resulting in selective suppression of the target gene [24]. siRNA libraries are composed of a series of siRNA molecules targeting a series of genes. These libraries can be used to screen for targets that are synthetic lethal with a given drug at a concentration that alone is not toxic. This allows the identification of sensitizing genes that modulate cell senstivity to sub-lethal concentrations of an anticancer compound. Since siRNA simulates pharmacological protein inhibition by preventing protein expression and function, a second compound, targeting the protein of the sensitizing gene, would be expected to have the same synthetic lethal effect as the siRNA when combined with the first compound (Figure 2).

The coupling of an siRNA technology with screening to form a sensitizing screen provides a fast method to identify synthetic lethal combinations. The application of siRNA to systematic genome-scale screening method was first demonstrated using C. elegans [25, 26]. Large libraries of siRNAs are commercially available, and can be used for large-scale synthetic lethal screening. Since our goal was to identify drug combinations, we were only interested in screening druggable targets, including such proteins as transcription factors, receptors and kinases [15]. Researchers have annotated a druggable genome of targets and developed siRNA libraries targeting those genes.

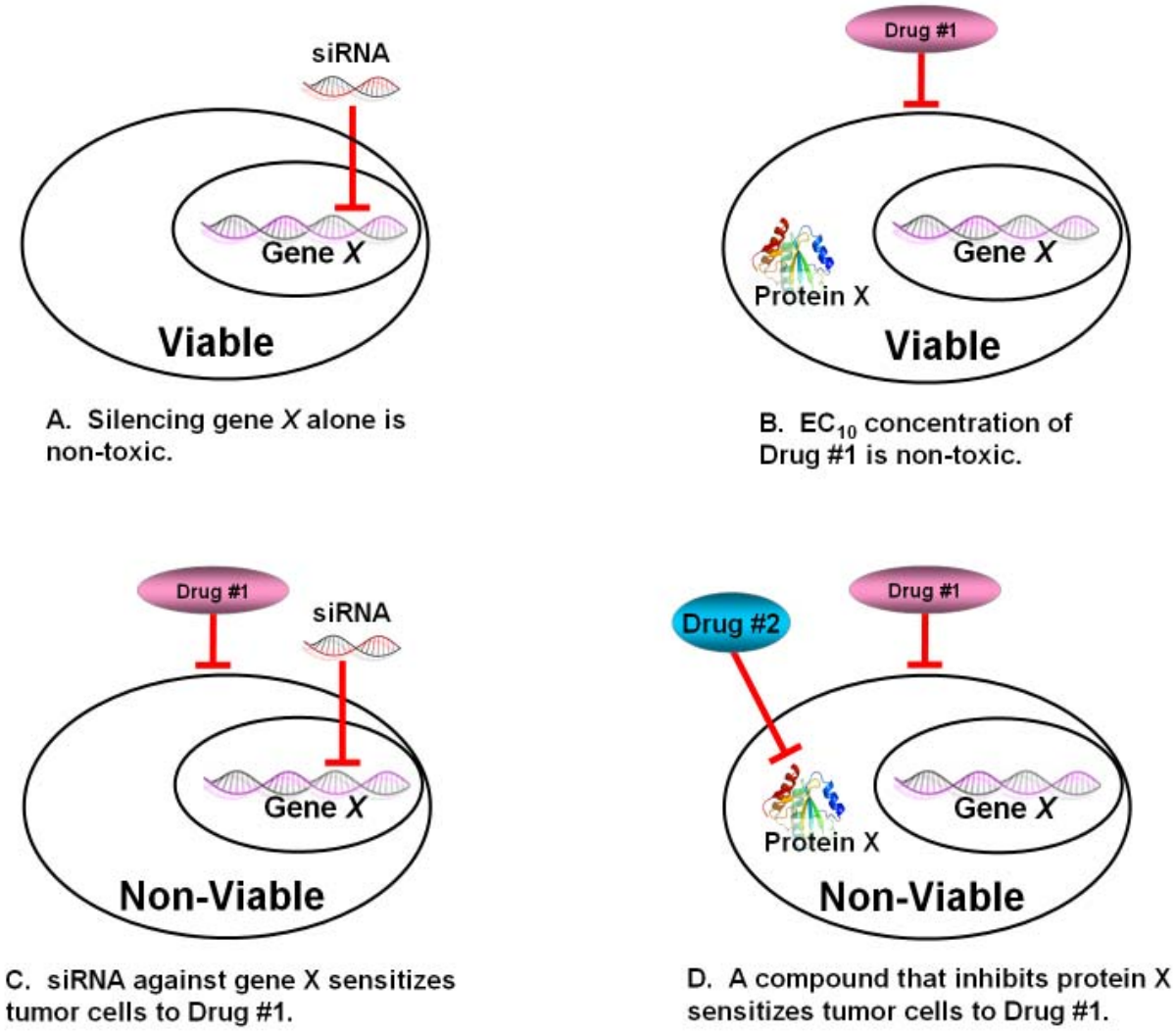

Figure 2. A general method to uncover druggable synthetic lethal interactions for a potential anticancer drug.

This model demonstrates how I used synthetic lethal siRNA screening to identify genes that sensitized cancer cells to non-toxic concentrations of a compound. In this model, Gene X represented a gene that was targeted by one of the siRNAs in the siRNA library, and protein X was the protein expressed from Gene X. In panel A, a library of siRNAs was screened, with interest only in siRNA that was able to silence protein expression of gene X, while not killing the

cancer cell. In panel B, this screen was coupled with a low concentration of a compound (Drug #1) that was not sufficient to kill the cancer cell. The combination of two non-toxic agents, siRNA and Drug #1, together lead to cell death (panel C). This identified a synthetic lethal relationship between the unknown effects of the compound (Drug #1) and the loss of protein X (by silencing gene X). Since I knew the identities of all siRNAs in the library and their target genes, I could combine the Drug #1 with a second compound (Drug #2) that directly targeted the expressed protein. In this way, I could mimic the synthetic lethal interaction to kill cancer cells using two synergizing drugs, which alone are non-lethal.

1.5 MICROTUBULE DISRUPTORS AS ANTICANCER AGENTS.

Screening a library of siRNA or compounds has previously been reserved primarily to large pharmaceutical and biotechnology industries. The decreasing cost of computer technology and increased availability of off-the-shelf screening solutions allow large scale screens to be performed in the university setting [27]. The synthetic lethal siRNA screening described in this dissertation was been miniturized to a 384-well plate format and automated, allowing fast and robust identification of genes that modulate tumor cell sensitivity to chemotherapeutic agents, such as taxanes, vinca alkaloids, and natural products. For this research, I chose two different chemotypes, the vinca alkaloid vinblastine, and the natural product disorazole C_1 to study microtubule disruption. Vinca alkaloids are isolated from the periwinkle plant, Vinca rosea, and include compounds such as vincristine, vinblastine, and vinorelbine. Vinblastine and disorazole C_1 are thought to share a similar molecular target, tubulin, and trigger microtubule destabilization, but details are lacking about precise details of the mechanism of action of

disorazole C_1. I speculate disorazole C_1's mechanism of cytotoxicity is unique from vinblastine, with a unique signaling profile. Both compounds enter cells and bind tubulin, preventing polymerization. This disruption impairs mitotic spindle formation in the M phase, preventing cells from proceeding through the spindle checkpoint, leading to programmed cell death [28-30].

Microtubules are a good target for cancer chemotherapy because proliferating cancer cells are dependent on proper microtubule dynamics, making cancer cells with high rates of proliferation more vulnerable to microtubule targeting drugs [31]. This vulnerability is born out of the unlimited replicative potential of cancer cells, enabling uncontrolled growth and cell division [32]. Further, the proliferating endothelial cells of tumor neovasculature is sensitive to microtubule destabilizers [33]. Tumor sensitivity to microtubule disruption makes depolymerizing drugs a valuable tool for chemotherapy [34].

The molecular signaling consequences of microtubule destabilizing agents (MDAs) provides great potential for enhancement by drug combination. Combination therapy typically achieves the same effect while requiring lower concentrations of each compound, and is well suited to microtubule-targeted drugs since the concentration required to suppress microtubule dynamics is lower than their maximum tolerated dose [34]. The synthetic lethal screen uses very low concentrations of each compound (IC_{20} or less), so that there is minimal apoptosis, but high enough for some microtubule binding and subsequent cellular stress signaling effects [35]. For example, vinblastine induces the expression and phosphorylation of the stress-associated signaling molecules JNK, c-Jun, and AP-1. At higher concentrations of vinblastine, JNK-dependent apoptosis occurs through AP-1 signaling [36, 37]. The consequences of microtubule

perturbing agents on intracellular protein kinase signaling pathways provides opportunities for a second agent to be used to synergistically enhance the apoptotic effects of MDAs on cancer cells. For example, ERK pathway inhibitor PD98059 potentiates vinblastine mediated apoptosis in ML-1 myeloid leukemia cells, and the EGFR inhibitor gefitinib synergizes with vinorelbine in human non-small cell lung cancer [38, 39]. An increased understanding of the mechanisms of MDAs and identification of synthetic lethal partners can provide effective chemotherapeutic effect at lower doses, minimizing side effects and neuropathy in patients with GBM.

For this research project, the tool of synthetic lethal siRNA screening was used as a means to identify new drug therapies for GBM, the most common and malignant central nervous system tumor [40]. GBM is a grade IV glioma, is the most aggressive primary brain tumor, and represents over half of all cases of glioma [41-43]. First line therapy for GBM is surgical removal, followed by radiotherapy and temozolomide treatment [44]. GBM is a morphologically heterogenous cancer, with a widely varied cellular composition with mixed histologic features [45]. Present chemotherapies for GBM are greatly hindered by glioblastoma's intrinsic resistance to both chemotherapy and radiation [46]. The radioresistant and chemoresistant profile of the GBM cell line T98G and the numerous literature reports on its responsiveness to antineoplastic agents made it a suitable candidate for HTS optimization in our synthetic lethal siRNA screen [46].

1.6 HYPOTHESIS AND SPECIFIC AIMS.

Cocktails of two or more cancer specific drugs acting synergistically at significantly lower doses provides a means to widen the chemotherapeutic window, giving more effective tumor killing while sparing the patient the side effects of high concentrations of drug. However, due to the complexities of cancer mentioned above, there is a need to develop an optimal, unbiased strategy to systematically elucidate the molecular underpinnings of GBM cell chemoresistance. In this dissertation, I proposed to develop a synthetic lethal siRNA screen and apply it to the glioblastoma T98G cell line to identify sensitivity determinants of microtubule destabilizing agents for use in predicting novel, synergistic drug combinations against GBM. Therefore, **I hypothesized that synthetic lethal screening can identify gene products that modulate glioma cell sensitivity to cancer therapy.** Thus, the specific aims of this dissertation were 1) develop a multi-component, high-throughput MDA-dependent synthetic lethal siRNA screen, 2) identify genes and networks that modulate tumor cell sensitivity to sub-lethal concentrations of microtubule perturbing agents, and 3) determine if functional inhibitors of the identified target proteins or networks enhance the toxicity of microtubule perturbing agents against human cancer in culture.

2.0 EXPERIMENTAL METHODS

2.1 REAGENTS.

DharmaFECT 2 transfection reagent, 5x siRNA resuspension buffer, and siGLO Green Transfection Indicator were from Dharmacon (Lafayette, CO). CellTiter-Blue Cell Viability Assay was from Promega (Madison, WI). The Silencer Druggable Genome siRNA Library was from Ambion (Austin, TX). 384-well tissue-culture treated microtiter plates were from Greiner Bio-One (GmbH, Frickenhausen, Germany). Antibodies recognizing TAU [phospho Serine 199], OptiMEM, McCoy's 5A Medium (modified), DMEM, EMEM, Stealth™ RNAi Negative Control Med GC scrambled siRNA, phosphate buffered saline (PBS), hoechst 33342, and Lipofectamine2000 were from Invitrogen (Carlsbad, CA). FITC donkey anti-mouse secondary antibody #715-095-152 and horseradish peroxidase-conjugated secondary antibodies was from Jackson Immunoresearch (West Grove, PA). ECL Western blotting substrate was from Pierce Biotechnology (Rockford, IL). Rabbit polyclonal neurokinin 1 receptor antibody #ab466 was from Abcam (Cambridge, UK). FuGENE transfection agent was from Roche (Nutley, NJ). Colchicine, vinorelbine, vincristine, vinblastine, doxorubicin, 37% formaldehyde, L-733,060, LY-294,002, WIN-51,708, DMSO, wortmannin, NeuroPorter transfection reagent and mouse monoclonal anti-alpha tubulin antibody #T9026 were from Sigma-Aldrich (St Louis, MO).

Disorazole C_1 was generously synthesized and provided by Peter Wipf (University of Pittsburgh, Pittsburgh, PA). Vinculin H300 antibody was from Santa Cruz Biotechnology (Santa Cruz, CA).

2.2 CELL CULTURE AND TREATMENTS.

MDA-MB-231 and Hela cells (ATCC, Rockville, MD) were maintained in DMEM supplemented with 1% L-glutamine, 100 U/mL penicillin/streptomycin (Invitrogen, Carlsbad, CA) and 10% fetal bovine serum (Cellgro, Manassas, VA). T98G, U87, and IMR-90 cells (ATCC, Rockville, MD) were maintained in EMEM supplemented with Earle's basic salt solution, nonessential amino acids, sodium pyruvate, 1% L-glutamine, 100 U/mL penicillin/streptomycin (Invitrogen, Carlsbad, CA) and 10% fetal bovine serum (Cellgro, Manassas, VA). T24 cells (ATCC, Rockville, MD) were maintained in McCoy's 5A medium supplemented with 1% L-glutamine, 100 U/mL penicillin/streptomycin (Invitrogen, Carlsbad, CA) and 10% fetal bovine serum (Cellgro, Manassas, VA).

All compounds were dissolved into DMSO for cell treatment. All compound treatments for synthetic lethal screening were added 48 hours after cell plating by replacing cell medium with fresh medium containing either vehicle or MDA compound at a final DMSO concentration of 0.5% for 48 hours in a humidified incubator at 37ºC with 5% CO_2. For combination studies, compounds were combined in DMSO in 96-well polypropylene plates, then added to media on cells 24 hours after cell plating, at a final DMSO concentration of 0.5%, and cells were incubated in the presence of compounds for 72 hours in a humidified incubator at 37ºC with 5% CO_2.

2.3 WESTERN BLOTTING.

For Western blotting, 6-well plates containing T98G, U87, Hela, T24, MDA-MB-231, and IMR-90 cells were placed on ice, washed with 5 ml of ice-cold PBS, and collected by scraping into lysis buffer containing a mini EDTA-free Protease Inhibitor Cocktail Tablet (Roche), Triton X-100, SDS, NaCl, EDTA, NaF, sodium beta-glycerol phosphate and Na_3VO_4 (Sigma). Relative protein concentrations of each sample were determined using the Bio-Rad protein assay kit (BioRad). Equivalent protein amounts from cell lysates were resolved on 4–20% SDS-polyacrylamide gels and transferred to nitrocellulose membranes (Protran, Schleicher & Schuell). Depending on the experiment, membranes were probed with either anti-phospho-TauSer199, anti-Lamin A/C, anti-NK1R, or anti-beta-tubulin antibodies. Beta-tubulin or vinculin were used as loading controls with mouse polyclonal anti-beta-tubulin antibody or vinculin H300 antibody, respectively. Positive antibody reactions were visualized using peroxidase-conjugated secondary antibodies (Jackson ImmunoResearch, West Grove, PA) and chemiluminescence by ECL Western Blotting Substrate (Pierce) according to manufacturer's instructions, and membranes were then exposed to X-ray film.

2.4 COMPOUND TREATMENT AND IMMUNOFLUORESCENCE.

T98G cells (1,000), U87 cells (1,000), Hela cells (1,000), IMR-90 cells (2,000), and MDA-MB-231 cells (3,000) were plated in 80 µL of medium into the wells of tissue-culture treated 96-well polystyrene plates (BD Falcon) and allowed to attach overnight. Compound combinations (40 µL) were added to the wells for a total of 120 µL medium at a final DMSO concentration of

0.5%. Cells were incubated in the presence of compounds for 72 hours in a humidified incubator at 37ºC with 5% CO_2. After incubation, cell viability was measured with the CellTiter-Blue cell viability assay for three hours, according to manufacturer's protocol, adding a 1:5 ratio of CellTiter-Blue to complete media (described further in Chapter 3, section 3.4.1). Cells were then fixed and stained with 3.7% formaldehyde and 1.2 μg/mL Hoescht 33342 for 10 minutes, then permeabilized with 0.5% Triton X-100 (Sigma-Aldrich) in PBS for five minutes. Cells were then immunostained with anti-alpha tubulin antibody (1:3000) for one hour, gently rinsed twice with PBS, and incubated with FITC donkey anti-mouse secondary antibody for one hour, gently rinsed twice with PBS, then sealed with 120 μL PBS per well. Cellular tubulin and nuclei for selected wells were visualized and photographed with the ArrayScanVTi.

2.5 SYNTHETIC LETHAL siRNA SCREEN.

The development and optimization of the synthetic lethal screen will be discussed in Chapter 3. Below are the selected screening parameters based on the optimization experiments of Chapter 3.

2.5.1 siRNA library sequences.

The 5,520 druggable targets of the Ambion Silencer Druggable Genome siRNA Library were selected by Ambion based on an internal bioinformatics analysis. The 109 categories composing this library are listed in Table 1. Three unique siRNAs duplexes targeting each gene

were designed, synthesized, and purified by Ambion (Austin, TX). Below are the sequences for the three unique siRNAs targeting MID2 and NK1R discussed in Chapters 4 and 5, respectively.

		Sense siRNA Sequence	Antisense siRNA Sequence
Midline 2	**Duplex #1**	**GCGCAACAGCGAACUAGAAtt**	**UUCUAGUUCGCUGUUGCGCtt**
Midline 2	**Duplex #2**	**CCUACCCGACUAAAAACAAtt**	**UUGUUUUUAGUCGGGUAGGtt**
Midline 2	**Duplex #3**	**CCAACCUGGUUAAGCGCAAtt**	**UUGCGCUUAACCAGGUUGGtg**
NK1 receptor	**Duplex #1**	**GGACAGUGACGAACUAUUUtt**	**AAAUAGUUCGUCACUGUCCtc**
NK1 receptor	**Duplex #2**	**GGGCUACUACUCAACCACAtt**	**UGUGGUUGAGUAGUAGCCCtg**
NK1 receptor	**Duplex #3**	**GCCUGGCAAAUUGUCCUUUtt**	**AAAGGACAAUUUGCCAGGCtg**

2.5.2 Automation.

The following automation and liquid handling platforms used in for the synthetic lethal siRNA screen:

- Velocity 11 V-Prep™ high speed automated precision microplate pipetting station.
- Titertek™ Zoom™ MV automated microplate dispenser.
- Molecular Devices SpectraMax M5 multi-detection plate reader and absorbance spectrophotometer, equipped with a Molecular Devices StakMax robotic plate handler.
- AquaMax™ DW4 liquid handling system (Molecular Devices).
- Abgene® SEAL-IT 100™ automated microplate sealer.
- Cellomics™ ArrayScan® VTi HCS reader.
- Bio-Stack™ Twister® II Microplate Handler, running iLink automation software.

2.5.3 Cell plating.

To maintain consistency of experiments from plate to plate and from week to week, special attention was made to ensure T98G cells in T-150 culture flasks were at a consistent log phase at the time of harvesting. To do this, 850,000 T98G cells were seeded in each of two T-150 flasks 72 hours before the day of the siRNA screen, ensuring at least 10 million cells on the day of harvest. On the first day of a screen, T98G cells in T-150 flasks were trypsinized for 7 minutes, counted, and resuspended in complete medium at a concentration of 9 cells/μL. T98G cells were then seeded at 450 cells per well in a volume of 51 μL per well into 384-well, tissue-culture treated black-side clear-bottom polystyrene microtiter plates (Greiner) using the Titertek Zoom bulk liquid dispenser (plates already contained siRNA transfection complexes, see next step). To ensure even settling and to avoid edge effect settling, I kept plates at room temperature for 20 minutes before they were placed in a humidified incubator at 37ºC with 5% CO2. To avoid edge effect due to edge well evaporation, I added two extra pans of water to the incubator to maintain humidity.

2.5.4 siRNA transient transfection.

T98G cells were forward transfected with the Ambion Silencer Druggable Genome siRNA library at a final concentration of 20 nM/target in a one-gene, one-well format. For each target, 4.13 μL of 833.3 nM siRNA was combined with 0.17 μL DharmaFECT2 transfection reagent and 33 μL of OptiMEM. The complexes were then split between two 384-well plates (14 μL per well), and 51 μL of T98G cell suspension was added directly onto the siRNA

complexes. siRNA complexes were prepared with DharmaFECT2 transfection reagent in pools of three unique siRNA duplexes per well, one gene per well across sixteen 384 well siRNA library plates. siRNA complexes were prepared at 50 nM per well, and the addition of cell suspension (20 minutes after complex preparation) to the siRNA complexes brought the siRNA concentration to 20 nM per well. Five hours later, medium containing siRNA complexes was removed and replaced with fresh complete medium. Cells were incubated for 48 hours in a humidified incubator at 37ºC with 5% CO2 to allow for gene silencing before vehicle or MDA compounds were added.

2.5.5 Drug treatment.

Forty-eight hours after cells were plated and transfected with library siRNA, medium was removed from the cells and replaced with fresh medium containing either 1.2 nM vinblastine, 350 pM disorazole C_1 , or 0.5% DMSO vehicle. Cells were incubated in the presence of compounds for 48 hours in a humidified incubator at 37ºC with 5% CO_2. After incubation, cell viability was measured with the CellTiter-Blue cell viability assay for three hours, according to manufacturer's protocol.

2.5.6 Cutoff for selecting sensitizing hits.

The synthetic lethal siRNA screen was performed three times for vinblastine, and three times for disorazole C_1, over six separate weeks. To quantify the degree of interaction between

siRNA plus drug or drug plus drug, I used the following equation to measure the percent greater-than-additive (%GTA) ratio:

$$C - (S + M) = \% \text{ GTA}$$

Where S was the percent inhibition caused by the target siRNA plus vehicle DMSO, M was the percent inhibition caused by the drug plus scrambled siRNA, and C was the percent inhibition caused by the combination treatment. This formula and its derivation will be described in greater detail in Chapter 3, section 3.4.2. "Inhibition" referred to the loss of cell viability relative to vehicle treated cells transfected with scrambled siRNA. A %GTA ratio of 10% or greater was considered a "hit".

2.6 DETERMINATION OF COMBINATION INDEX FOR DRUG INTERACTIONS.

To determine if drug combinations were additive, synergistic, or antagonistic to cancer cells at different effect levels, the combination index (CI) method of Chou and Talalay was used [47-50]. These methods of evaluating drug interactions were selected because they take into account the potencies of each drug and combinations (Dm value), as well as the shape of the dose-effect curves (m values), calculating how the experimental effect differs from the effect expected with additivity. CI values of <1, 1, and >1 indicate synergism, additivity, and antagonism, respectively. Briefly, cells were plated in a 8x8 grid of a 96-well plate and horizontal rows were treated with a range of seven concentrations of the first compound and one row of DMSO, and treated vertically with a range of seven concentrations of the second

compound and one row of DMSO. The final DMSO concentration of all wells was 0.5%. Cells were incubated for 24 hours after plating before compound treatment, and cell viability was measured by CellTiter-Blue after 72 hours in the presence of compound. After cell viability measurement, cells were simultaneously fixed and stained for ten minutes with a PBS solution containing 4% formaldehyde and 1.2 µg/mL Hoescht 33342. The 8x8 grid arrangement of compound treatment provided 64 unique drug combination ratios of the two compounds and/or DMSO, including a DMSO vehicle-only well. This scheme enabled CI values to be determined at many different effect levels and different dose levels. CI values and plots were automatically generated using the computer software program CalcuSyn version 2.1 [51, 52]. The CalcuSyn program calculates the CI values and plot through the median-effect equation of Chou, enabling a correlation between the dose or concentration of compound and the effect in terms of cell viability [51]. According to the CalcuSyn product manual:

$$f_a/f_u = (D/D_m)^m \qquad \text{[Eq. 1]}$$

where:

D: the dose of drug

D_m: the median-effect dose signifying the potency. It is determined from the x-intercept of the median-effect plot.

f_a: the fraction affected by the dose

f_u: the fraction unaffected, $f_u=1-f_a$

m: an exponent signifying the sigmoidicity (shape) of the dose effect curve. It is determined by the slope of the median effect plot.]

The alternative forms of the median-effect equation are:

fa = 1/[1+ (Dm/D)m] [Eq. 2]

D = Dm[fa/(1-fa)]1/m [Eq. 3]

From Eq. 2, if Dm and m are known, the effect (fa) can be determined for any dose (D).

From Eq. 3, if Dm and m are known, the dose (D) or (Dx) can be determined for any effect (fa). Thus, Dm and m parameters representing the potency and shape, respectively, determine the entire dose-effect curve.

Synergism is defined as a more than expected additive effect, and antagonism as a less than expected additive effect. CI = 1 is designated as the additive effect, thus from the multiple drug effect equation of two drugs, we obtain:

$$CI = \frac{(D)_1}{(D_x)_1} + \frac{(D)_2}{(D_x)_2} \qquad \text{[Eq. 4]}$$

CI < 1, = 1, and > 1 indicates synergism, additive effect, and antagonism, respectively. Eq. 4 dictates that drug 1, (D)1, and drug 2, (D)2, (in the numerators) in combination inhibit x% in the actual experiment. Thus, the experimentally observed x% inhibition may not be a round number but most frequently has a decimal fraction. (Dx)1 and (Dx)2 (in the denominators) of Eq. 4 are the doses of drug 1 and drug 2 alone, respectively, inhibiting x%. Dx can be readily calculated from Eq. 3. The axes of the combination index (CI) plot are illustrated in figure 3.

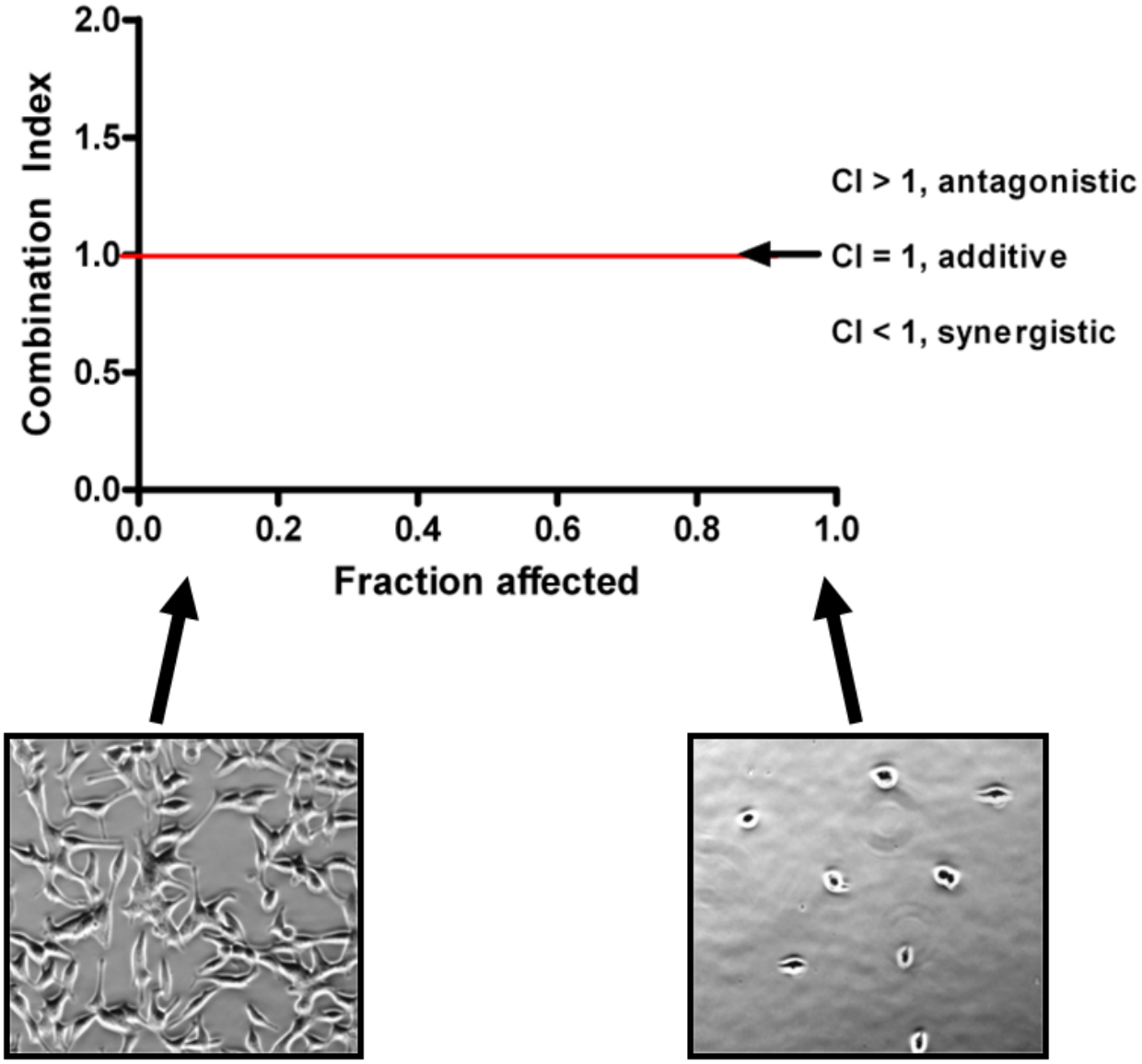

Figure 3. Description of the combination index plot.

The combination index plots generated by CalcuSyn provided a quantitative measure of the degree of drug interaction in terms of additive effect, synergism, or antagonism for a given endpoint of the effect measurement. For each combination, Calcusyn plots a single data point onto a graph illustrated above. The location of the data point on the Y-axis illustrated whether a particular combination was antagonistic, additive, or synergistic, plotted above, on, or below a

combination index value of 1.0. The location of the data point on the X-axis illustrated the % of cells affected by a combination, termed fraction affected. As illustrated, a fractional affect at 0.1 would indicate the level of synergy or antagonism when only 10% of the cells were affected, either by a 10% inhibition of cell proliferation or a toxic effect in 10% of cells. Likewise, at a fraction affect level of 0.9 displays the interaction of the drug combination when 90% of cells are affected.

3.0 DEVELOPMENT AND APPLICATION OF A SYNTHETIC LETHAL SCREEN TO IDENTIFY GENE PRODUCTS AND NETWORKS THAT MODULATE GLIOMA CELL SENSITIVITY TO CANCER THERAPY

The first specific aim of this thesis was to develop a synthetic lethal screen to identify gene products that modulate GBM cell sensitivity to cancer therapy. To develop this screen, I used a miniaturized, 384-well format for transiently transfecting T98G cells with siRNA from a druggable genome siRNA library, silencing specific druggable genes in cells treated with minimal concentrations of MDAs, and coupled this to a semi-automated, high-throughput, cell-based cytotoxicity assay. This chapter describes the development and application of this synthetic lethal assay. The objectives of this aim were to 1) develop a workflow for high-throughput transfection and MDA treatment in microtiter plates, 2) optimize reproducible cell culture plating and compound treatment conditions, 3) optimize siRNA library transient transfection conditions in T98G cells, and 4) establish methods for collection and analysis of large screening data sets.

3.1 SYNTHETIC LETHAL siRNA SCREENING ASSAY WORKFLOW.

The workflow of the synthetic lethal screen, which was fully optimized by me, consisted of a five-day week, illustrated in Figure 4. The transfection reagent DharmaFECT2 was combined with OptiMEM and uniformly distributed into a series of sterile polystyrene V-bottom 384-well plates using a Titertek Zoom bulk dispenser. siRNA molecules were added to the wells, targeting one gene per well, plus in-plate scrambled siRNA control wells on every plate. I had three unique siRNAs for each of the 5,520 genes that were targeted across 16 plates. I pooled the three siRNAs to reduce the cost and improve throughput. The druggable genome siRNA library was screened at a final concentration 20 nM siRNA. Transfection complexes were prepared using automated liquid handling instruments, and after 15-20 minutes, transfection complexes were divided among two new 384-well plates (16 x 2 = 32 plates total) followed by the addition of T98G cells in suspension. Plate pairs were incubated for 48 hours, then treated with either vehicle (0.5% DMSO) or a microtubule perturbing agent. Fourty-eight hours later, cell viability was measured by the CellTiter-Blue assay. The assay was limited to a total of 96 hours due to minimize variability while still providing sufficient time for gene silencing and MDA impact on dividing T98G cells. For each compound tested, three individual screens were performed over separate weeks.

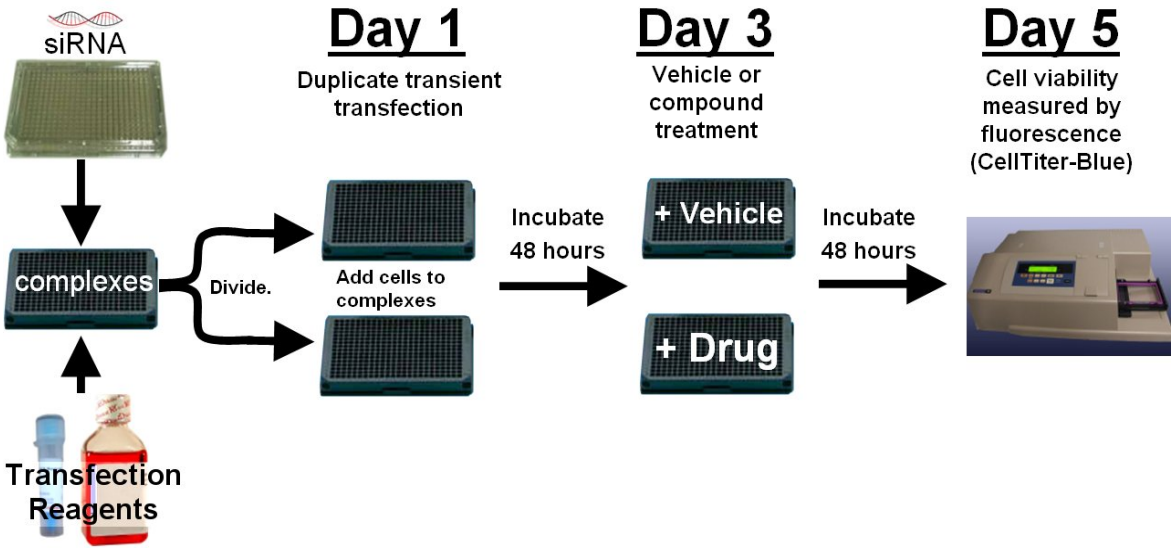

Figure 4. Synthetic lethal siRNA screening assay workflow diagram.

The five-day workflow of the synthetic lethal screen consisted of a five-day week. Cells were transfected on Day 1, treated with either vehicle (0.5% DMSO) or a microtubule perturbing agent on Day 3, and cell viability was measured on Day 5 by the CellTiter-Blue assay. For each compound tested, three individual screens were performed over separate weeks.

3.2 OPTIMIZATION OF T98G CELL CULTURE CONDITIONS AND MDA TREATMENT

3.2.1 Cell seeding in 384 well plates.

A cell seeding density experiment was conducted to determine the optimal number of T98G cells to be seeded per well of the 384-well microtiter plate for the five day assay (96 hour

incubation). Plating density was extremely important to this type of assay, as this assay was very sensitive to the final number of cells surviving siRNA transfection and compound treatment. Too many cells per well resulted in early confluency and over confluency, muting the effects of minor cell inhibition. In addition, crowding leads T98G cells to enter a viable G1 arrested state. Too few cells will result in under confluency at the end of the 96 hours, and decrease reproducibility. To determine the optimal number of cells to plate, I plated T98G cells using a semi-automated Titertek Zoom liquid dispenser to minimize plate-to-plate and day-to-day variability. Target T98G cell density on day 1 was 30% well confluency, to achieve 90-100% confluency by day 5. Logarithmically growing T98G cells were seeded in 384-well plates and incubated for 96 hours before measuring cell viability. CellTiter-Blue viability assay (Figure 5A) and microscopic evaluation (Figure 5B) indicated that seeding 400-500 T98G cells was sufficient to provide 90 -100% confluency after 96 hours. Based on these data and similar reproductions of this experiment, a seeding density of 450 T98G cells per well was selected for all further assay development.

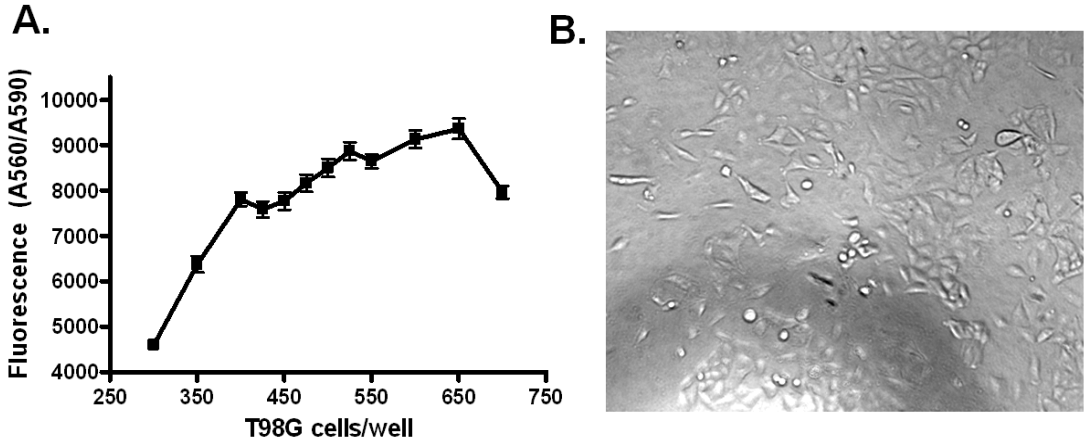

Figure 5. Cell seeding density for T98G cells.

T98G cells were seeded at a range of cell densities with 25 μL/well in 384-well polystyrene tissue-culture-treated plates in complete medium and incubated for 96 hours at 37°C and 5% CO_2. (A) After incubation, CellTiter-Blue viability reagent (5 μL) was added to each well and the fluorescence was read on the SpectraMax M5 after three hours. Fluorescence was proportional to the ability of living cells to convert the non-fluorescent resazaurin dye to fluorescent resorufin. Data represent the mean value of four well replicates $\pm$ S.E.M. (B) Brightfield image of T98G cells 96 hours after seeding 450 cells in a 384-well microtiter plate.

3.2.2 Compound treatment.

The purpose of this assay was to identify siRNAs that sensitized T98G cells to concentrations of disorazole C_1 or vinblastine that alone would be sub-lethal. To determine the minimal growth inhibition of compound, I conducted a concentration response curve for both disorazole C_1 and vinblastine in T98G cells transfected with scrambled siRNA (Figure 6). Based on these data, I selected concentrations of 0.35 nM and 1.2 nM concentrations of disorazole C_1 and vinblastine, respectively, as suitable sub-lethal (EC_{15}) concentrations for treating cells in the siRNA screening assay. By using these concentrations, it was easier to visualize any synergistic synthetic lethal response. Compound concentrations causing less than 10% inhibition of cell viability decreased the ability of the assay to detect sensitization by target gene silencing, and compound concentrations causing a greater than 20% inhibition of cell viability were less reproducible, as they approached the downward slope of the concentration response curve, frequently triggering a greater than intended toxicity.

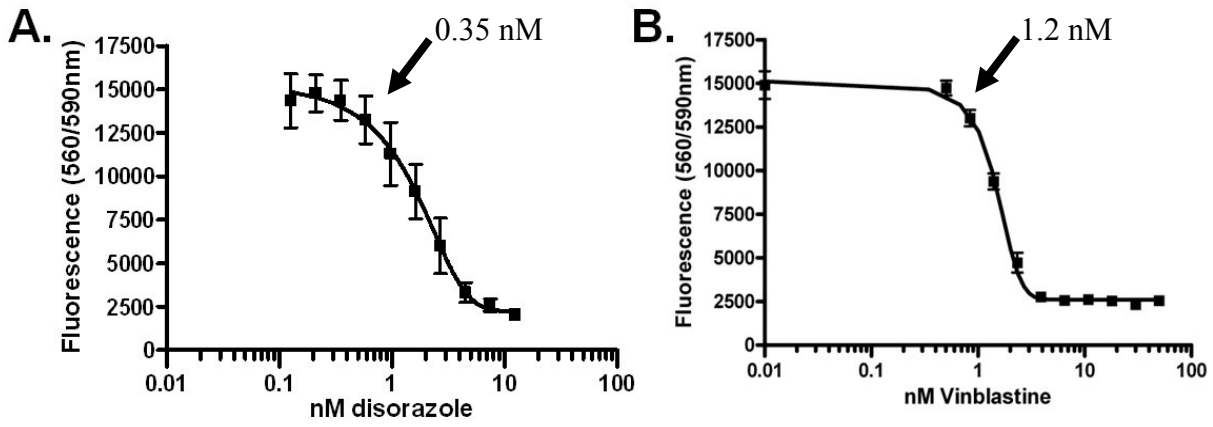

Figure 6. Disorazole C1 and vinblastine concentration response in T98G cells.

T98G cells were seeded at 450 cells/well in 50 µL in 384-well plates and transfected with non-targeting scrambled siRNA. After 48 hours of incubation at 37°C and 5% CO_2, cells were treated with a range of concentrations of either (A) disorazole C_1 or (B) vinblastine. After incubation, CellTiter-Blue viability reagent (10 µL) was added to each well and the fluorescence was read pm the SpectraMax M5 after three hours. Fluorescence was proportional to cell viability. Data represent the mean values of four well replicates + S.E.M.

3.3 OPTIMIZATION OF HIGH-THROUGHPUT TRANSIENT siRNA LIBRARY TRANSFECTION OF T98G CELLS.

siRNA transfection optimization was necessary to assure a high transfection efficiency with minimal cytotoxicity. A successful RNAi transient transfection provides high target knockdown with high cell viability. There are at least seven key considerations when optimizing siRNA transfection: (1) choice of transfection reagent, (2) transfection method, (3) amount of

transfection reagent, (4) cell density per well, (5) cell exposure time to reagent, (6) amount of siRNA, and (7) timing of the assay.

3.3.1 Transfection procedure.

To silence the genes in this study, I used transient transfection of siRNA because of its ease of use and cost efficiency while still providing sufficient gene silencing within 48-72 hours for most gene targets [53]. siRNA molecules are transfected into the cell as duplexes, and do not require the endogenous processing needed by short hairpin RNA (shRNA) [53]. One limitation of siRNA transfection is the transient nature of the effect, with decreased silencing after 96 hours, unlike shRNA, which provides stable, long term silencing. Because the synthetic lethal assay is only 96 hours, siRNA was sufficient, and its flexibility was preferable for automation of this assay.

Further, there are several methods of siRNA transient transfection beyond the standard forward transfection, such as dry reverse transfection, and wet reverse transfection. Forward transfection refers to plating cells, allowing the cells to grow for 24 hours before adding siRNA complexes. Wet reverse transfection involves plating out the siRNA complexes then adding cells in suspension directly to the complexes. Dry reverse transfection is performed by plating out siRNA molecules alone into dry plates, and letting all moisture evaporate away from the plate, allowing daughter siRNA plates to be stored while awaiting resuspension in transfection media and cell suspension. Preliminary studies comparing forward to wet reverse transfection gave me nearly identical transfection efficiencies, measured by fluorescent siGLO siRNA. For the siRNA library screening, I used wet reverse transfection because it allowed same-day

transfecting and plating cells, eliminating the 24 hour incubation waiting period and removed the handling step of replacing cell media with complexes 24 hours after plating.

3.3.2 Transfection reagents.

To get optimal transfection efficiency with minimal toxicity, I had to select an appropriate transfection reagent. siRNA experiments required a transfection reagent that was specially optimized for siRNA delivery into mammalian cells, and the best transfection reagent for plasmids was not always the best reagent for siRNA, as in Figure 7 panel A and B. To determine the best siRNA transfection reagent for T98G cells, I transiently transfected T98G cells in quadruplicate in a 384-well plate with fluorescently labelled siRNA (75 nM final concentration of Invitrogen BLOCK-IT fluorescent oligo siRNA) using four transfection reagents: Lipofectamine2000, FuGENE6, NeuroPorter, and DharmaFECT. DharmaFECT siRNA transfection reagent is specifically designed for siRNA transfection, while the other three reagents are suitable for plasmid or siRNA transfection. There are four versions of DharmaFECT reagent: DharmaFECT1, DharmaFECT2, DharmaFECT3, and DharmaFECT4, which slightly different formulations for transfecting different cell lines. According to manufacturer's protocol, DharmaFECT2 is the optimal DharmaFECT reagent for T98G. To compare DharmaFECT2 to the other transfection reagents, T98G cells were fixed and stained with Hoescht 33342, and transfection efficiency was determined by handcounting (# transfected cells / # total cell nuclei) (illustration in Figure 7 panel C). Noticeably, the small size of siRNA compared to plasmids allowed a much higher transfection efficiency with siRNA (Figure 7, compare A to B). Visually, the fluorescent siRNA could be seen in nearly every T98G cell in Figure 7 panel C. While FuGENE had the greatest transfection efficiency of plasmids in T98G,

it could not achieve higher than 11% transfection efficiency of siRNA. Lipofectamine2000 enabled transfection of both plasmid and siRNA, but was unpredictably toxic to most wells and required complexes to be removed 3-5 hours after transfection to prevent 100% cell death. Importantly, this toxicity could adversely affect results of this siRNA screen, for toxic reagents such as Lipofectamine have been reported to alter gene expression of over 2,000 genes after transfection of cells with plasmids (without inserts) [54]. The DharmaFECT2 reagent, however, had both a high transfection efficiency and minimal toxicity. DharmaFECT2 was selected for all further assay development.

A.

GFP Plasmid	Transfxn efficiency	Toxicity (death 96h)
FuGENE	25%	5%
Lipo2000	10%	95%
DharmaFECT	—	—

B.

Fluor. siRNA	Transfxn efficiency	Toxicity (death 96h)
FuGENE	.2-11%	5%
Lipo2000	87-99%	95%
DharmaFECT	87-99%	5%

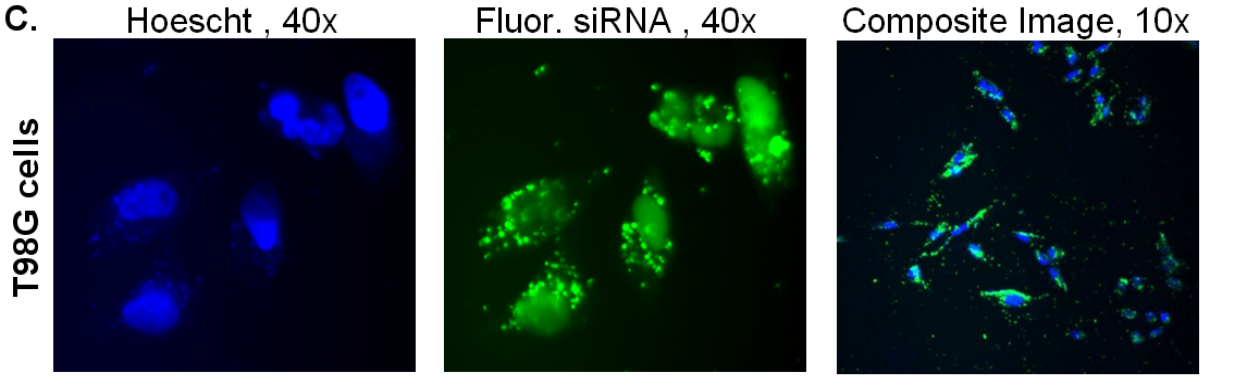

Figure 7. T98G cell transfection efficiencies.

T98G cells were seeded at 1000 cells/well in 50 µL in 384-well plates in complete medium and allowed to attach overnight at 37°C and 5% CO2. Cells were then transiently

transfected in quadruplicate with (A) green fluorescent protein expressing pEGFP-C1 plasmid or (B) 75 nM (final concentration) Invitrogen BLOCK-IT fluorescent (fluor.) oligo siRNA (non-targeting scrambled) using various transfection reagents according to manufacturer's protocols, scaled from 96-well format down to 384-well plate format. Twenty-four hours after transfection, cells were fixed and stained with 3.7% formaldehyde and 1.2 μg/mL Hoescht 33342, respectively. Transfection (transfxn) efficiency was assessed by manual counting fluorescent cells divided by total nuclei per field. Panel C illustrates Hoescht 33342 stained nuclei, fluorescent siRNA, and a merged image overlaying nuclear staining with fluorescent siRNA clusters.

3.3.3 Transfection conditions.

To confirm gene silencing with DharmaFECT2 deprived T98G cells of target protein, I transfected T98G cells with siRNA against lamin A/C and assessed lamin A/C silencing by two methods: (1) protein silencing in whole cell lysates by Western blot, and (2) % of cells silenced, as measured by lamin A/C antibodies and read with ArrayScan for fluorescence of lamin A/C-Alexa594 antibodies.

Lamin A/C immunoblotting is presented in Figure 8. The transfection conditions were capable of delivering lamin A/C siRNA and reducing protein levels. DharmaFECT-mediated siRNA transfection reduced protein levels after 48 and 72 hours, but not 24 hours. Since some proteins have long half lives (like lamin), to prevent false positives, the siRNA screen should provide 48 hours for silencing before addition of drug. This assay was optimized to keep

proteins silenced between 48-96 hours after transfection, to coincide with the duration of the 48 hour drug treatment period.

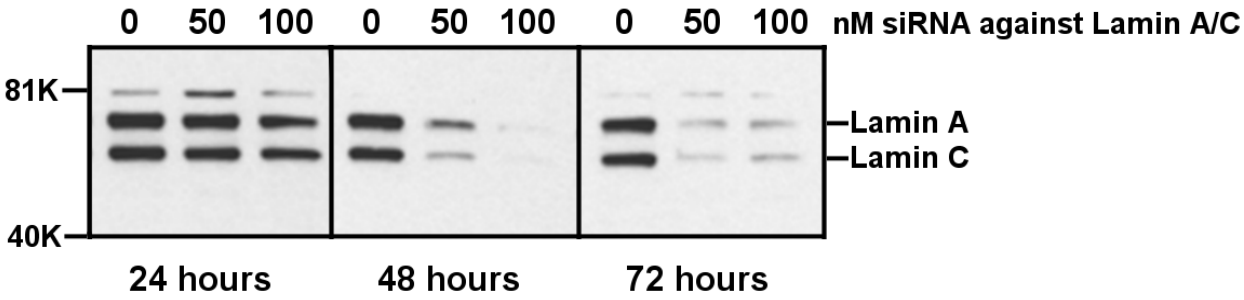

Figure 8. Lamin A/C protein depletion by siRNA against lamin A/C.

T98G cells were transiently transfected in 6-well plates with 0, 50, or 100 nM final concentration of siRNA targeting lamin A/C using DharmaFECT2 transfection reagent. 24, 48, or 72 hours after transfection, cells were lysed for Western blot analysis. Lamin A/C protein was detected by immunoblotting using lamin A/C primary rabbit antibody (Cell Signaling). Lamin A/C protein levels were only not affected after 24 hours, but were dimished after 48 and 72 hours in the presence of siRNA against lamin A/C.

Lamin A/C silencing in 384-well plate format was detected by ArrayScan VTi as described in the legend of Figure 9. Lamin A/C signal could be seen in the first column, where cells did not receive siRNA against lamin A/C. Lamin A/C signal was dramatically decreased in cells by both 50 nM and 100 nM final concentrations of siRNA, however, 100 nM was slightly more toxic to cells. In both this immunofluoresce assay, and the previous immunoblotting assay, 50 nM siRNA concentration was sufficient for silencing lamin A/C, so 50 nM was chosen as the final concentration of siRNA for future library transfections. A lower range of siRNA concentrations (10, 20, and 50 nM) was later tested, revealing that 20 nM was sufficient for

silencing. Library screening was performed using a final concentration of 20 nM siRNA per well.

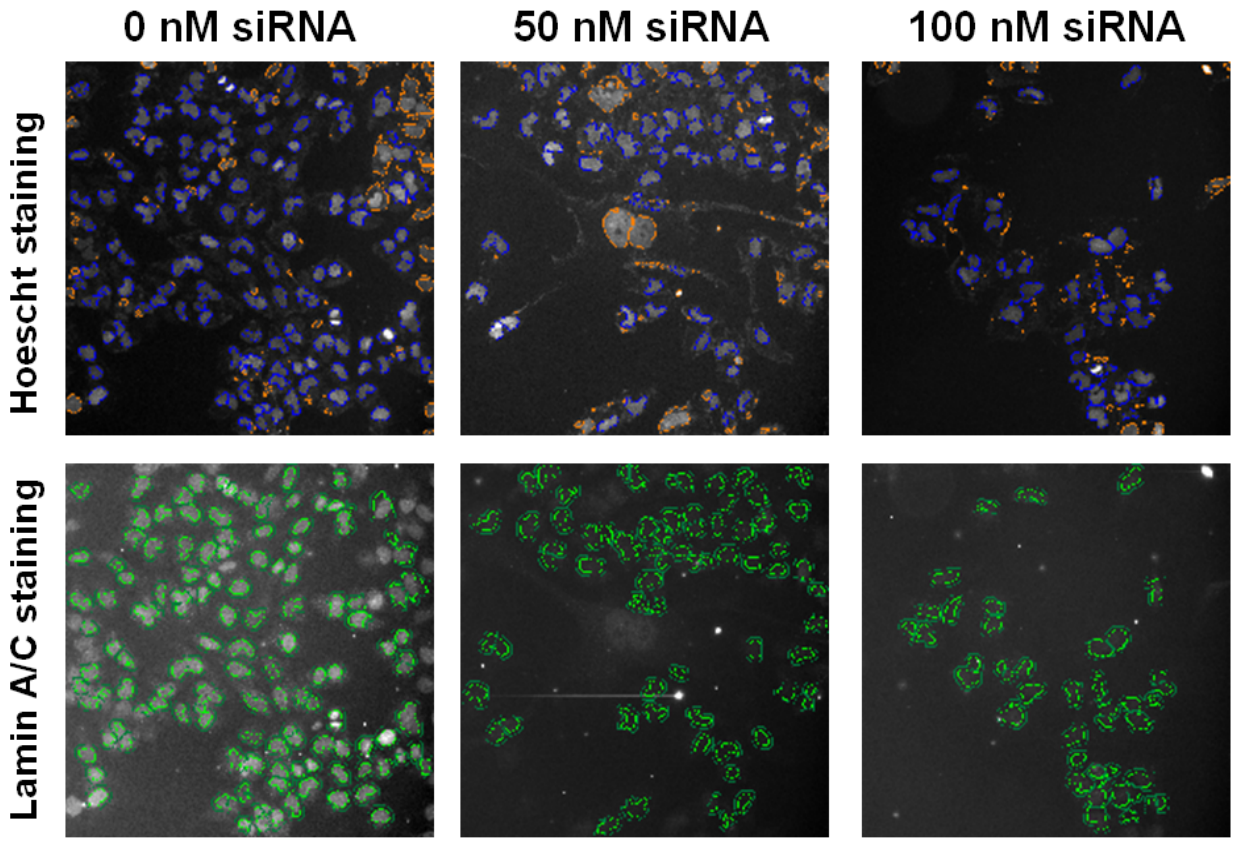

Figure 9. siRNA silencing of lamin A/C in T98G cells.

T98G cells were seeded at 450 cells/well in 50 µL in 384-well plates in complete medium and allowed to attach overnight at 37°C and 5% CO_2. Cells were then transiently transfected in quadruplicate with 0, 50, or 100 nM final concentration of siRNA targeting lamin A/C using DharmaFECT2 transfection reagent. Seventy-two hours after transfection, cells were fixed and stained with 3.7% formaldehyde and 1.2 µg/mL Hoescht 33342, respectively. Lamin A/C protein was detected using lamin A/C primary rabbit antibody (Cell Signaling) and Alexa594-conjugated secondary goat-anti-rabbit (Cell Signaling). Transfection efficiency was assessed by

ArrayScan VTi. Briefly, cells were defined by drawing a nuclear mask (blue line) around Hoescht 33342-stained nuclei in the first fluorescence channel (top row of panels), and this mask was used to detect lamin A/C-Alexa594 staining in the second fluorescence channel (green outline, bottom row of panels).

3.3.4 siRNA library.

We relied on siRNA technology as a means of gene silencing by pools of three individual siRNAs per gene, in a one-gene one-well format, performed three times independently. Due to the focus of this project on chemotherapeutics, we relied on a commercially available library targeting gene products that are either affected by existing drugs or have the potential to be used by drug-like compounds [55, 56]. In this research, I used the Ambion Silencer Druggable Genome siRNA Library, which contains 16,560 unique siRNA sequences to target 5,520 genes (categories of this library are listed in Table 1). This library contains members of all of the major functional protein categories including G-protein coupled receptors (GPCRs), transporters, ion channels, kinases, phosphatases, deacetylases, oxidoreductases, polymerases, reductases, and other enzymes (Figure 10).

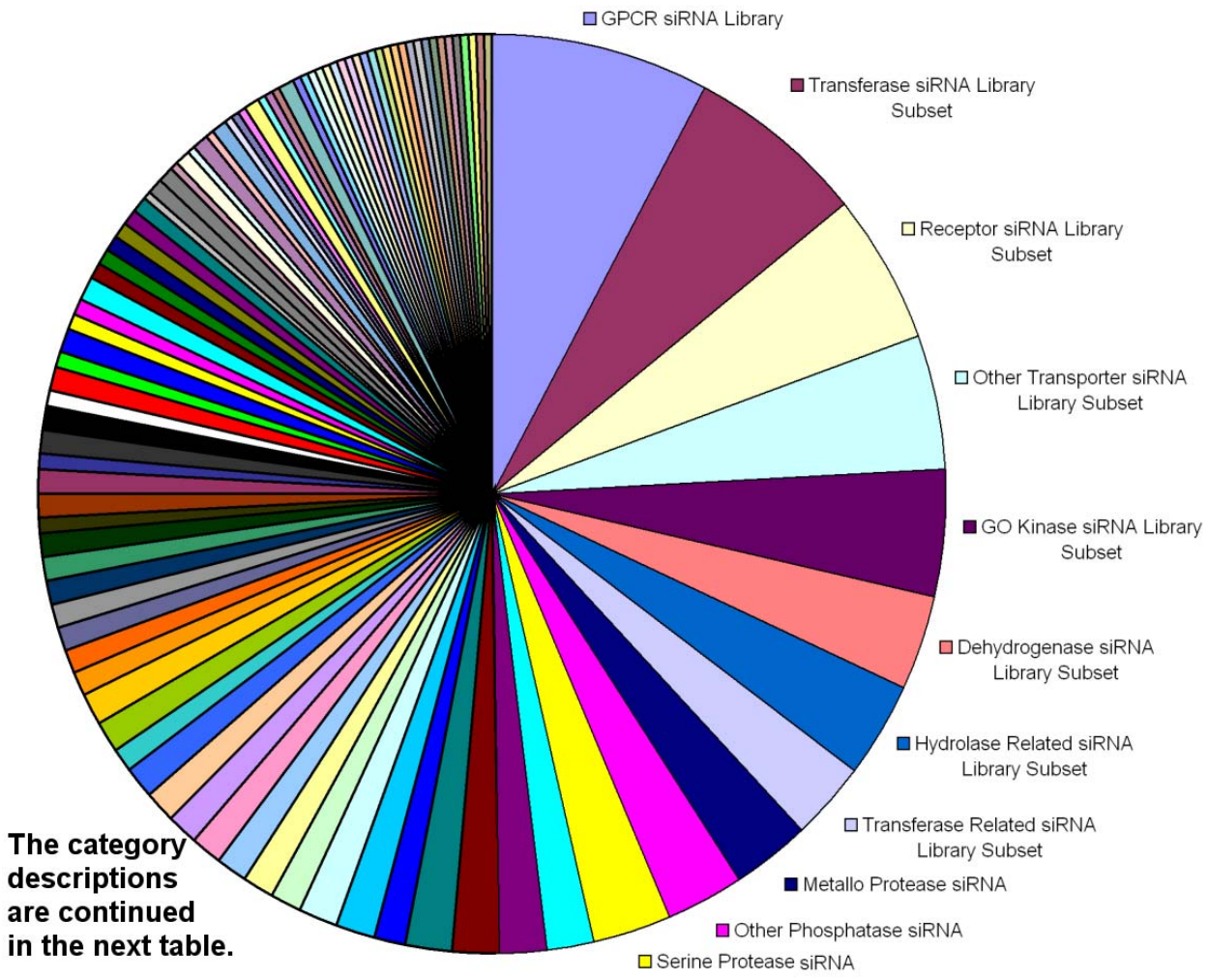

Figure 10. Gene Categories in Silencer® Druggable Genome siRNA Library.

Functional categories in Silencer Druggable siRNA Library. I utilized a library of 16,560 siRNAs corresponding to three unique siRNA duplexes, targeting 5,520 unique human genes in a one-gene per well format on 384-well plates. The list of categories is provided in Table 1, in order of appearance in piechart, clockwise from the top (GPCR first).

Ambion Silencer Druggable Genome siRNA Library v. 1.1

Gene categories from Figure 3.7 are displayed clockwise from top:

Subset	Genes	% of library
GPCR siRNA Library	431	7.8%
Transferase siRNA Library Subset	345	6.3%
Receptor siRNA Library Subset	295	5.3%
Other Transporter siRNA Library Subset	257	4.7%
GO Kinase siRNA Library Subset	253	4.6%
Dehydrogenase siRNA Library Subset	186	3.4%
Hydrolase Related siRNA Library Subset	173	3.1%
Transferase Related siRNA Library Subset	164	3.0%
Metallo Protease siRNA Library Subset	157	2.8%
Other Phosphatase siRNA Library	151	2.7%
Serine Protease siRNA Library Subset	141	2.6%
Ras G Protein siRNA Library Subset	101	1.8%
Other G Protein siRNA Library Subset	96	1.7%
Cysteine Protease siRNA Library Subset	87	1.6%
TK Kinase siRNA Library Subset	84	1.5%
Voltage Gated Potassium Channel siRNA Library S	76	1.4%
Silencer®Other Kinase siRNA Library Subset	72	1.3%
CAMK Kinase siRNA Library Subset	68	1.2%
Dehydrogenase Related siRNA Library Subset	67	1.2%
Reductase siRNA Library Subset	65	1.2%
Other Ion channels siRNA Library Subset	63	1.1%
Miscellaneous siRNA Library	62	1.1%
Carrier Related siRNA Library Subset	59	1.1%
AGC Kinase siRNA Library Subset	58	1.1%
CMGC Kinase siRNA Library Subset	57	1.0%
Other Protease siRNA Library Subset	57	1.0%
Oxidase siRNA Library Subset	56	1.0%
Nuclear Hormone Receptor siRNA Library	53	1.0%
Cytochrome P450 siRNA Library Subset	52	0.9%
ATP Binding Cassette (ABC) Transporter siRNA Li	50	0.9%
Isomerase Related siRNA Library Subset	46	0.8%
Ubiquitin siRNA Library	46	0.8%
Receptor Related siRNA Library Subset	45	0.8%
Hydroxylase siRNA Library Subset	43	0.8%
Kinesin siRNA Library Subset	42	0.8%
Lipase Related siRNA Library Subset	42	0.8%
STE Kinase siRNA Library Subset	42	0.8%
TKL Kinase siRNA Library Subset	41	0.7%
Tyrosine Phosphatase siRNA Library Subset	41	0.7%
Atypical Kinase siRNA Library Subset	40	0.7%
Isomerase siRNA Library Subset	40	0.7%
Synthetase siRNA Library Subset	40	0.7%
Hydrogen Transporter siRNA Library Subset	39	0.7%
Caspase siRNA Library Subset	38	0.7%
Phosphodiesterase Library	38	0.7%
Myosin siRNA Library Subset	37	0.7%
Proteinase siRNA Library	34	0.6%
Peptidase siRNA Library Subset	33	0.6%
Solute Carrier siRNA Library Subset	33	0.6%
Glutamate Neurotransmitter siRNA Library Subset	32	0.6%
ATPase siRNA Library Subset	31	0.6%
Cyclin siRNA Library Subset	31	0.6%
Lipase siRNA Library Subset	28	0.5%
Voltage Gated Calcium Channel siRNA Library Sul	28	0.5%
Esterase siRNA Library Subset	27	0.5%
Carboxylase Related siRNA Library Subset	25	0.5%
Other Ligand Ion channels siRNA Library Subset	25	0.5%
Oxygenase siRNA Library Subset	25	0.5%
Unassigned siRNA	25	0.5%
Anion channels siRNA Library Subset	23	0.4%
Tubulin siRNA Library	23	0.4%
Kinase Related siRNA Library Subset	22	0.4%
Carboxylase siRNA Library Subset	21	0.4%
GABA Neurotransmitter siRNA Library Subset	20	0.4%
Synthase siRNA Library Subset	20	0.4%
Adhesion Molecule siRNA Library	19	0.3%
ATP Carbohydrate Transporter siRNA Library Subs	19	0.3%
Dynein siRNA Library Subset	19	0.3%
Peptidase Inhibitor siRNA Library Subset	19	0.3%
Acetylcholine Neurotransmitter siRNA Library Sub	18	0.3%
Esterase Related siRNA Library Subset	18	0.3%
Oxidoreductase siRNA Library	18	0.3%
Reductase Related siRNA Library Subset	18	0.3%
Integrin siRNA Library Subset	17	0.3%
Ligase siRNA Library Subset	17	0.3%
Lyase and Related siRNA Library	17	0.3%
Oxidase Related siRNA Library Subset	17	0.3%
Aspartic Protease siRNA Library Subset	16	0.3%
BCL2 and Related siRNA Library	16	0.3%
Polymerase siRNA Library	16	0.3%
Protein Exchange G Protein siRNA Library Subset	16	0.3%
Amino AcidTransporter siRNA Library Subset	15	0.3%
Heterotrimeric G Protein siRNA Library Subset	15	0.3%
Ribonuclease siRNA Library Subset	15	0.3%
Dehydratase siRNA Library Subset	14	0.3%
Voltage gated - sodium siRNA Library Subset	14	0.3%
Other Neurotransmitter siRNA Library Subset	13	0.2%
Deaminase siRNA Library Subset	12	0.2%
CK Kinase siRNA Library Subset	11	0.2%
ATPase Related siRNA Library Subset	10	0.2%
Hydroxylase Related siRNA Library Subset	10	0.2%
Guanylate Cyclase siRNA Library Subset	9	0.2%
Adenylate Cyclase siRNA Library Subset	8	0.1%
Cyclic Nucleotide Gated Ion Channel siRNA Librar	8	0.1%
Dehydratase Related siRNA Library Subset	8	0.1%
Helicase siRNA Library Subset	7	0.1%
Glucosidase siRNA Library Subset	7	0.1%
Oxygenase Related siRNA Library Subset	7	0.1%
Protease Inhibitor siRNA Library	7	0.1%
Deacetylase siRNA Library Subset	6	0.1%
Integrin Related siRNA Library Subset	6	0.1%
Synthase Related siRNA Library Subset	6	0.1%
Synthetase Related siRNA Library Subset	6	0.1%
Cytochrome P450 Related siRNA Library Subset	5	0.1%
Endonuclease siRNA Library Subset	5	0.1%
Non Solute Carrier siRNA Library Subset	5	0.1%
Other Cyclase siRNA Library Subset	4	0.1%
RNA Binding siRNA Library Subset	3	0.1%
Exonuclease siRNA Library Subset	2	0.0%

Table 1. List of gene categories in Silencer Druggable Genome siRNA Library.

List of functional categories in Silencer Druggable siRNA Library from Figure 10. The list of categories is provided in order of appearance in Figure 10 piechart, clockwise from the top (GPCR first).

The siRNA library consisted of three sets of 16 microtiter plates, each containing a different set of 5,520 siRNA 19-mer duplexes. For each target gene, three unique siRNA duplexes were provided, thus 16,560 wells of siRNA targeting 5,520 genes. I resuspended the library in 100 μL/well sterile siRNA resuspension buffer (Dharmacon) to a concentration of 2.5 μM. A small volume of each of the three sets of 16 plates were pooled together to creating a daughter set of 16 plates, each well containing three duplexes against a particular gene. The majority of the library was left unpooled for future single-duplex use. Pools were created for screening to reduce initial screening cost by two thirds, as well as to increase speed of throughput. This approach provided significantly higher efficiency in time and cost than running the screen with individual siRNAs. Another major advantage of siRNA pooling is the reduction of off-target effects. Off-target effects refer to when an unintended gene target is silenced, such as when an siRNA silences an mRNA that is not the intended target. Silencing of unintended targets can lead to incorrect results. Each duplex alone may silence its own specific set of off-target genes, but as a pool of three, this reduces the off-target silencing by roughly two-thirds for each duplex, while the three duplexes together still target the same desired mRNA.

Each 384-well plate of the siRNA library had two columns of empty wells. To those columns I added non-targeting scrambled siRNA for each newly created pooled daughter plate to serve as in-plate controls for toxicity caused by siRNA transient transfection in the absence of gene silencing.

3.4 DATA COLLECTION AND ANALYSIS.

3.4.1 Data collection: Assessment of cell viability.

To determine the effect of siRNA or compound treatment on T98G cells at the end of the screen, I used the CellTiter-Blue cell viability assay, described in Figure 11. CellTiter-Blue was selected because it was economical, easy to use, and non-toxic to the cells and to humans, unlike other viability assays such as MTT (dimethyl thiazolyl diphenyl tetrazolium) assay. Forty-eight hours after compound or vehicle treatment, thus 96 hours after siRNA transfection, cell viability was assessed using the CellTiter-Blue assay. Following a fluorometer reading, cells were fixed with 3.7% formaldehyde to preserved cells for later immunofluorescence analysis.

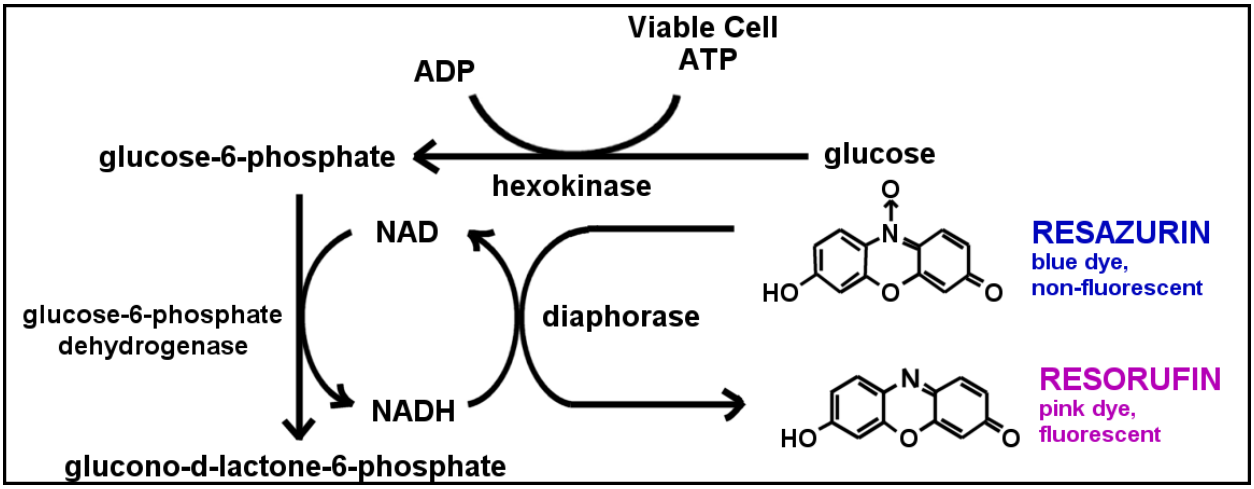

Figure 11. Resazurin reduction mechanism of CellTiter-Blue cell viability assay.

This diagram illustrates the cell viability assay mechanism of resazurin conversion triggered by ATP from viable cells. Viable cells produce NADH, which in the presence of

diaphorase and resazurin, was used to drive the diaphorase-catalyzed production of the fluorescent resorufin product. Resazurin could enter living cells where it is reduced to the fluorescent resorufin product. The conversion of resazurin to resorufin was proportional to the number of metabolically active, viable cells present in a population. The CellTiter-Blue Cell Viability Assay used an optimized reagent containing resazurin. The homogeneous procedure involved adding the reagent directly to cells in culture. The assay plates were incubated at 37°C for 1–4 hours to allow viable cells to convert resazurin to the fluorescent resorufin product. The signal is recorded using a standard multiwell fluorometer.

3.4.2 Data analysis.

Performing this screen in triplicate, with controls, using two different microtubule disrupting agents – vinblastine and disorazole C_1 – involves a total of 73,728 wells:

16 plates in library * 384 wells per plate * 2 (1st set with drug, 2nd set with vehicle) * triplicate * 2 compounds (vinblastine and disorazole C_1) = 73,728 wells

Due to this large number of wells, individual visual inspection was impossible. The following formula was derived to provide a meaningful estimate of the ability of an siRNA to sensitize T98G cells to the MDA compound:

$$\mathbf{C - (S + M) = \% \ GTA}$$

Where:

%GTA = the % of cell inhibition that is greater than the additive inhibition caused by the target siRNA transfection and the inhibition caused by the MDA compound.

C = % inhibition of cell viability caused by the **c**ombination of both target siRNA transfection plus MDA compound.

S = % inhibition of cell viability caused by target **s**iRNA plus vehicle.

M = % inhibition of cell viability caused by scrambled siRNA plus **M**DA compound.

The three values of C, S, and M are calculated by:

C = cell viability of cells transfected with scrambled control and treated with vehicle minus cell viability of cells transfected with target siRNA and treated with MDA compound.

S = cell viability of cells transfected with scrambled control and treated with vehicle minus cell viability of cells transfected with target siRNA and treated with vehicle.

M = cell viability of cells transfected with scrambled control and treated with vehicle minus cell viability of cells transfected with scrambled control and treated with MDA compound.

For example, in Figure 12A, the cell viability of T98G cells under various conditions was compared as a % of control, where control was T98G cells transfected with scrambled siRNA and treated with vehicle, set to 100% cell viability. Transfection of cells with the target siRNA (against a proteasome subunit) inhibited cell viability by 10%, 10%, and 5% over three screens, an average of 8% loss of cell viability compared to control. As defined above, S = 8% (Figure 12B). Similarly, the effect of 350 pM disorazole C_1 alone over three independent screens was an average of 6% inhibition compared to control, so M = 6%. Cells that were both transfected with

siRNA against proteasome subunit and treated with 350 pM had an average % cell inhibition of 47% relative to the control cells, so C = 47%. When we used these values in the formula C – (S + M) = % GTA, we calculated the greater-than-additive effect to be 33% (Figure 12C).

A.

Effect of 350 pM disorazole C_1 and siRNA against [proteasome subunit] on T98G cell viability

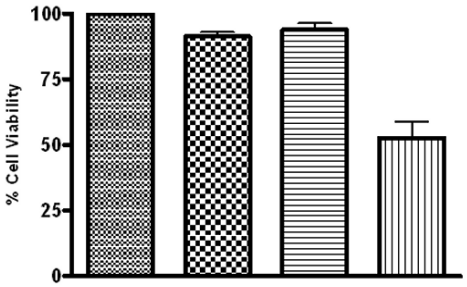

350 pM disorazole C_1:	-	-	+	+
target siRNA:	-	+	-	+
N#1	100	90	99	64
N#2	100	90	91	43
N#3	100	95	91	51
Average loss, relative to control 100%:		**8**	**6**	**47**

B.

[– Drug – siRNA] – [+ Drug + siRNA] – [– Drug – siRNA] – [– Drug + siRNA] + [– Drug – siRNA] – [+ Drug – siRNA]

47% "C" 8% "S" 6% "M"

C.

Combination siRNA & drug – [siRNA + drug] = % GTA

47% – [8% + 6%] = 33%

Figure 12. Example of how to calculate % greater-than-additive effect.

To identify specific siRNAs that sensitize cells to sub-lethal concentrations of MDA compounds, I needed to identify a cutoff value. Figure 13 illustrates a frequency distribution of %GTA sensitization resulting from each of 11,040 siRNA pool averages (5,520 from disorazole C_1 screening plus 5,520 from vinblastine screening). From these combined data, I chose a selection cutoff at two standard deviations above the mean, which was 10%GTA. With this cutoff, 34 genes were identified as sensitizers to both disorazole C_1 and vinblastine. For example, with this cutoff, the siRNA against the proteasome subunit in Figure 12 was declared a "hit", since its 33% GTA was greater than 10%. A cutoff of three standard deviations above the mean was too stringent, leaving only 3 siRNAs as sensitizers, and a cutoff at one standard deviation above the mean was too relaxed, yielding 276 sensitizers.

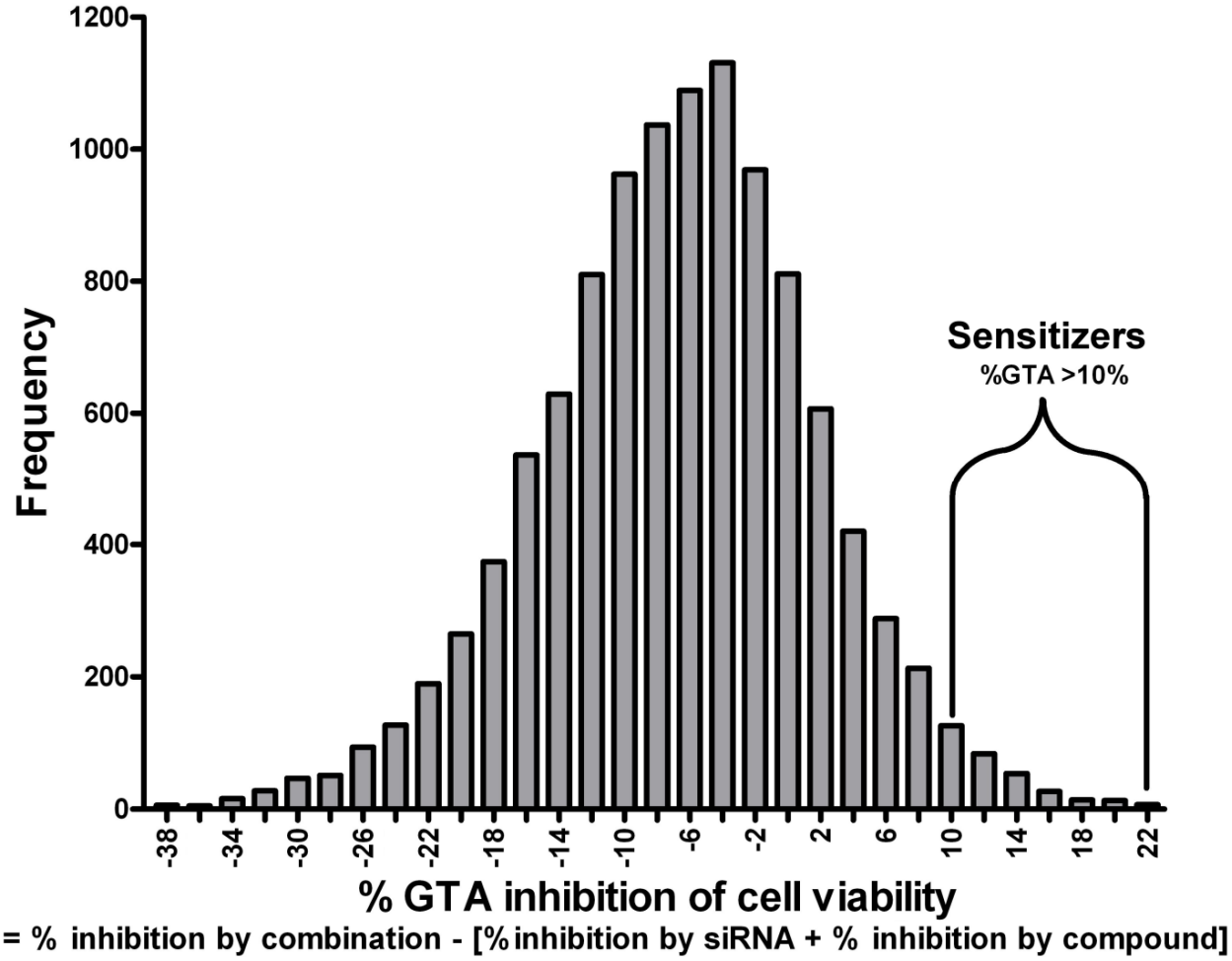

Figure 13. Frequency distribution of screening hit averages from six whole library screens.

Frequency distribution of sensitization resulting from each of 11,040 siRNA pool averages (5,520 from disorazole C_1 screening plus 5,520 from vinblastine screening). %GTA is a measure of the greater-than-additive inhibition of cell viability, defined in figure 12. From this histogram, I chose a hit cutoff of 10%, which was two standard deviations above the mean.

3.5 DISCUSSION

3.5.1 Data application #1: identification of survival genes.

The data from this screen provided several applications in addition to synthetic lethality. The first application was the detection of survival genes, similar to the work of MacKeigan [57]. MacKeigan screened a library of kinases and phosphatases to identify kinases and phosphatases that when inhibited contribute to apoptosis [57]. Survival genes are loosely defined as genes whose expressed proteins are essential for cell survival and proliferation. The proteins of T98G survival genes could be novel drug targets, particularly proteins which are essential for T98G survival but not essential for normal cells. These survival genes could also provide an explanation for the chemoresistant profile of T98G, especially if these survival genes are overexpressed in T98G relative to normal cells. Since the siRNA library was screened in duplicate plates, one treated with vehicle (DMSO), the other one with compound, the data needed to identify survival genes had already been gathered. To identify gene products that regulated T98G cell survival, I analyzed the data from plates that were screened in the presence of vehicle alone. Wells in which these survival genes had been silenced had significantly fewer cells than wells with siRNA against non-essential genes or control siRNA. To quantify the ability of a target siRNA to either increase or decrease T98G cell viability, the % cell viability of each well transfected with target siRNA against any of 5,520 genes was calculated. Percent cell viability was measured by dividing the target siRNA well viability by the average scrambled siRNA well viability for that plate. The % cell viability data from three individual screens was averaged together and the frequency distribution is displayed in figure 14. An arbitrary cutoff of two standard deviations below the mean was chosen to declare survival genes. A survival gene

was thus defined as a gene that, when silenced, led to an average of at least 66% inhibition of T98G cell viability, n=3. This cutoff identified 188 genes as T98G survival genes. The top 40 genes from this list are shown in Table 2. These survival genes were uploaded to Ingenuity Pathway Analysis (IPA), a web based data analysis program, to identify potential pathways or networks of T98G survival genes. IPA analysis of T98G survival genes identified over a dozen networks of associated proteins. Three networks were connected by their relationships to histone H3, and are displayed in Figure 15. IPA analysis is useful for identify the biological context of clusters of survival genes, and to identify the shortest path between multiple identified genes.

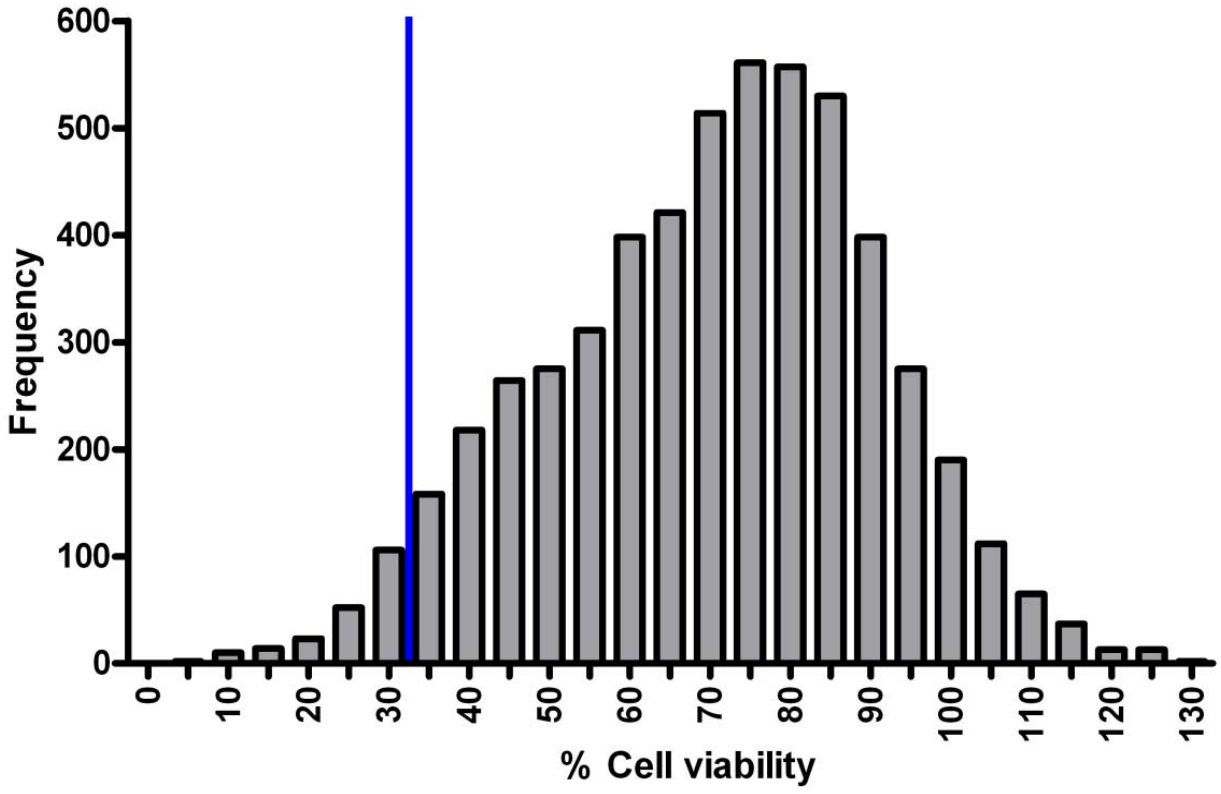

Figure 14. Frequency distribution of average % cell viability of siRNA treated T98G cells from three whole library screens.

Frequency distribution of % cell viability of T98G cells 96 hours after being transfected with siRNA. Data represent averages of three experiments, one average data point per gene target, 5,520 gene targets, using pools of three siRNA sequences per gene. Blue bar indicates cutoff for two standard deviations below the mean. The T98G survival genes were defined as the 188 gene targets that fell below the cutoff.

Cell viability	Symbol	Gene Name
5%	RAN	RAN, member RAS oncogene family
7%	DDX39	DEAD (Asp-Glu-Ala-Asp) box polypeptide 39
8%	SIAT4B	ST3 beta-galactoside alpha-2,3-sialyltransferase 2
8%	PSMC3	proteasome (prosome, macropain) 26S subunit, ATPase, 3
9%	K-ALPHA-1	K-ALPHA-1
10%	SIAT7E	ST6 N-acetylgalactosaminide alpha-2,6-sialyltransferase 5
11%	HLCS	holocarboxylase synthetase (biotin ligase)
11%	PSMD14	proteasome (prosome, macropain) 26S subunit, non-ATPase, 14
11%	POLR2F	polymerase (RNA) II (DNA directed) polypeptide F
12%	SPTLC1	serine palmitoyltransferase, long chain base subunit 1
12%	TLR2	toll-like receptor 2
12%	TUBGCP6	tubulin, gamma complex associated protein 6
13%	PSMC6	proteasome (prosome, macropain) 26S subunit, ATPase, 6
14%	RAB40B	RAB40B, member RAS oncogene family
14%	SRCRB4D	scavenger receptor cysteine rich domain containing, group B (4 domains)
14%	BTN2A3	butyrophilin, subfamily 2, member A3
15%	PIGQ	phosphatidylinositol glycan, class Q
16%	GRHPR	glyoxylate reductase/hydroxypyruvate reductase
16%	NQO3A2	NAD(P)H:quinone oxidoreductase type 3, polypeptide A2
16%	CHN1	chimerin (chimaerin) 1
16%	CGI-04	tyrosyl-tRNA synthetase 2 (mitochondrial)
17%	GABRB2	gamma-aminobutyric acid (GABA) A receptor, beta 2
17%	RAB40C	RAB40C, member RAS oncogene family
17%	CLCN3	chloride channel 3
17%	RALB	v-ral simian leukemia viral oncogene homolog B (ras related; GTP binding)
17%	ITGAV	integrin, alpha V (vitronectin receptor, alpha polypeptide, antigen CD51)
18%	POMT1	protein-O-mannosyltransferase 1
18%	COX7A2	cytochrome c oxidase subunit VIIa polypeptide 2 (liver)
18%	PSMC5	proteasome (prosome, macropain) 26S subunit, ATPase, 5
18%	CARM1	coactivator-associated arginine methyltransferase 1
19%	SORCS1	sortilin-related VPS10 domain containing receptor 1
19%	ITGA3	integrin, alpha 3 (antigen CD49C, alpha 3 subunit of VLA-3 receptor)
19%	VCP	valosin-containing protein
19%	IL18R1	interleukin 18 receptor 1
20%	LOC144125	olfactory receptor, family 2, subfamily AG, member 1
20%	DKFZP434L1717	DKFZP434L1717
20%	IDH3B	isocitrate dehydrogenase 3 (NAD+) beta
20%	CYB5R2	CYB5R2
20%	UBL5	ubiquitin-like 5
20%	SLC7A2	solute carrier family 7 (cationic amino acid transporter, y+ system), member 2

Table 2. Top 40 T98G survival genes.

This table displays the top 40 T98G survival genes, which are defined as genes that, when silenced, inhibit T98G cell viability by at least 66%, relative to scrambled siRNA control. The first column displays the % cell viability of T98G cells when transfected with siRNA against the displayed gene, for 96 hours, relative to scrambled siRNA control.

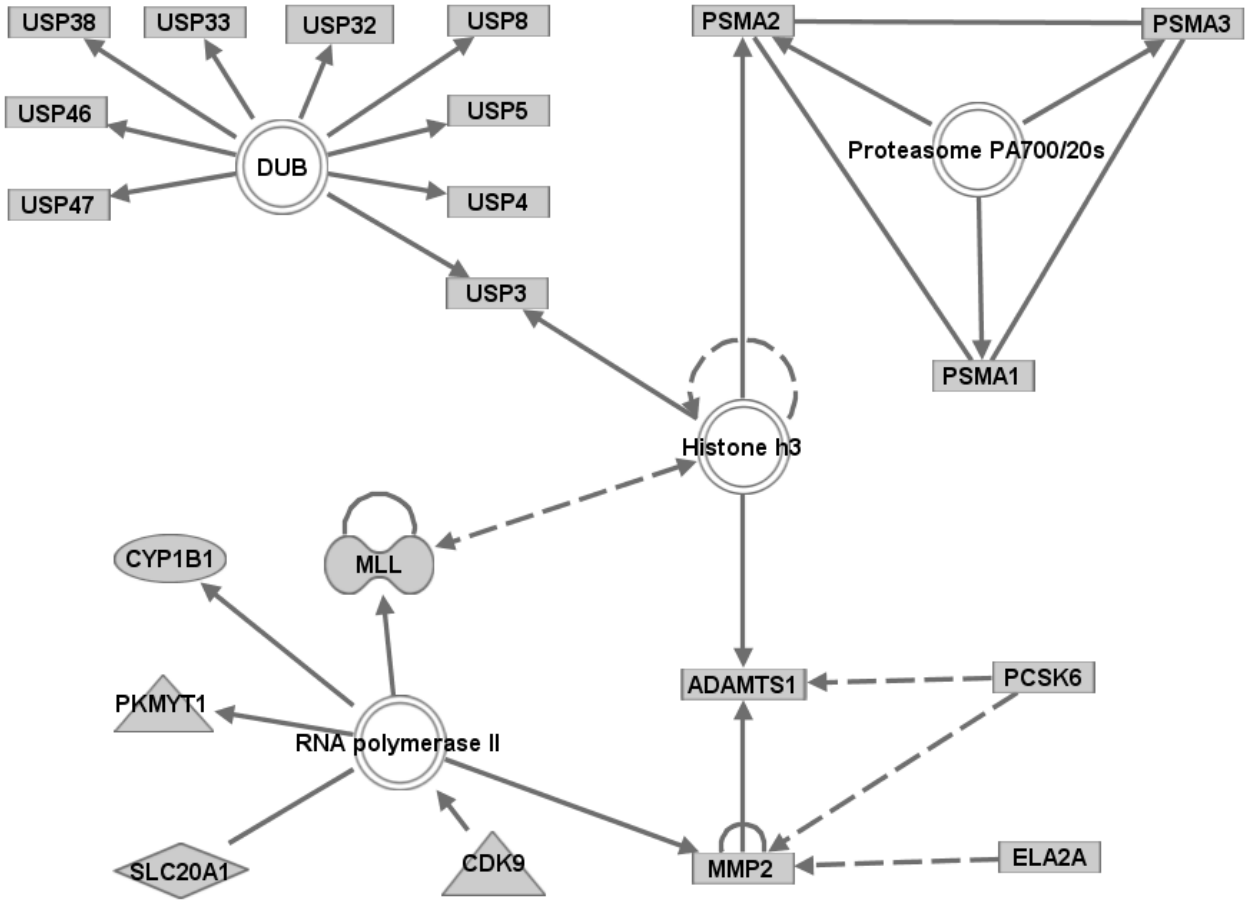

Figure 15. Networks of survival genes identified by IPA analysis.

An example of an IPA network analysis of T98G survival genes. Upper left network: The USP3, 4, 5, 8, 32, 33, 38, 46, and 47 proteins are a cluster of associated deubiquitinating enzyme (DUBs) that have ubiquitin specific peptidase activity [58-60]. Upper right network: The PSMA1, 2, and 3 proteins in this cluster are members of the 26S proteasome, which is formed by the PA700 proteasome activator and the 20S proteasome [61, 62]. Lower network: CYP1B1, PKMYT1, SLC20A1, MLL, and MMP2 bind to RNA polymerase II, which is activated by the survival kinase CDK9. The peptidase MMP2 has relationships with the peptidases ADAMTS1, PCSK6, and ELA2A.

3.5.2 Data application #2: identification of protective siRNAs.

A second application of the data obtained from this screen was protective siRNAs. The frequency distribution (Figure 13) illustrates that while there are a number of siRNAs that sensitized T98G cells to MDAs, there were also siRNAs that would seem to protect T98G cells. In a separate research project, I have applied this protective screening concept in other research to identify genes which, when silenced, protect cultured human cells from ionizing radiation. Data from three independent siRNA screens with ionizing radiation in T98G cells provided information for visualizing both sensitizing siRNAs and protective siRNAs. One example of a protective siRNA was siRNA against the gene mixed lineage kinase 4 (KIAA1804), shown in figure 16. Silencing KIAA1804 with siRNA increased T98G cell viability by 5%, and a 25 Gy dose of ionizing radiation inhibited cell viability by 53%. Silencing KIAA1804 48 hours before ionizing radiation treatment protected cells by 31%. Screening the siRNA library with an EC50 dose of ionizing radiation to identify both protective and sensitizing genes of T98G helped us understand what genes regulated its radiation resistance profile, and helped us identify molecular targets to made T98G more sensitive to radiation therapy.

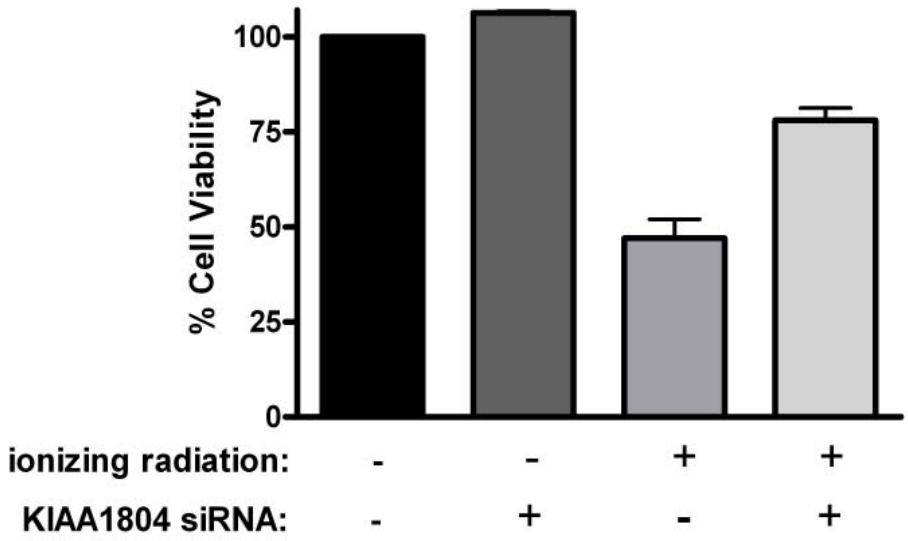

Figure 16. Silencing mixed lineage kinase 4 (KIAA1804) with siRNA protects T98G cells from ionizing radiation.

Bar graphs demonstrate cell viability of T98G cells 3 days after 25 Gy ionizing radiation (or mock) either scrambled control siRNA or KIAA1804 gene siRNA. T98G cells were treated with 25 Gy irradiation 48 hours after siRNA transfection. Cell viability was measured with CellTiter-Blue and is shown as a percentage of the viability of cells transfected with control siRNA. Data are plotted as the mean $\pm$ SD of three different experiments.

3.5.3 Data application #3: identification of sensitizing siRNAs.

The research of this dissertation was focused on identifying siRNAs that sensitized T98G cells to MDAs, and the data from this work is described in chapters 4 and 5 of this dissertation. In addition, this synthetic lethal siRNA screening methodology can be applied more broadly to other therapeutic agents. This assay is not limited to small molecules, as I am currently

employing this technique to identify siRNAs that sensitize these radioresistant T98G cells to sub-lethal doses of ionizing radiation. This synthetic lethal siRNA screen is a valuable tool for identifying genes products that sensitize or protect cells to any number of mechanistically distinct small molecules and other therapeutic agents and modalities.

4.0 SYNTHETIC LETHAL SCREENING PREDICTS A NOVEL MECHANISM FOR SYNERGISM OF PI3K INHIBITORS AND MICROTUBULE DISRUPTING AGENTS FOR TUMOR CELL DEATH

Combination drug regimens expand the therapeutic window for cancer treatment. Identifying the chemosensitivity nodes that produce synergy is challenging. I have exploited an unbiased, 16,560-member siRNA synthetic lethal screen capable of quickly identifying novel drug targets for sensitizing cancer cells to sublethal concentrations of microtubule-perturbing agents. I employed this high-throughput siRNA screen with human T98G glioblastoma cells to isolate a high-confidence list of 142 and 152 siRNAs that enhanced the cytotoxicity of the natural products vinblastine and disorazole C_1 , respectively, with 34 siRNAs being common to both agents. These results suggested that the two inhibitors of tubulin polymerization could have different mechanisms of action or binding sites. Silencing of microtubule-associated midline proteins potentiated the cytotoxicity of both vinblastine and disorazole C_1 , but not cisplatin or ionizing radiation. Microtubule-associated proteins are controlled by the PI3K/Akt axis, and inhibition of upstream PI3K/Akt pathway elements with wortmannin and LY-294,002 acted synergistically with microtubule perturbing agents to increase cytotoxicity in cancer cells. These results demonstrate the power of combining siRNA libraries with automated phenotypic assays to uncloak previously unknown drug pathways and to identify potential novel drug combinations.

4.1 INTRODUCTION

The vinca alkaloids gained status as a novel class of anticancer agents in the early 1960s [63]. Since then, microtubule destabilizing agents (MDAs) have been recognized as powerful chemotherapeutic agents for the treatment of cancer by their ability to alter microtubule dynamics, arresting cell cycle progression at mitosis and leading to apoptotic cell death. However, the neurological and hematological toxicities of MDAs hinders their effectiveness for cancer therapy.

To circumvent the problems associated with dose-dependent side effects, I sought to identify genes mediating sensitivity to MDAs using a synthetic lethal siRNA screen. Previous groups have used siRNA screening to categorize determinants of taxane sensitivity and predict novel drug combinations [64]. siRNA screens rely on RNA interference, the cellular mechanism that inhibits gene expression post-transcriptionally by sequence-specific mRNA transcript degradation [24]. siRNA screening is made feasible by large libraries of siRNA reagents, targeting a wide range of transcripts [65]. When coupled to automation, high-throughput siRNA screening enables efficient analysis of genome-wide screens [66]. The application of siRNA to systematic genome-scale screening method was first demonstrated using C. elegans [25, 26].

Druggable genome libraries are increasingly popular siRNA libraries, as they target genes that are considered potential targets for therapeutics, such as ion channels, proteases, protein kinases and phosphatases [67]. The druggable genome reflects targets that are considered both druggable and disease modifying [56]. In this study, I have used a druggable genome synthetic lethal siRNA screen to identify determinants of sensitivity to the microtubule disruptors

vinblastine and disorazole C_1. The identification of novel mediators of the cellular response to microtubule disruptors may indicate novel potential combination therapies.

4.2 RESULTS

4.2.1 Uncloaking novel sensitizers of microtubule disruptor cytotoxicity using synthetic lethal siRNA screening.

I sought to use synthetic lethal siRNA screening to identify new drug therapies for GBM, the most common and malignant central nervous system tumor [40]. To detect novel sensitizers of disorazole C_1 and vinblastine, three independent synthetic lethal screens were performed for each of the two microtubule disrupting compounds. Screening data were averaged and revealed a normal distribution (Chapter 3), and the frequency distribution of all screening data indicated that a 10% sensitization was two standard deviations above the mean. Therefore, siRNAs that sensitized T98G cells to compounds by 10% or more were selected as hits. This cutoff yielded 152 and 142 hits for disorazole C_1 and vinblastine, respectively, with 34 siRNAs being common to both agents (Figure 17B). The list of 34 genes is summarized in Table 2. One of the common 34 hits for both vinblastine and disorazole C_1, midline 2 (MID2), was of particularly interest due to its colocalization with microtubules, its role in tethering a key regulator of intracellular signaling (protein phosphatase 2A, PP2A) to microtubules, and its potential role in microtubule stability through PP2A binding [68, 69]. In the screen, siRNA against MID2 in the presence of vehicle DMSO inhibited T98G cell viability by 13% compared to scrambled siRNA, and treatment of cells with scrambled siRNA and 1.4 nM vinblastine inhibited T98G cell viability by

22% (Figure 17C). Combining vinblastine and MID2 siRNA led to a 78% inhibition of cell viability (Figure 17C). The combinations of vinblastine plus MID2 siRNA and disorazole C_1 plus MID2 siRNA yielded 43% and 22% greater-than-additive inhibition of T98G cell viability, indicating the importance of MID2 in sensitizing GBM cells to microtubule disruption (Figure 17C). To confirm the specificity of the MID2 silencing-mediated cell death with MDAs, I investigated interactions with ionizing radiation and found cell death was not enhanced by MID2 siRNA (Figure 17C).

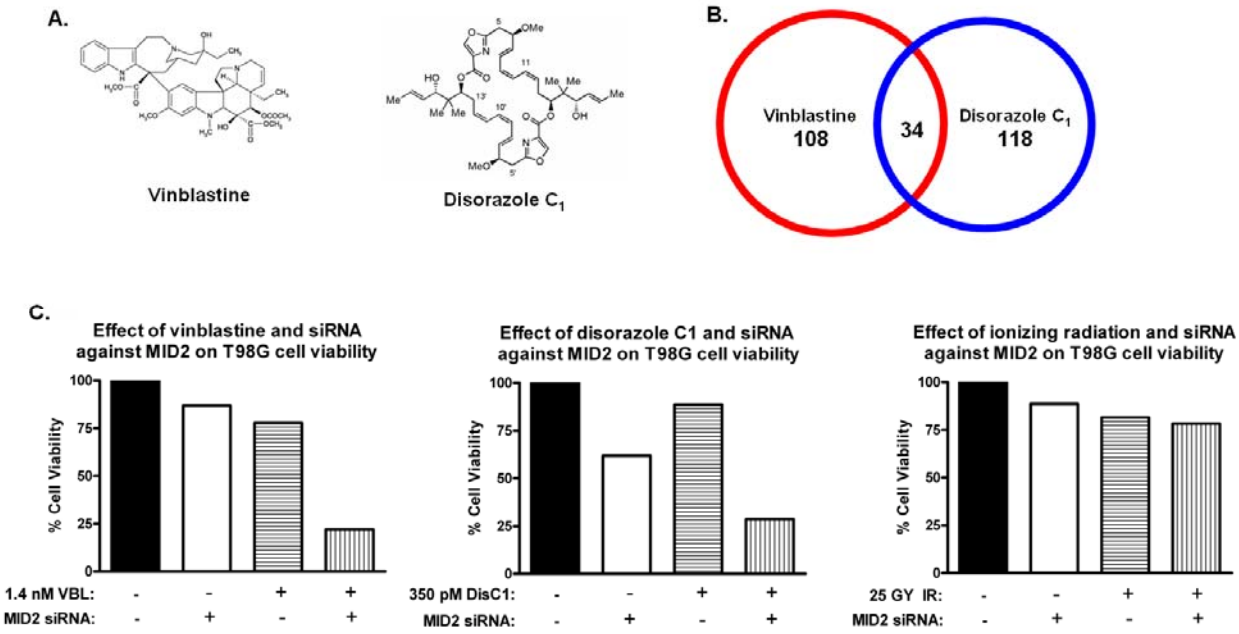

Figure 17. Silencing midline2 (MID2) with siRNA sensitizes T98G cells to microtubule destabilizers.

(A) Structures of the compounds vinblastine and disorazole C_1 (B) Three independent screens for each of two MDAs were performed. Screening data were averaged and siRNAs that sensitized T98G cells to compounds were selected as hits. siRNA against MID2 was one of the common 34 hits for both vinblastine and disorazole C_1 (C) Bar graphs demonstrate cell viability of T98G cells 2 days after drug treatment (1.2 nM vinblastine, 350 pM disorazole C_1 , 25 GY

ionizing radiation (IR) or 0.5% DMSO vehicle). T98G cells were treated with drug 48 hours after siRNA transfection. Silencing MID2 with siRNA sensitizes T98G cells to low concentrations of both compounds, but not ionizing radiation. Cell viability was measured with CellTiter-Blue and is shown as a percentage of the viability of cells transfected with control siRNA. Graphs are representative of mean data from three independent screens.

GenBank	Symbol	Gene Name
NM_138340	ABHD3	abhydrolase domain containing 3
NM_001024946	ASL	argininosuccinate lyase
NM_138578	BCL2L1	BCL2-like 1
NM_032966	BLR1	Burkitt lymphoma receptor 1, GTP binding protein
NM_016382	CD244	CD244 natural killer cell receptor 2B4
NM_004661	CDC23	CDC23 (cell division cycle 23, yeast, homolog)
NM_130901	C15orf16	chromosome 15 open reading frame 16
NM_015510	DKFZp566O084	DKFZp566O084
NM_007026	DUSP14	dual specificity phosphatase 14
NM_022066	E2-230K	E2-230K
NM_173641	FLJ33655	EPH receptor A10
NM_152873	TNFRSF6	Fas (TNF receptor superfamily, member 6)
NM_002014	FKBP4	FK506 binding protein 4, 59kDa
NM_178557	FLJ37478	FLJ37478
NM_178135	SCDR9	hydroxysteroid (17-beta) dehydrogenase 13
NM_012302	LPHN2	latrophilin 2
NM_000255	MUT	methylmalonyl Coenzyme A mutase
NM_033115	MGC16169	MGC16169
NM_052817	MID2	midline 2
NM_004685	MTMR6	myotubularin related protein 6
NM_000303	PMM2	phosphomannomutase 2
NM_000918	P4HB	procollagen-proline 4-hydroxylase beta polypeptide
NM_206876	PPP1CB	protein phosphatase 1, catalytic subunit, beta isoform
NM_001664	RHOA	ras homolog gene family, member A
NM_032918	RERG	RAS-like, estrogen-regulated, growth inhibitor
NM_016544	RBJ	RBJ
NM_014715	RICS	RICS
NM_005778	RBM5	RNA binding motif protein 5
NM_006919	SERPINB3	serine (or cysteine) proteinase inhibitor, clade B (ovalbumin),3
NM_006217	SERPINI2	serine (or cysteine) proteinase inhibitor, clade I (pancpin),2
NM_004174	SLC9A3	solute carrier family 9 (sodium/hydrogen exchanger), 3
NM_001058	TACR1	tachykinin receptor 1
NM_003844	TNFRSF10A	tumor necrosis factor receptor superfamily, member 10a
NM_152444	ZADH1	zinc binding alcohol dehydrogenase, domain containing 1

Table 3. Overlapping siRNA screening hits for vinblastine and disorazole C_1 synthetic lethal screens.

Thirty-four genes were identified that, when silenced by siRNA, sensitized T98G cells to vinblastine and disorazole C_1 by more than two standard deviations above the mean of all sensitization values (see also Figure 17).

4.2.2 Microtubule sensitization by loss of MID2.

Identifying the underlying mechanisms of MDA sensitization by MID2 silencing should enable prediction of suitable compounds for combination chemotherapy, and may help assessment of the clinical relevance of this combination. I hypothesize that MID2 silencing sensitizes T98G cells to MDAs due to the role of MID2 in tethering PP2A to the microtubules [69]. As illustrated in Figure 18, homodimers and heterodimers of MID1 and MID2 tether α4, a regulatory subunit of PP2A, to microtubules [69]. In this way, the dimerized midline proteins tether PP2A to the microtubules.

The localization of PP2A at the microtubules allows it maintain the dephosphorylated status of the microtubule-associated protein (MAP) tau; inhibition of PP2A promotes hyperphosphorylation of tau [70]. As predicted, silencing of MID2 induced the phosphorylation of tau on Ser^{199} (Figure 18A). Ser^{199} was selected as one of several motifs that are phosphorylated in its hyperphosphorylated state. Kinase-mediated hyperphosphorylation of tau reduces its ability to bind and stabilize microtubules, so the role of PP2A is important in maintaining microtubule structural integrity [34, 71]. The relevance of this to chemotherapy lies in rapamycin-sensitive α4.

The interaction of α4 with PP2A is dependent on phosphorylation by the mammalian target of rapamycin (mTOR) kinase [69]. I hypothesized that inhibitors of the PI3K-AKT-mTOR pathway might sensitize T98G cells to MDAs by a mechanism similar to MID2 silencing. Indeed, Kohno et al. reported the synergistic effect of a combination of PI3K pathway inhibitors with vincristine only in tumor cells in which the PI3K pathway is constitutively activated: T98G

GBM, T24 bladder cancer, and Hela cervical cancer [72]. Perhaps the ability of T98G cells to resist MDA-mediated apoptosis is due to microtubule stabilization by a constitutive PI3K pathway.

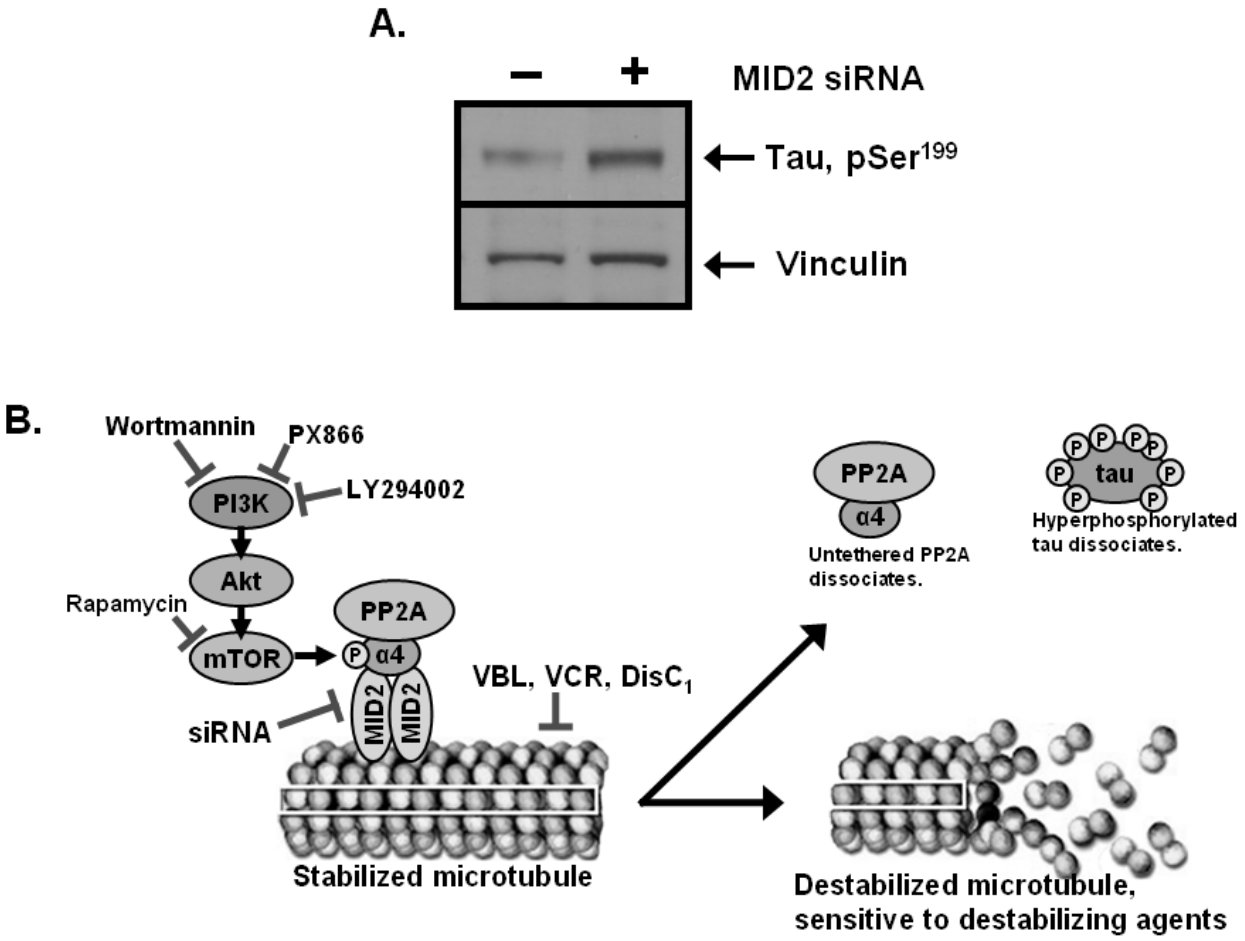

Figure 18. Disruption of PI3K-mediated Tau dephosphorylation sensitizes PI3K-active cells to microtubule disruptors.

(A) MID2 siRNA transfection induces hyperphosphorylation of the microtubule-associated protein tau. Western blot analysis of cellular Ser199- phosphorylated tau, and vinculin (loading control) in T98G cells. Cells were transiently transfected with a pool of three siRNAs targeting MID2. Scrambled control siRNA-transfected cells received a nonsense siRNA sequence. (B) Proposed model of microtubule sensitization. PP2A prevents tau

hyperphosphorylation when tethered to microtubules by MID2 and phosphorylated-α4. PP2A can be displaced from the microtubules by MID2 silencing or by inhibiting α4 phosphorylation by the PI3K pathway. In the absence of PP2A, tau becomes hyperphosphorylated and dissociates from the microtubules, destabilizing them. This model predicts that cells can be sensitized to microtubule disrupting agents by either MID2 siRNA or inhibition of α4 phosphorylation.

4.2.3 Disorazole C_1 and PI3K inhibitor combinations produce synergistic inhibition of T98G cell growth.

To assess additive, synergistic, or antagonistic interactions between PI3K inhibitors and vinblastine or disorazole C_1, I exploited the combination index (CI) method of Chou and Talalay [47-50]. This method of evaluating drug interactions was selected because it examines the potencies of each drug and combinations (Dm value), as well as the shape of the concentration-effect curves (m values), calculating how the experimental effect differs from the effect expected with additivity.

The combination effects of wortmannin and the microtubule disruptors vinblastine and disorazole C_1 are represented in Figure 19. For these curves, CI values of <1, 1 (dotted line), and >1 indicated synergism, additivity, and antagonism, respectively. The combination index plot (Figure 19) indicated that a 1:2000 ratio of disorazole C_1 plus wortmannin (1 nM disorazole C_1 to 2 μM wortmannin) achieved a greater than additive effect, with the data points of all combinations falling well below a CI value of 1 at 90% (CI = 0.38), 75% (CI = 0.40), and 50% (CI = 0.44) levels of cell inhibition. As expected from the screen, the combination of

wortmannin with vinblastine was also synergistic, but to a lesser effect. Exposure of T98G cells to both combinations resulted in increasing levels of synergism with increasing effect levels.

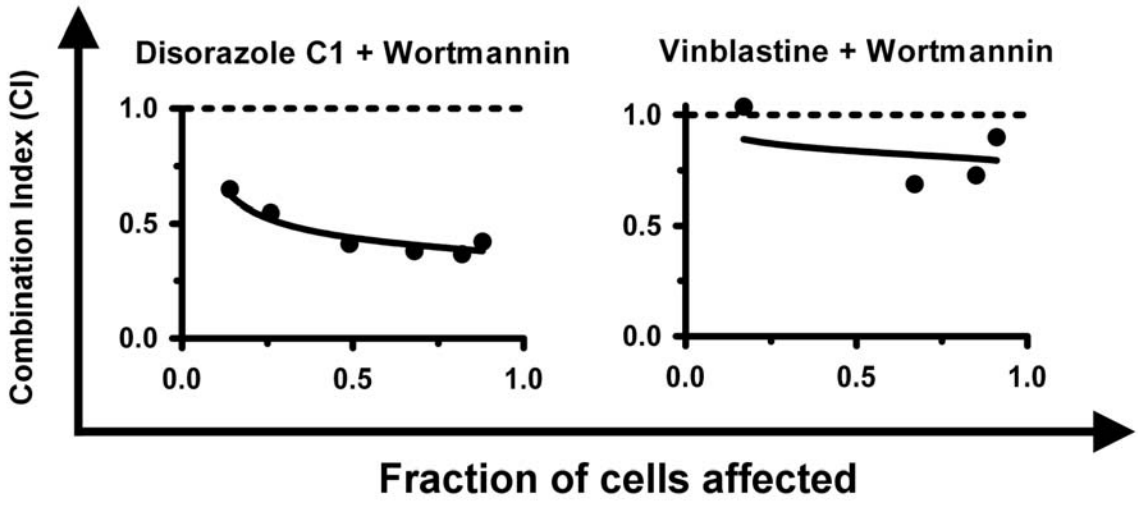

Figure 19. Synergism between MDAs and wortmannin in T98G cells.

T98G cells were plated at low density and treated with concentration gradients of disorazole C_1, vinblastine, vehicle (0.5% DMSO), or mixtures thereof in an 8x8 grid of a 96-well plate, providing 64 unique combinations. Cells were incubated in the presence of compounds for 72 hours. Cell viability was measured with the CellTiter-Blue assay. To quantify the interaction between drug treatments, I generated combination index plots of the treatments at constant molar ratios. For these curves, CI values of <1, 1 (dotted line), and >1 indicated synergism, additivity, and antagonism, respectively. Data were analyzed assuming mutually exclusive drug effects and are representative of two or more separate experiments.

While wortmannin has antitumor activity against tumor xenografts in animals, it is biologically unstable and is accompanied by liver and hematologic toxicity [73, 74]. This led to the development of PX866, a novel, less toxic, and significantly more biologically stable PI3K inhibitor [74, 75]. Because of the potential greater clinical relevance of PX866 over

wortmannin, I performed combination studies with disorazole C_1 and PX866 at various ratios. PX866 and disorazole C_1 were synergistic at ratios of 8 µm : 1 nM, 5 µm : 1 nM, 3 µm : 1 nM, 2 µm : 1 nM, especially when higher fractions of cells are affected (Figure 20). The effect was decreased at ratios outside of this range (data not shown).

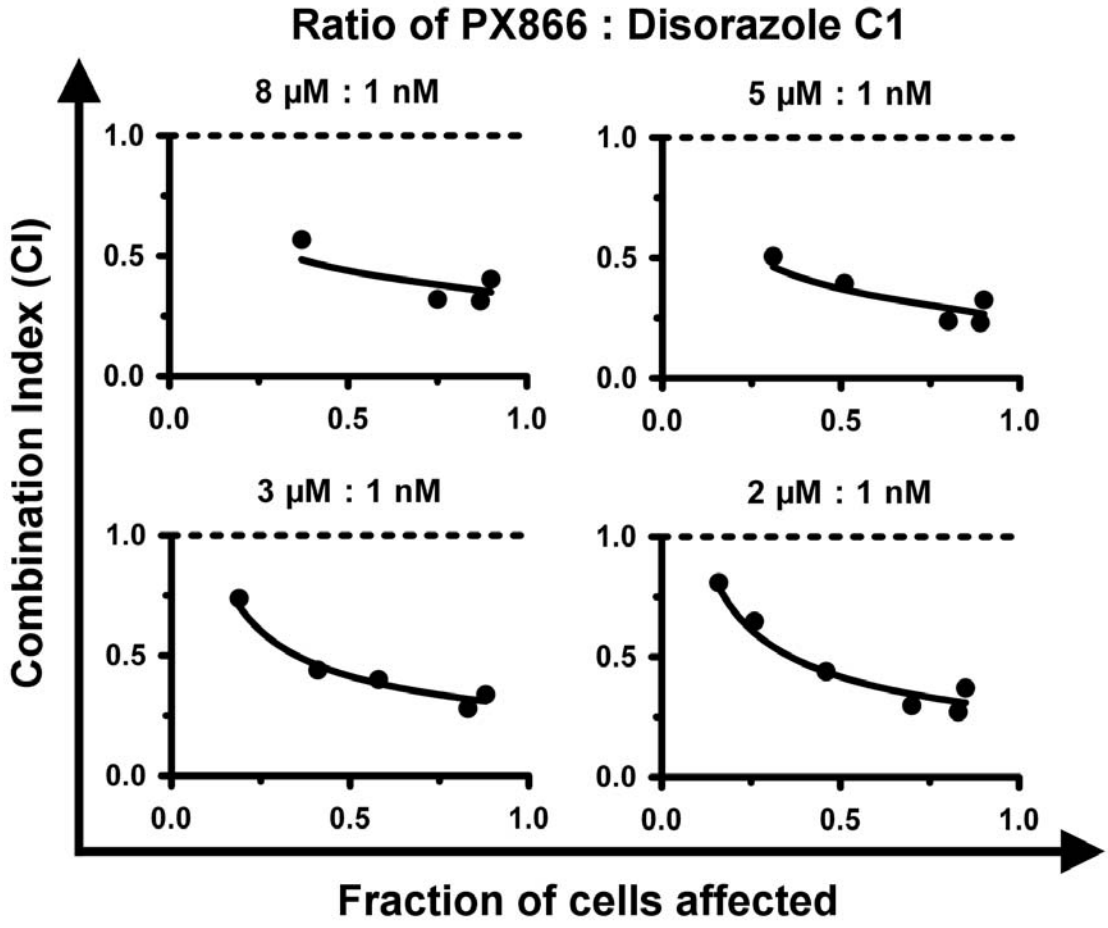

Figure 20. Analysis of the combination of PX866 and disorazole C_1 in T98G cells at four different ratios.

Combination index plot analysis of the combination of PX866 with disorazole C_1 in T98G cells at µM:nM ratios of 8:1, 5:1, 3:1, and 2:1 for PX866 to disorazole C_1. Combination index values at <1.0, 1.0, and >1.0 indicate synergy, additivity, and antagonism, respectively.

PI3K inhibition is a potentially relevant target for GBM chemotherapy, as AKT activation has been detected in several types of human cancers and is associated with resistance to chemotherapy and radiotherapy [76-78]. PI3K inhibitors are currently being used in early clinical trials for patients with glioblastoma [79]. This past year, Kohno et al. reported the synergistic effect of a combination of PI3K pathway inhibitors with vincristine only in tumor cells in which the PI3K pathway is constitutively activated [72]. Both the GBM cell line T98G and the bladder cancer cell line, T24, have a constitutively active PI3K pathway, sensitizing both to PI3K inhibition [80]. I therefore performed combination studies to plot the CI curve for vinblastine with PX866 in both T98G and T24 cell lines (Figure 20). As predicted, vinblastine synergized with PX866 for inhibition of T98G cell viability at a ratio of 1μM to 2nM of PX866 to vinblastine in both the T98G and T24 cell lines Figure 21). In agreement with my model (Figure 18), synergy was also seen with MDAs combined with inhibitors of the mTOR but not with the DNA damaging agent cisplatin (Figure 22). Other combinations of PI3K inhibitors and MDAs also synergize together, (Figure 22) and the combination effects of disorazole C_1, vinblastine, vincristine, cisplatin, rapamycin, wortmannin, LY-294,002, and PX866 are summarized in Table 4 for direct comparison across all drug combination studies (Table 4).

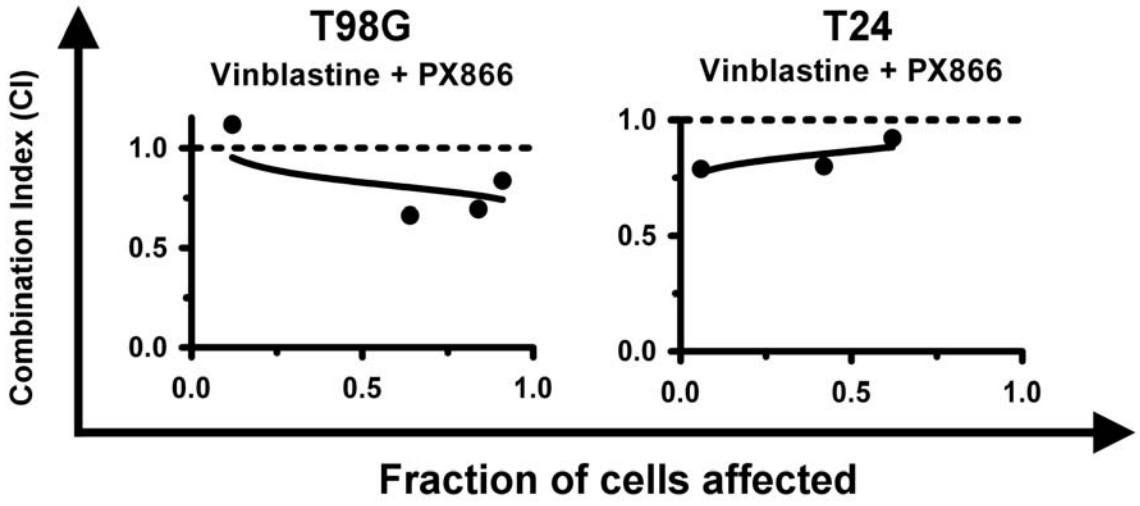

Figure 21. Synergy of PX866 and vinblastine in cell lines with constitutively active PI3K.

Combination index plots for the combination of PX866 with vinblastine in T98G and T24 cell lines at a ratio of 1 μM PX866 : 2 nM vinblastine. Combination index values at <1.0, 1.0, and >1.0 indicate synergy, additivity, and antagonism, respectively.

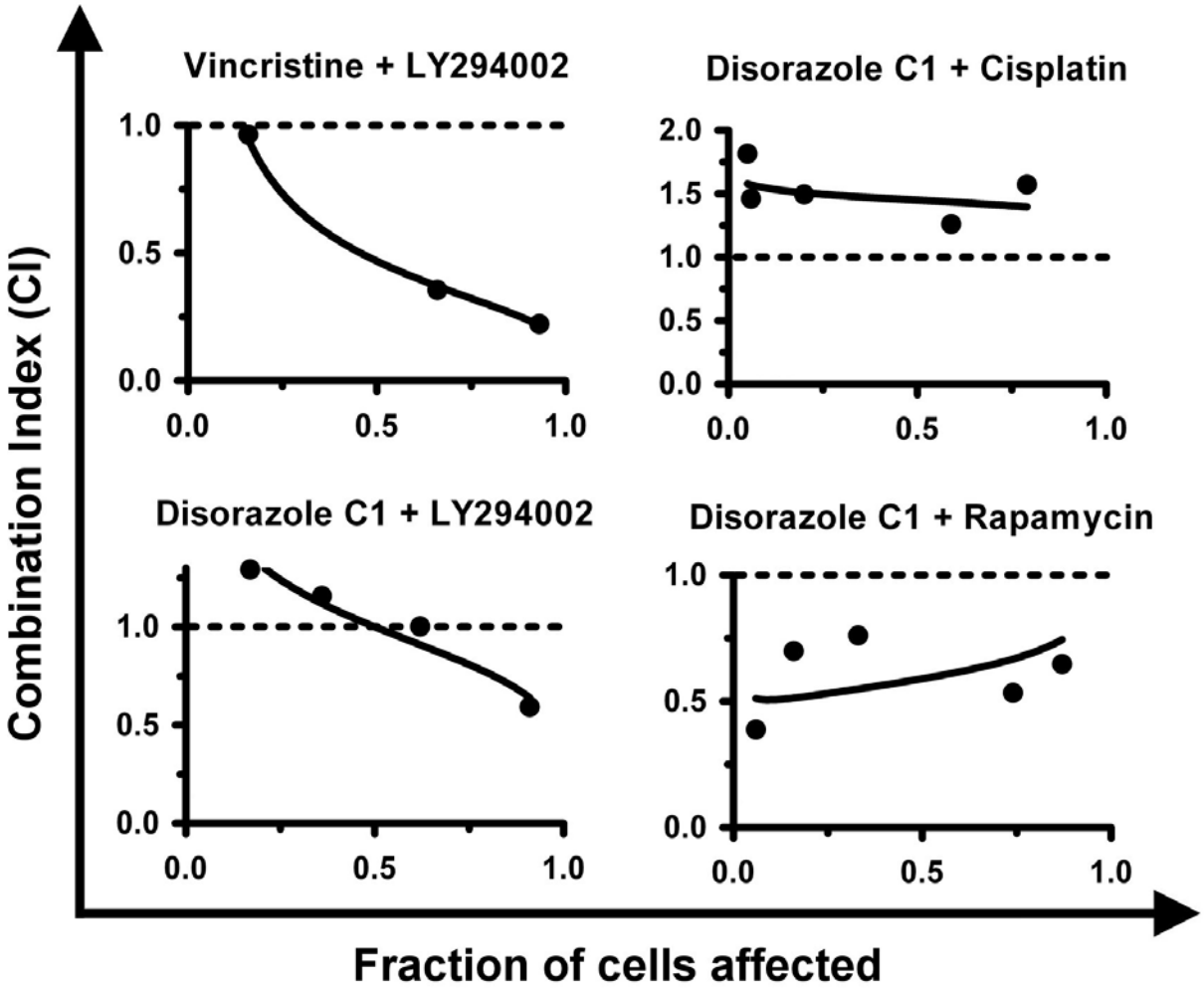

Figure 22. Combination index plot analysis of MDAs with a LY-294,002, cisplatin, or rapamycin in T98G cells.

Combination index plots for combinations of the PI3K inhibitor LY-294,002 with vincristine or disorazole C_1, and combinations of disorazole C_1 with cisplatin or rapamycin. Combination index values at <1.0, 1.0, and >1.0 indicate synergy, additivity, and antagonism, respectively.

Cell line	Combination	CI value at EC50	EC75	EC90	r
T98G	Disorazole C1 + PX-866 (5.1 nM : 1 μM)	0.37	0.30	0.27	0.97
	Disorazole C1 + Wortmannin (1 nM : 2.2 μM)	0.44	0.40	0.38	1.00
	Disorazole C1 + Cisplatin (1 nM : 2 μM)	1.45	1.41	1.36	1.00
	Disorazole C1 + LY-294,002 (1 nM : 18.8 μM)	1.00	0.81	0.65	0.99
	Disorazole C1 + Rapamycin (1 nM : 10 nM)	0.59	0.67	0.77	0.98
	Vinblastine + PX-866 (2 nM : 1 μM)	0.83	0.78	0.74	0.95
	Vincristine + LY-294,002 (1 nM : 1.4 μM)	0.47	0.32	0.24	1.00
	Vinblastine + Wortmannin (1 nM : 2.5 μM)	0.84	0.81	0.80	0.95
T24	Vinblastine + PX-866 (3 nM : 1 μM)	0.87	0.91	0.95	1.00

Table 4. Concentration-effect relationships and combination index values for compound combinations in T98G and T24 cells.

Multiple drug effect analysis was performed using the PI3K inhibitors wortmannin, LY-294,002, and PX866 in combination with either one of the three microtubule destabilizing agents (vinblastine, disorazole C_1, or vincristine). Experiments were performed in the bladder cancer cell line T24 and the glioblastoma cell line T98G. CalcuSyn was used to quantitatively describe the interaction of drug combination and to derive combination index plots (Figures 19-22). This table lists the actual experimental values for the combination indices as a function of fractional inhibition of cell viability by a mixture of the PI3K inhibitor and a microtubule destabilizer. Combination index values are listed for three different fractional effects, wherein EC50 represents the level of interaction at 50% cell inhibition. Combination index values at <1.0, 1.0, and >1.0 indicated synergy, additivity, and antagonism, respectively. "r" is the linear correlation coefficient for the median effect line of the median effect plot. Commonly referred to as r value, this value indicates the conformity of the data.

4.3 DISCUSSION

I have used a synthetic lethal siRNA screen to identify MID2 as a sensitizing link between PI3K pathway inhibitors and microtubule destabilizing agents (MDAs). Previously, Kohno et al. demonstrated that blockade of the PI3K-Akt pathway enhanced apoptosis by MDAs in cells with a constitutively active PI3k pathway [72]. They showed that the enhancement of MDA apoptosis by PI3K inhibitors was mediated by activation of glycogen synthase kinase-3β (GSK-3β) and consequent tau phosphorylation, decreasing its ability to bind and stabilize microtubules [34, 71, 72]. The PI3K pathway regulates the phosphorylation of Tau through the respective phosphatase and kinase activities of GSK-3β and PP2A [81]. Given the role of MID1 and MID2 homo- and heterodimers in tethering PP2A to microtubules, the induction of tau hyperphosphorylation after MID2 silencing was predictable; sensitization of T98G and T24 cell lines to low concentrations of MDAs was less obvious and previously unknown. Importantly, the redundancy of MID1 and MID2 ensures that silencing MID2 alone was not sufficient to induce full microtubule destabilization and resultant cell death. It is interesting to note that MID1 siRNA did not sensitize T98G cells to MDAs. I speculate that MID2 could play a more prominent role in α4 tethering in T98G cells than MID1.

Since PI3K inhibitors sensitize T98G cells to disorazole C1 or vinblastine, I would expect that PI3K siRNA should also sensitize T98G cells. However, PI3K has numerous isoforms and subunits. The Ambion siRNA library has siRNA against many different subunits of PI3K, including five PI3K regulatory subunits, four PI3K catalytic subunits, and three PI3K polypeptides. Silencing only one particular isoform or subunit may not be enough to disrupt the

redundant or overlapping functions of the other forms, preventing siRNA against any single subunit or isoform to be identified as a sensitizer. However, it should be noted that siRNA against the following three PP2A subunits did sensitize T98G cells to vinblastine, possibly because loss of any of these subunits was sufficient to enhance tau hyperphosphorylation and subsequent microtubule destabilization:

PPP2R2A - protein phosphatase 2 (formerly 2A), regulatory subunit B, alpha isoform

PPP2R1B - protein phosphatase 2 (formerly 2A), regulatory subunit A, beta isoform

PPP2R5D - protein phosphatase 2, regulatory subunit B', delta isoform

This synthetic lethal methodology is a broad platform; thus the pattern of screening hits for vinblastine and disorazole C_1 can be used as a screening profile for each compound, similar to microarray reference profiling. The data from our vinblastine and disorazole C_1 screens will be used in our current siRNA-mediated compound sensitization profiling. The principle of this technique is that the unique sensitization profile from a compound-driven synthetic lethal siRNA screen can be directly compared with the profile of other similar and dissimilar compounds. With a battery of compound profiles, it may become feasible to use siRNA screening data to predict the mechanism of action of novel small molecule inhibitors and classify the compound by its pattern of sensitivity to the druggable genome siRNA library.

MID2 was just one of 34 silencing targets that modulated T98G sensitivity to both vinblastine and disorazole C_1. The remaining screening hits identified by this screen could potentially predict other mechanisms in GBM for resistance to MDAs, and I am currently investigating several of these other targets. Interestingly, there were a number of siRNA targets

that modulated T98G cell sensitivity to only one or the other MDA, illustrating unique, diverse responses of each agent on signal transduction pathways. This differential response may be due to the broad array of signaling molecules that interact with microtubules and the diverse effects of MDAs on signaling pathways such as the JNK, hedgehog, MAPK, and Wnt networks [82]. Disruption of microtubules can prevent their ability to position signaling molecules to allow signal transduction in these pathways. Although all MDAs are defined by their effect of destabilizing microtubules at high concentrations, different MDAs can elicit different effects in the cell, such as disorazole C_1 more readily inducing senescence than vinblastine (Brisson, M. et al., unpublished) [34]. Microtubules have also been demonstrated to be affected by signaling pathways, potentially further contributing to the criss-cross of downstream signal transmission [82]. It will be very interesting to tease out the pathway distinctiveness of disorazole C_1 and vinblastine.

The complexity and multi-factorial nature of GBM make it very challenging to address with single agent chemotherapy. Combination chemotherapy addresses the need to target interconnected pathways through mechanistically distinct small molecule inhibitors. This synthetic lethal siRNA screen provides an unbiased tool for probing the druggable genome to identify determinants of cellular sensitivity to novel microtubule destabilizing compounds like disorazole C_1. Using this screen, I have demonstrated that inhibition of either MID2 or upstream PI3K pathway elements is sufficient to sensitize T98G and T24 cells to MDAs, highlighting the importance of this PP2A tethering molecule in mediating the effects of this synergy in tumor cells with constitutively active PI3K signaling. Numerous survival-related genes have been identified in the PI3K signaling pathway in GBM, making PI3K inhibitors a critical therapy for

glioma patients [83]. The application of microtubule disrupting agents in combination with PI3K glioma chemotherapy has great potential for patients with GBM. These results demonstrate the ability of this synthetic lethal screen to unveil novel biology that can be exploited to predict synergistic drug combinations. The benefits of this type of predictive screen are uniquely able to identify determinants of MDA sensitization while pinpointing the specific molecular target regulating that sensitivity.

5.0 SYNTHETIC LETHAL SCREENING REVEALS CANCER SPECIFIC SYNERGY BETWEEN MICROTUBULE DESTABILIZING AGENTS AND NK1R ANTAGONISM

5.1 INTRODUCTION

The previous two chapters described the development and application of the synthetic lethal siRNA screen. As described in chapter 4, the screen was used to identify 142 and 152 genes that, when silenced, enhanced the cytotoxicity of vinblastine and disorazole C_1 by greater than two standard deviations, respectively. One of the 34 common hits for both agents was the neurokinin 1 receptor (NK1R). NK1R is also known as the tachykinin 1 receptor, TACR1, or the substance P receptor, SPR, and is a member of the G protein-coupled receptor (GPCR) family [84]. NK1R is expressed in neuronal, non-neuronal, and non-innervated tissues, both normal and neoplastic, and is agonized by neuronal tachykinins, such as substance P, as well as by non-neuronal tachykinins, such as hemokinin-1 and endokinins [84-94]. Due to the antiapoptotic signaling of NK1R in tumor cells, I hypothesized that antagonism of this receptor would inhibit the cytoprotective effect of NK1R in tumor cells, sensitizing them to sub-lethal concentrations of antimitotic agents, concentrations that alone would be too low to induce apoptosis. L-733,060, a potent and selective antagonist of NK1R, was selected for synergy studies due to its antitumor effect in numerous cancer cell lines. I demonstrated that low

concentrations of L-733,060 greatly sensitized the breast cancer cell line MDA-MB-231 and the GBM cell lines T98G and U87 to sub-lethal concentrations of the vinca alkaloids vinblastine, vincristine, and vinorelbine. I also found remarkable synergy between L-733,060 and vinblastine in the bladder cancer cell line T24 and the cervical cancer cell line Hela in addition to MDA-MB-231, T98G and U87, but only an additive effect in the normal lung fibroblast cell line IMR-90. In contrast to synergy seen between NK1R antagonists WIN-51,708 and L-733,060 and the MDAs disorazole C_1 and vinca alkaloids, I observed additive or antagonistic effects when L-733,060 was combined with the microtubule stabilizer paclitaxel and the non-microtubule targeting agent doxorubicin. This chapter presents the novel finding that NK1R antagonists synergize specifically with MDAs in multiple cancer cell lines. The lack of synergistic cytotoxicity in normal cells illustrates the tremendous potential of this strategy for combination chemotherapy for multiple forms of cancer.

5.2 RESULTS

5.2.1 NK1R silencing sensitizes T98G cells to MDAs

Based on my screen of the 16,560-member druggable genome siRNA library in a synthetic lethal screen with MDAs using T98G human GBM cells (Table 3), I identified the neurokinin 1 receptor (also known as NK1R, the tachykinin receptor, TACR1, or the substance P receptor) as one of the 34 genes targets that modulated T98G sensitivity to both vinblastine and disorazole C_1 was NK1R. I observed that siRNA against NK1R sensitized T98G cells to the MDAs vinblastine and disorazole C_1. (Figure 23B). Interestingly, silencing NK1R had minimal effect

on sensitizing cells to the microtubule stabilizing agent discodermolide, indicating a potential specificity of this sensitization towards microtubule destabilizers.

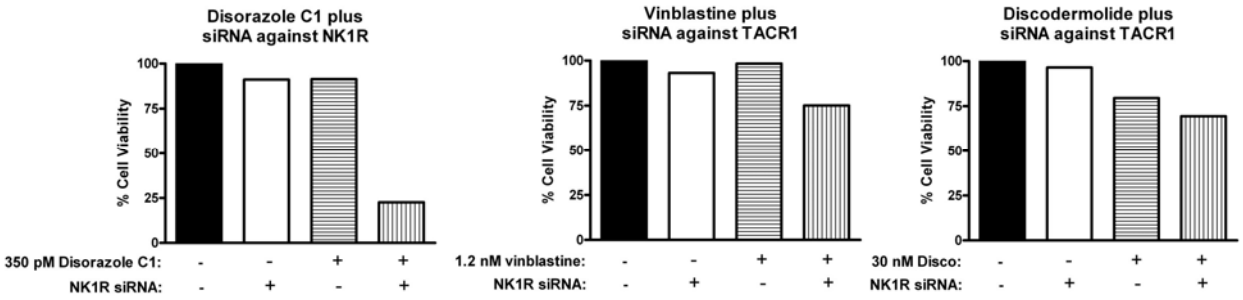

Figure 23. Silencing NK1R with siRNA sensitizes T98G cells to microtubule destabilizers.

Bar graphs demonstrate cell viability of T98G cells 2 days after drug treatment (1.2 nM vinblastine, 350 pM disorazole C_1, 30 nM discodermolide or 0.5% DMSO vehicle). T98G cells were treated with compound 48 hours after siRNA transfection. Silencing NK1R with siRNA sensitizes T98G cells to low concentrations of vinblastine and disorazole C_1, but not discodermolide. Cell viability was measured with CellTiter-Blue and is shown as a percentage of the viability of cells transfected with control siRNA. Graphs are representative of data from three independent screens.

5.2.2 NK1R antagonist L-733,060 sensitizes T98G cells to MDAs

The objective of this druggable genome siRNA screen was to identify gene products that have commercially available inhibitors, to develop synergistic drug combinations for cancer therapy. The identification of NK1R as a determinant of sensitivity for microtubule disruption

was of great interest due to the antitumor properties of NK1R antagonists [95] and the availability of numerous commercially available compounds targeting NK1R. The NK1R antagonist L-733,060 was selected for synergy studies with MDAs because this compound has antiproliferative activity against human neuroblastoma and glioma cell lines (Figure 24) [96, 97]. To determine if combinations of the NK1R antagonists and microtubule disruptors were additive, synergistic, or antagonistic to cancer cells at different effect levels, I used the combination index (CI) method of Chou and Talalay, described in Chapter 2 [47-50]. The combination index method of evaluating drug interactions was selected because it incorporated consideration of the potencies of each drug and combinations (Dm value), as well as the shape of the concentration-effect curves (m values), calculating how the experimental effect differs from the effect expected with additivity.

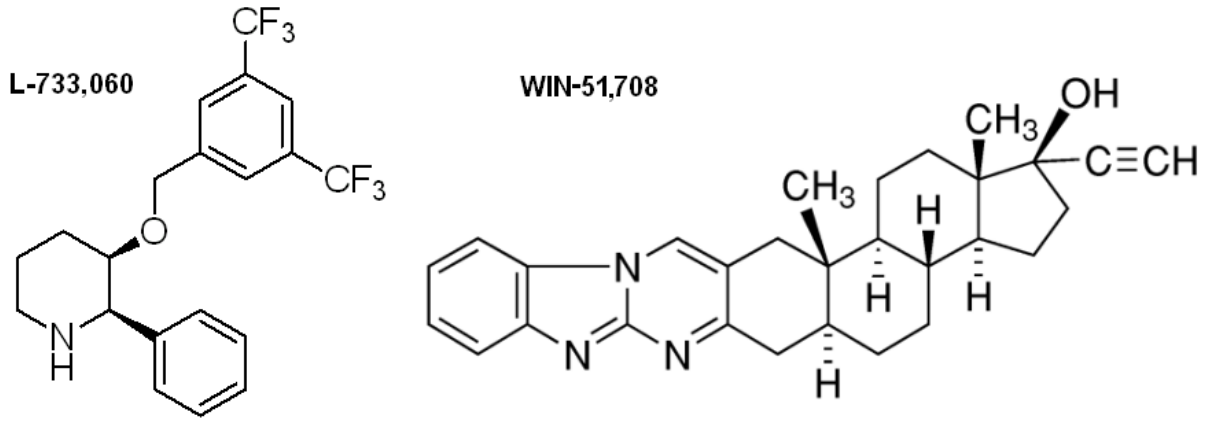

Figure 24. Chemical structures of the NK1R antagonists L-733,060 and WIN-51,708.

The combination effects of the NK1R antagonist L-733,060 and the MDAs vinblastine and disorazole C_1 are represented in Figure 25 and summarized in Table 5. The combination index plot (Figure 25) shows that the combination of L-733,060 plus vinblastine at a 6000:1 (6 μM L-733,060 to 1 nM vinblastine) ratio achieved a synergistic effect, with the data points of all

combinations falling well below a CI value of 1 at 90% (CI = 0.50), 75% (CI = 0.53), and 50% (CI = 0.57) levels of cell inhibition. As predicted from the screen, the combination of L-733,060 with disorazole C_1 was also synergistic. Exposure of T98G cells to both combinations resulted in increasing synergism with increasing effect levels. The 8x8 grid format of my experiment allowed me to test for synergy at multiple compound to compound ratios in any given experiment (method described in Chapter 2). I observed that these two compounds synergize at μM:nM ratios of 14:1, 9:1, 6:1, and 4:1 for L-733,060 to vinblastine, respectively, especially when higher fractions of cells are affected (Figure 26). The effect was decreased at ratios outside of this range (data not shown).

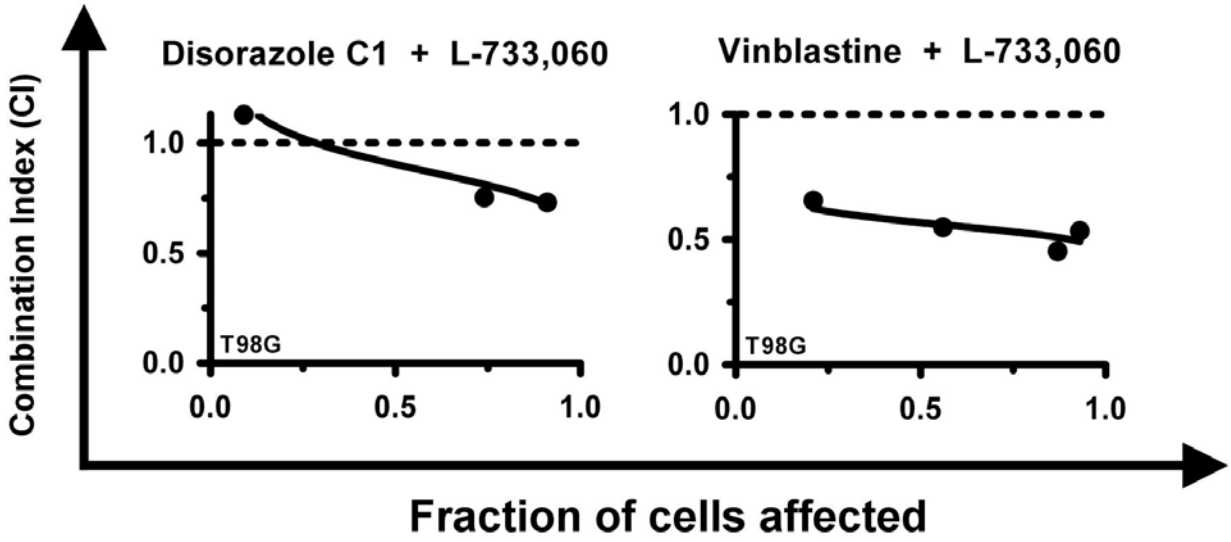

Figure 25. Synergism between MDAs and NK1R antagonist L-733,060 in T98G cells.

T98G cells were plated at low density and treated with concentration gradients of disorazole C_1, vinblastine, vehicle (DMSO), or mixtures thereof in an 8x8 grid of a 96-well plate,

providing 64 unique combinations. Cells were incubated in the presence of compounds for 72 hours. Cell viability was measured with CellTiter-Blue. To quantify the interaction between drug treatments, I generated combination index plots of the treatments at constant molar ratios. For these curves, CI values of <1, 1 (dotted line), and >1 indicated synergism, additivity, and antagonism, respectively. Data were analyzed assuming mutually exclusive drug effects and were representative of two or more separate experiments.

		CI value at			
Cell line	**Combination**	**EC50**	**EC75**	**EC90**	**r**
U87	L7 + VBL (6.3 μM : 1 nM)	0.58	0.49	0.44	0.99
	L7 + VEL (1 μM : 4.5 nM)	0.80	0.62	0.53	1.00
	L7 + VCR (9.4 μM : 1 nM)	0.86	0.81	0.77	1.00
	L7 + PTX (1 μM : 1.3 nM)	1.21	1.37	1.70	0.99
	L7 + Dox (4.7 μM : 1 nM)	1.11	1.04	0.98	0.89
T98G	L7 + VBL (6.2 μM : 1 nM)	0.57	0.53	0.50	0.99
	L7 + DisC1 (6.9 μM : 1 nM)	0.90	0.81	0.73	0.99
	L7 + VEL (1 μM : 4.5 nM	0.66	0.56	0.52	1.00
	L7 + VCR (4.2 μM : 1 nM)	0.50	0.32	0.21	1.00
	L7 + PTX (1 μM : 1.5 nM)	1.01	0.98	0.95	0.99
MDA-MB-231	L7 + VBL (4.2 μM : 1 nM)	0.77	0.84	0.92	0.98
	L7 + VEL (1 μM : 6.8 nM)	0.47	0.37	0.31	1.00
	L7 + VCR (6.3 μM : 1 nM)	0.89	0.80	0.71	0.98
T24	L7 + VBL (9.4 μM : 1 nM)	0.47	0.39	0.34	0.99
	Win + VBL (4.7 μM : 1 nM)	0.96	0.84	0.73	0.99
Hela	L7 + VBL (9.3 μM : 1 nM)	0.57	0.52	0.48	1.00

Table 5. Concentration-effect relationships and combination index values for compound combinations in normal and cancer cell lines.

Multiple drug effect analysis was performed using the NK1R antagonist L-733,060 (L7) or WIN-51,708 (Win) combination with either one of the four microtubule destabilizing agents, vinblastine (VBL), vincristine (VCR), vinorelbine (VEL), or disorazole C_1 (DisC1) or the microtubule stabilizing agent paclitaxel (PTX) or doxorubicin (Dox). Experiments were performed in six cell lines: the normal lung fibroblast cell line IMR-90, the breast cancer cell line MDA-MB-231, the bladder cancer cell line T24, the cervical cancer cell line Hela, and the glioblastoma cell lines T98G and U87. CalcuSyn was used to quantitatively describe the interaction of drug combination and to derive combination index plots (Figures 25, 26, 29, 30, and 31). This table lists the actual experimental values for the combination indices as a function of fractional inhibition of cell viability by a mixture of L-733,060 and either a microtubule destabilizer or a stabilizer. Combination index values are listed for three different fractional effects, wherein EC_{50} represents the level of interaction at 50% cell inhibition. Combination index values at <1.0, 1.0, and >1.0 indicated synergy, additivity, and antagonism, respectively. "r" is the linear correlation coefficient for the median effect line of the median effect plot. Commonly referred to as r value, this value indicates the conformity of the data.

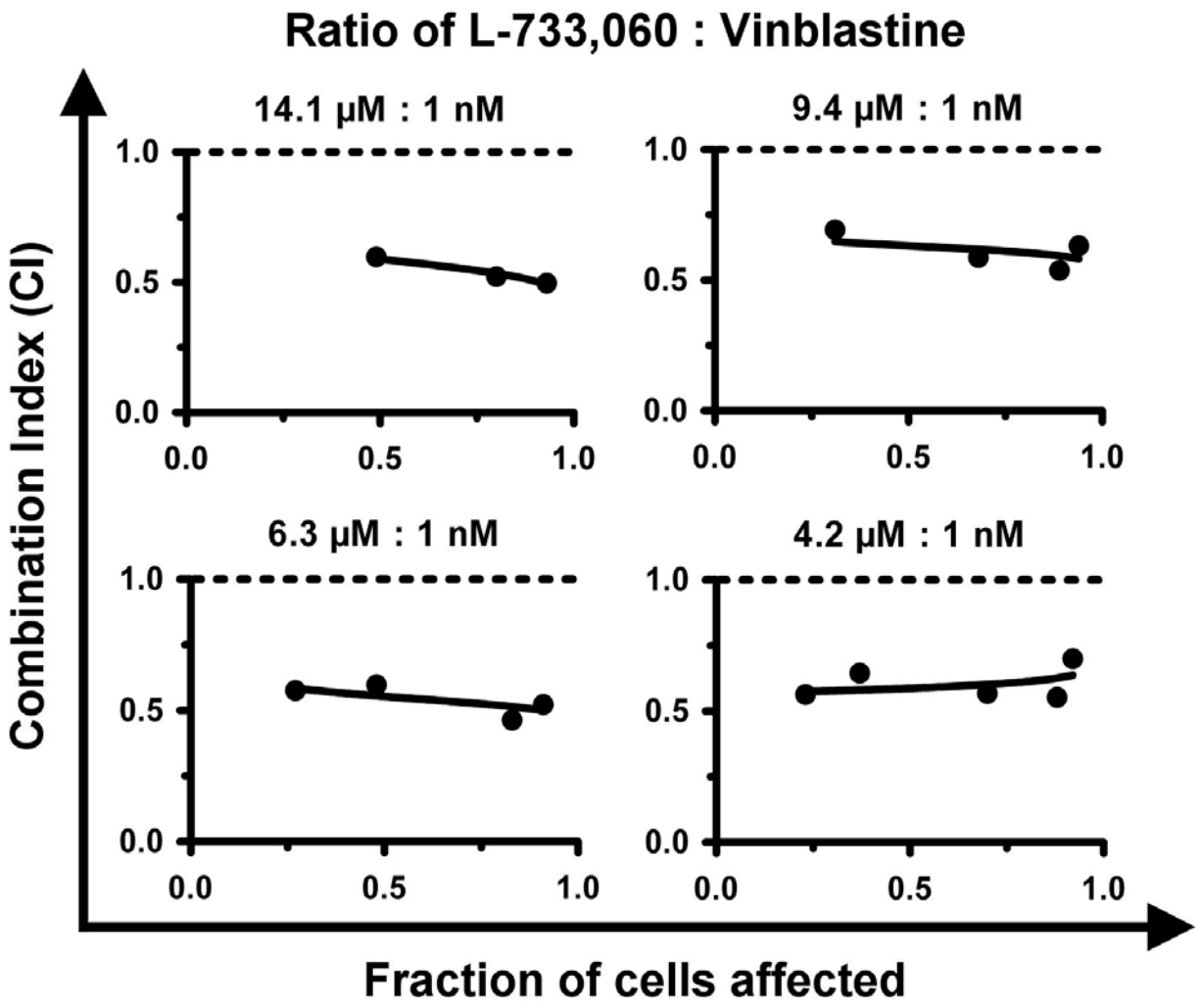

Figure 26. Analysis of the combination of vinblastine and L-733,060 in T98G cells at four different ratios.

Combination index plot analysis of the combination of L-733,060 with vinblastine in T98G cells at µM:nM ratios of 14.1:1, 9.4:1, 6.3:1, and 4.2:1 for L-733,060 to vinblastine. Combination index values at <1.0, 1.0, and >1.0 indicate synergy, additivity, and antagonism, respectively.

5.2.3 NK1R protein levels in six cell lines

To provide the molecular basis for the synergy, I next investigated the expression of NK1R and the promiscuity of this synergy across normal and cancer cell lines. NK1R receptors are present in numerous glioma, glioblastoma and astrocytoma cell lines, including T98G, U373, U87, UC11, and SJ-G4 [85-91]. NK1R expression has also been demonstrated in squamous cell carcinoma, pancreatic cancer, human B lymphoblastoma, hepatoma, and breast cancer cell lines [86, 95, 98-100]. I used immunoblotting to detect the presence of NK1R in six cell lines: normal lung fibroblast IMR-90, glioblastoma T98G and U87, bladder cell carcinoma T24, breast adenocarcinoma MDA-MB-231, and cervical cancer Hela cells (Figure 27). Cells were grown in culture and total cell protein extracts were resolved by polyacrylamide gels, then transferred to membranes and incubated with an antibody against NK1R. A band was observed in all five cell lines, with a molecular weight correlating with the predicted 53 kDa band for NK1R. Notably, this is the first time NK1R protein expression has been documented in the T24, IMR-90, and Hela cell lines.

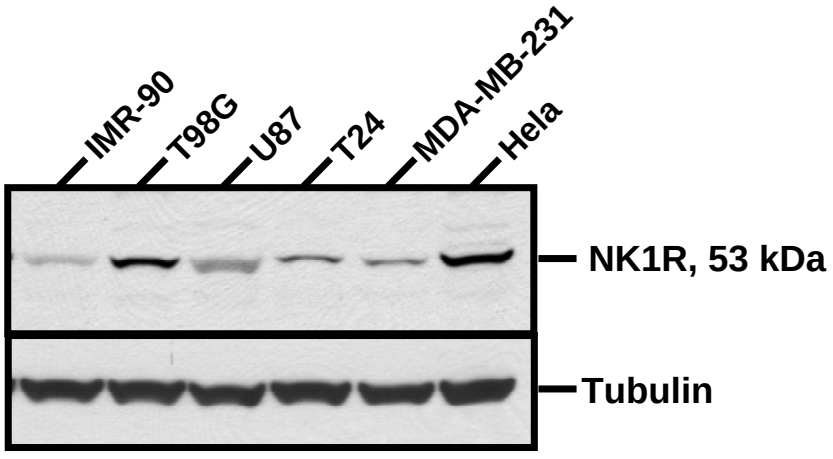

Figure 27. Western blot analysis of NK1R in normal and cancer cell lines.

Immunoblotting was used to detect relative amounts of NK1R protein in six cell lines: normal lung fibroblast IMR-90, glioblastoma T98G and U87, bladder cell carcinoma T24, breast adenocarcinoma MDA-MB-231, and cervical cancer Hela cells. The mass of NK1R has been reported to be 53 kDa.

5.2.4 Promiscuity of synergy in five cancer cell types

Due to the high levels of NK1R expression in these cancer cell lines, I sought to demonstrate the synergy of NK1R antagonism with microtubule disruption in these cells by combining vinblastine and L-733,060 at a constant ratio over multiple effect levels. L-733,060 was used due to its wide range of cytotoxic activity against various cell lines, including human glioma, neuroblastoma, retinoblastoma, laryngeal, melanoma, and pancreas carcinoma cell lines [96, 97, 101-104]. However, to our knowledge L-733,060 has not been previously reported to be cytotoxic in our particular cell lines. Treatment of T98G, U87, Hela, T24, and MDA-MB-231 cancer cells with L-733,060 resulted in a concentration-dependent cytotoxicity (Figure 28). I then performed combination studies to plot the CI curve for vinblastine plus L-733,060 in each of these cell lines (Figure 29). As predicted, the combination yielded optimal synergistic inhibition of cell proliferation in U87, MDA-MB-231, T24, and Hela, at μM L-733,060 : nM vinblastine ratios of 6:1, 4:1, 9:1, and 9:1, respectively.

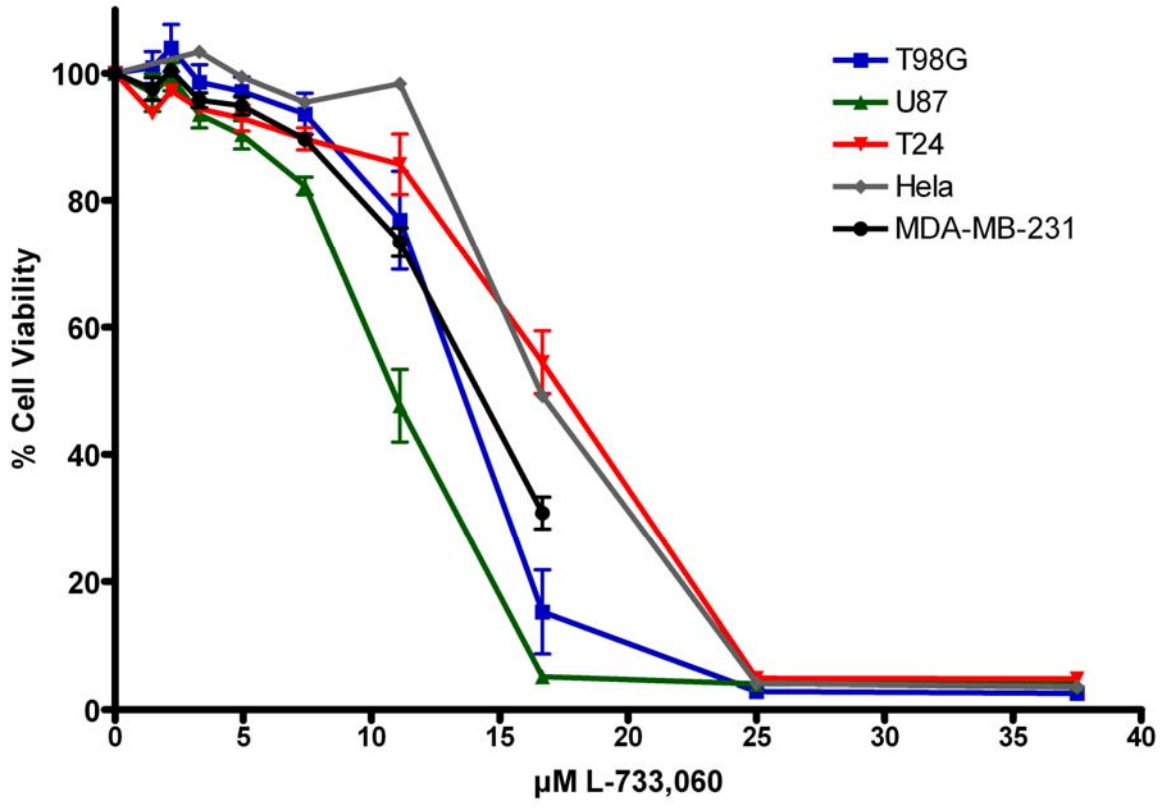

Figure 28. Inhibition of cancer cell viability by NK1R receptor antagonist L-733,060.

Cell viability of T98G, U87, Hela, T24, and MDA-MB-231 cancer cells 72 hours following the addition of increasing concentrations of L-733,060. Cell viability was measured with CellTiter-Blue and is shown as a percentage of the viability of cells treated with vehicle (0.5% DMSO). Values are means ± SD (bars) from independent experiments. Number of experiments per cell line represented: T98G n=10, U87 n=10, T24 n=4, Hela n=1, and MDA-MB-231 n=4.

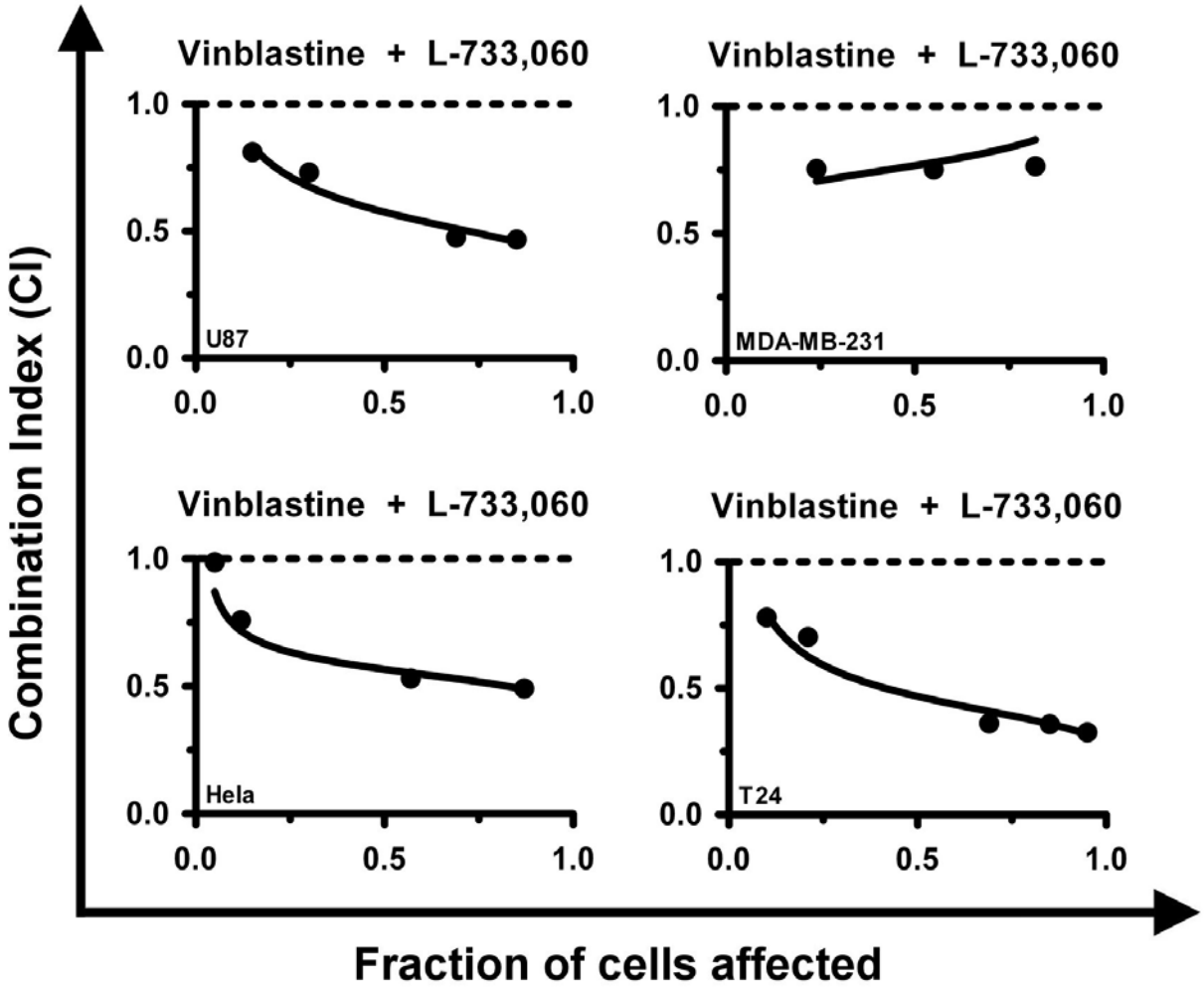

Figure 29. Synergy of vinblastine and L-733,060 in T98G in four different cancer cell lines.

Combination index plots for the combination of L-737,060 with vinblastine in U87 glioblastoma (6.3 μM : 1 nM), MDA-MB-231 breast cancer (4.2 μM : 1 nM), Hela cervical cancer (9.4 μM : 1 nM), and T24 bladder cancer cells (9.4 μM : 1 nM). Combination index values at <1.0, 1.0, and >1.0 indicated synergy, additivity, and antagonism, respectively.

5.2.5 L-733,060 specifically sensitizes cancer cells to MDAs.

Since cancer cells were sensitized to vinblastine and disorazole C_1 by NK1R siRNA and NK1R antagonism, I questioned whether this interaction was specific to these two agents, or was common among other microtubule destabilizers and stabilizers. Therefore, I tested two additional MDAs, vincristine and vinorelbine, and one microtubule stabilizer, paclitaxel, for potential cooperative cytotoxicity with L-733,060. Combination index studies confirmed that L-733,060 combined with either vincristine or vinorelbine was synergistic in U87, MDA-MB-231, and T98G cancer cell lines (Figure 30). However, the combination of a microtubule stabilizing agent, paclitaxel, was additive in T98G cells and antagonistic in U87 cell lines (Figure 31). These results suggested that the synergy between NK1R antagonism and MDAs was not shared by microtubule stabilizing agents.

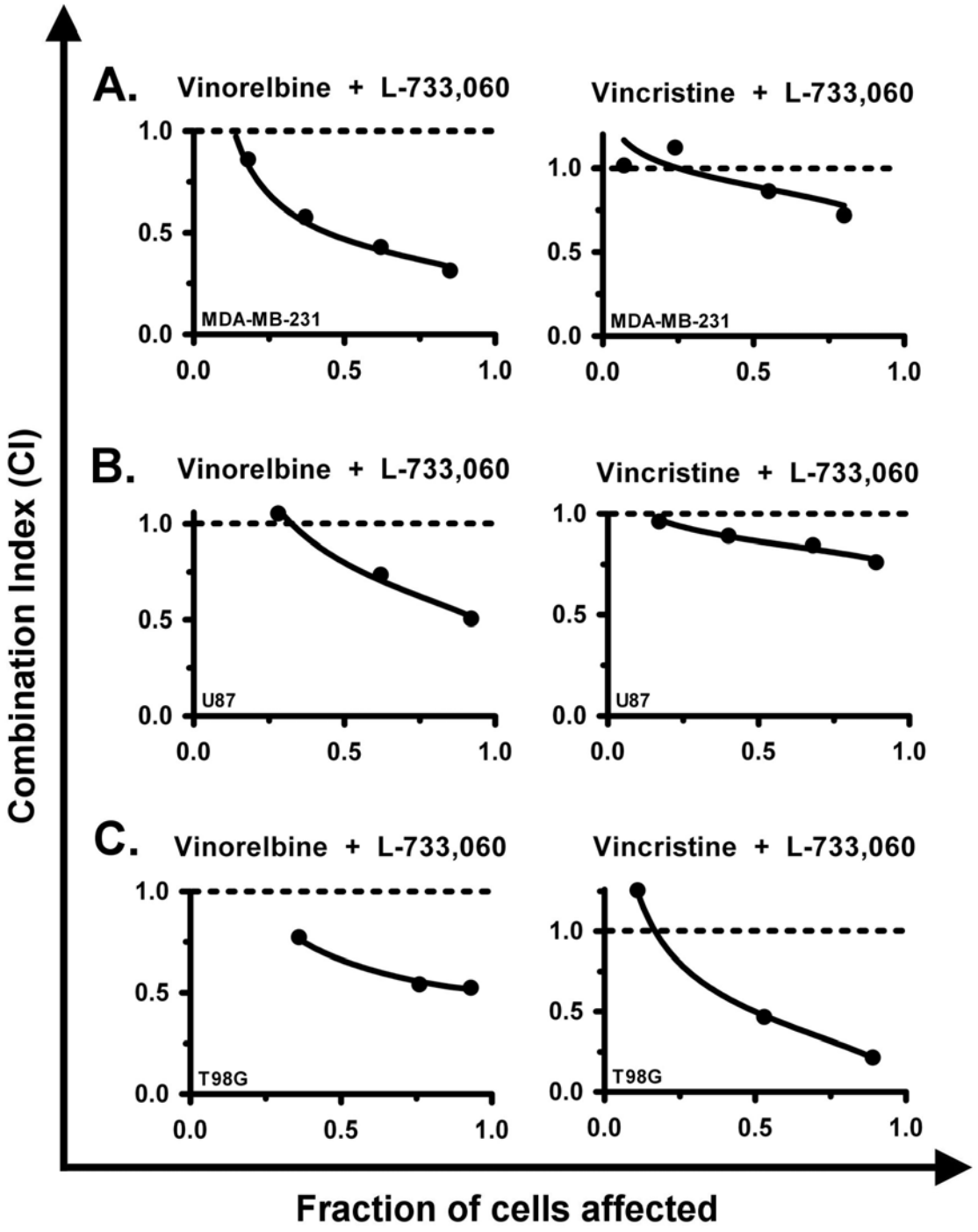

Figure 30. Combination index plot analysis of L-733,060 combined with the vinca alkaloids vincristine and vinorelbine.

(A) Combination index plots for the combination of L-733,060 with vinorelbine (ratio 1 μM : 6.8 nM) or vincristine (ratio 6.3 μM : 1 nM) in MDA-MB-231 cells. (B) Combination

index plots for the combination of L-733,060 with vinorelbine (ratio 1 μM : 4.5 nM) or vincristine (ratio 9.4 μM : 1 nM) in U87 cells. (C) Combination index plots for the combination of L-733,060 with vinorelbine (ratio 1 μM : 4.5 nM) or vincristine (ratio 4.2 μM : 1 nM) in T98G cells. Combination index values at <1.0, 1.0, and >1.0 indicate synergy, additivity, and antagonism, respectively.

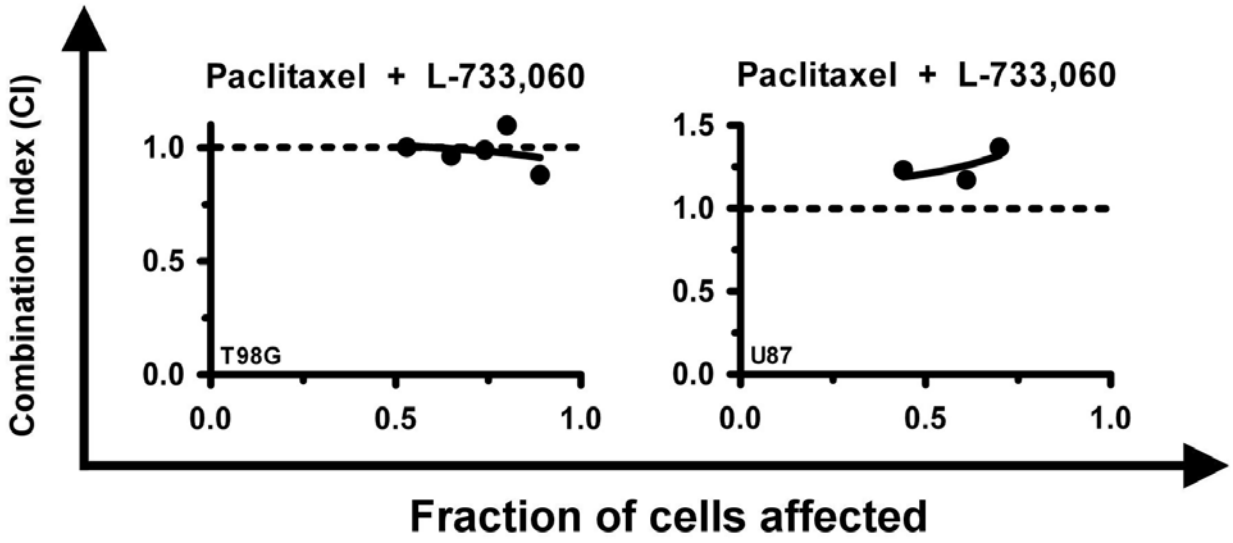

Figure 31. Analysis of the combination of paclitaxel and L-733,060 in two glioblastoma cell lines.

Combination index plots for the combination of L-733,060 with paclitaxel in T98G cells (ratio 1 μM : 1.5 nM) and U87 cells (ratio 1 μM : 1.3 nM). Combination index values at <1.0, 1.0, and >1.0 indicate synergy, additivity, and antagonism, respectively.

5.2.6 Visualization of combination treatment effects on intracellular tubulin and nuclei by immunofluorescence.

After calculating cell viability for 96-well plates, the cells in all wells were simultaneously fixed and stained for ten minutes with a PBS solution containing 4% formaldehyde and 1.2 μg/mL Hoescht 33342. This nuclear staining provided a means to count cells by nuclei to confirm cell viability reads, and also allowed visual inspection of nuclear shape, chromatin condensation, and multinucleation in the presence of compound. To observe the effects of individual compound and combination treatment on cellular microtubule structure, I incubated the treated, fixed cells with immunofluorescent antibodies against tubulin. Figure 32A illustrates MDA-MB-231 breast cancer cells treated with either vehicle, 1.2 nM vinblastine, 7.4 μM L-733,060, or the combination of vinblastine and L-733,060. As described in Chapter 2, the final DMSO concentration of in all wells was 0.5%. As seen in the figure, breast cancer cells treated with low concentrations either vinblastine or L-733,060 alone did not inhibit cell growth or proliferation, and the cells are visually healthy with uniform nuclei and well organized tubulin. However, interaction of the two agents in MDA-MB-231 cells induces a heterogeneous response of tubulin disorganization, cell rounding, and multinucleation, possibly suggesting mitotic slippage. The amorphous, rounded cellular appearance in the dual compound treatment is a hallmark of microtubule destabilization, which we hypothesized reflected sensitization of the breast cancer cells to concentrations of vinblastine [105]. Figure 32B presents the cell viability of the four wells from which these photos were taken, measured prior to fixing and staining.

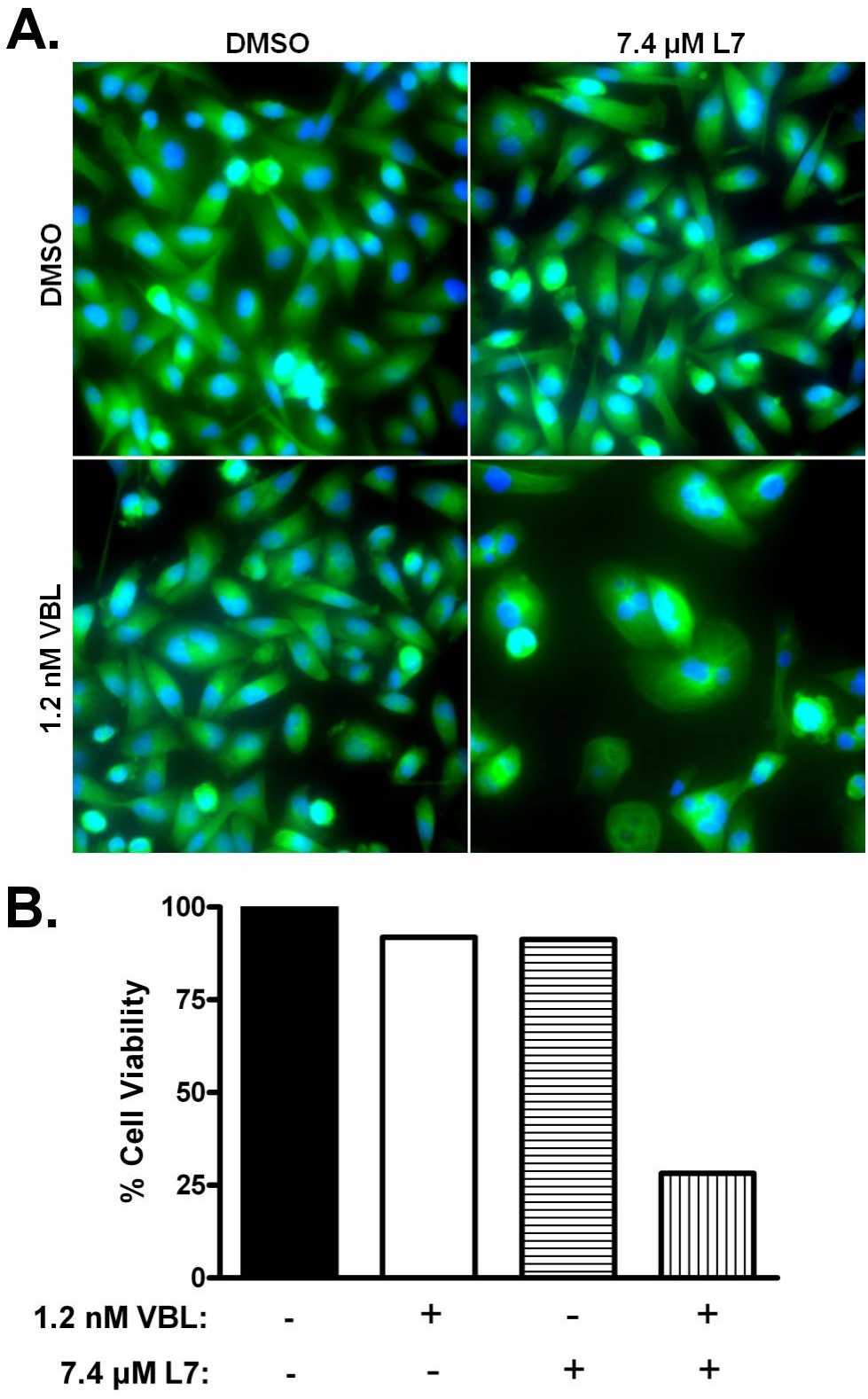

Figure 32. Quantification and visualization of MDA-MB-231 cells treated with a NK1R antagonist plus a vinca alkaloid.

Immunofluorescence images (A) and cell viability (B) of MDA-MB-231 breast cancer cells treated with vehicle (DMSO), 7.4 μM L-733,060 (L7), 1.2 nM vinblastine (VBL), or a combination of 7.4 μM L-733,060 and 1.2 nM vinblastine.

5.2.7 The combination of L-733,060 and MDAs is not synergistic in normal lung fibroblasts.

To determine the limits of the synergy between microtubule destabilizers and L-733,060, I tested numerous cell lines and compound combinations, summarized in Table 5. To confirm that the synergy was due to L-733,060 mediated antagonism of NK1R, I also showed that the NK1R antagonist WIN-51,708 also synergized with vinblastine, with combination index plot data points falling well below a CI value of 1 at 90% (CI = 0.73), 75% (CI = 0.84), and 50% (CI = 0.96) levels of cell inhibition. To test whether the synergy of L-733,060 was limited to microtubule targeted drugs, I combined the DNA intercalating compound doxorubicin with L-733,060, yielding only an additive response (Table 5).

The use of NK1R inhibition in cancer therapy is of great interest due to potential selectivity in cancer cells. Notably, NK1R is overexpressed in tumorigenic breast cancer cell lines relative to nontumorigenic breast cancer cell lines [86]. Since the goal of our research was to identify novel drug combinations for cancer therapy, I sought to determine whether the interaction of vinca alkaloids and L-733,060 would produce synergistic toxicity in normal cells. I repeated the synergy studies of vincristine and L-733,060 in normal lung fibroblast IMR-90 cells at multiple ratios and effect levels, and found that the combination was not synergistic in this cell line. To confirm the cell viability data used to measure synergy, I fixed and stained

IMR-90 cells following the synergy study to visualize tubulin structure, nuclei shape and cell morphology following treatment of IMR-90 cells with vincristine and L-733,060 (Figure 33). Figure 33A illustrates the results when IMR-90 cells were treated with either vehicle, 1.2 nM vincristine, 7.4 μM L-733,060, or the combination of vincristine and L-733,060. Unlike the MDA-MB-231 breast cancer cells, the IMR-90 cells appeared healthy, with organized tubulin even with the combination treatment. Figure 33B reports the cell viability for these conditions, measured prior to fixing and staining. These data suggested that drug combinations targeting microtubules in tandem with NK1R antagonism represented a valuable strategy for specific targeting of cancer cells.

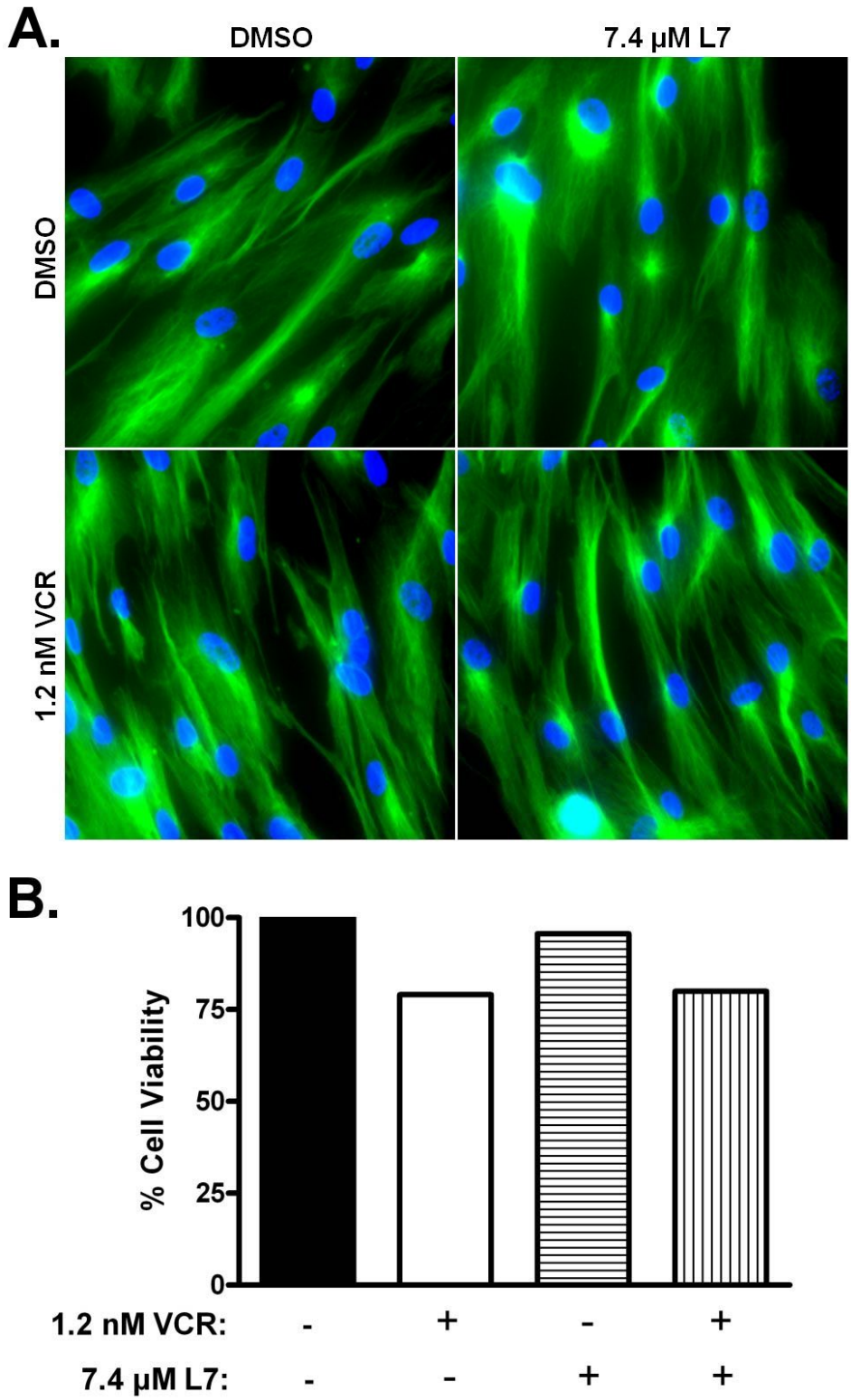

Figure 33. Quantification and visualization of IMR-90 cells treated with a NK1R antagonist plus a vinca alkaloid.

Immunofluorescence images (A) and cell viability (B) of normal lung fibroblast IMR-90 cells treated with vehicle (DMSO), 7.4 μM L-733,060 (L7), 1.2 nM vincristine (VCR), or a combination of 7.4 μM L-733,060 and 1.2 nM vincristine.

5.3 DISCUSSION

I performed synthetic lethal screening to identify genes that, when silenced, would sensitize cancer cells to MDAs. The goal of this research was to identify druggable protein targets for pharmacological inhibition and to replicate the MDA sensitization observed with the target siRNA. I discovered that silencing NK1R sensitized T98G cells to non-toxic concentrations of both vinblastine and disorazole C_1. The use of NK1R inhibition in cancer therapy is of great interest due to potential selectivity in cancer cells. Notably, NK1R is overexpressed in tumorigenic breast cancer cell lines relative to nontumorigenic breast cancer cell lines [86]. In addition, NK1R activity influences numerous life and death signaling pathways in both normal and neoplastic cells.

5.3.1 NK1R in normal cells: agonists and antagonists.

The tachykinin substance P (SP), also known as neurokinin 1 (NK1), is the preferential, but not exclusive, ligand for NK1R, agonizing neurotransmission [94]. Substance P (SP) was long considered to be the main pain neurotransmitter of pain [95, 106]. Later, SP was classified into the tachykinin family with other peptides containing the amino acid consensus sequence

FxGLM-NH2 at their C-terminus [90]. Tachykinins were traditionally viewed as peptides expressed by neuronal cells, however, there is now evidence for tachykinin expression in non-neuronal cells, such as endothelial, muscle, and inflammatory cells [92], such as the tachykinins hemokinin 1 and endokinins, which exhibit selectivity for NK1R [93]. Thus NK1R acts as receptor for ligands derived from both neuronal and non-neuronal cells, and itself is expressed in tissues other than the brain, including endothelial cells, muscle cells, inflammatory cells, and in different parts of the female reproductive system [84, 91, 92].

NK1R antagonism is clinically very beneficial, and numerous NK1R antagonists have been developed. The NK1R antagonist L-754,030 (aprepitant) is a widely used anti-emetic, preventing chemotherapy induced nausea in cancer patients [107-109]. The NK1R antagonists CP96345 and SR140333 have demonstrated anti-inflammatory properties in astroglioma cells and in mouse autoimmune encephalomyelitis, respectively [110, 111]. Several NK1R antagonists have provided an analgetic effect in mice (FK888) and in humans (CP99994) [112, 113]. Interestingly, NK1R antagonists have also been shown to have antiproliferative properties.

5.3.2 NK1R antiapoptotic signaling: NK1R as a drug target for cancer.

Several studies have shown NK1R antagonists can inhibit NK1R mediated tumor cell proliferation. SP is implicated in inducing mitogenesis of human astrocytoma cells, through activation of mitogen-activated protein kinase (MAPK) signaling pathway through NK1R [114]. DeFea et al. demonstrated that SP induces expression of antiapoptotic Bcl-2 and protects cells against apoptosis, dependent on NK1R and ERK1/2 signaling [115]. NK1R agonists activate ERK1/2 by the formation of a complex of NK1R, β-arrestin and ERK1/2 at the plasma

membrane [115]. The activated ERK1/2 translocates to the nucleus to induce proliferation and protect cells from apoptosis [114, 115]. The protective antiapoptotic effects of SP through NK1R in human colonocytes and rat cerebellar granule cells is mediated through Akt-activation, preventing apoptosis [116, 117]. SP promotes tumor cell proliferation in human retinoblastoma, breast carcinoma, neuroblastoma, glioma, and pancreatic cancer cells [96-98, 103, 104, 118]. NK1R antagonists inhibit tumor cell proliferation in these cell lines, as well as in human small cell lung cancer, suggesting that the proliferative and protective effects of SP in cancer cells is through NK1R [119]. NK1R overexpression in breast cancer and in the GBM cell line T98G further suggests a potential role for NK1R in tumor growth, supporting NK1R as a potential drug target for cancer therapy [86, 91].

5.3.3 Synergy between MDAs and NK1R antagonists.

The proliferative and antiapoptic signaling by NK1R provides a possible explanation for the synergy observed between NK1R antagonists and MDAs. MDAs like vinblastine trigger apoptotic signaling through JNK, and modulation of MAPK pathway elements can enhance or inhibit MDA-induced apoptosis. The pro-death JNK/AP-1 pathway is required for vinblastine-mediated apoptosis, while ERK pathway inhibition by the upstream MEK inhibitor U0126 strongly potentiates vinblastine-mediated apoptosis [36, 120]. Similarly, I hypothesized that the proliferative and antiapoptotic signaling of NK1R inhibited the apoptotic signaling of MDAs. Therefore, the NK1R antagonist L-733,060 sensitized cancer cells to MDA-mediated inhibition of cell viability by reducing this antiapoptotic NK1R signaling, potentiating vinblastine-induced cell death. It would be valuable to explore the effects of the combination of MDAs and NK1R antagonists on MAPK pathway elements ERK, JNK, and AP-1, and to determine if ERK, JNK,

or AP-1 are necessary for this synergistic toxicity in cancer cell lines containing NK1R. Elucidating the underlying mechanisms of this interaction may help assessment of the clinical relevance of this novel, synergistic combination.

5.3.4 Potential cancer cell specificity.

The cytotoxic combination synergy of microtubule disrupting agent and NK1R antagonism was observed with the cancer cell lines but we found only additive effects with normal cells (Figures 32 and 33, and Table 5). Because NK1R protein was detected in both normal and cancer cell lines (Figure 27), it was unlikely that the cancer specific synergy was due to NK1R levels. The NK1R receptor may be activated by autocrine signaling in the cancer cells, making L-733,060-mediated NK1R antagonism more pronounced in cancer cells, similar to autocrine and paracrine stimulation of EGFR signaling in cancer [121-124]. It was also possible that the cancer cell lines I used were more dependent on microtubule dynamics than the normal lung fibroblast cell line, making the cancer cells more vulnerable to microtubule targeting drugs [31]. The specificity of this synergy to cancer cells and not normal cells suggested that this combination could be useful for cancer combinatorial chemotherapy. However, experiments in other normal cell lines and animal models will be required to confirm cancer specificity with minimal normal cell toxicity.

Interestingly, NK1R antagonist treatment sensitized cancer cells to the microtubule destabilizer vinblastine, but not to the microtubule stabilizer paclitaxel (Figure 31). Recent research by Kolomeichuk et al. revealed distinct signaling pathways of microtubule inhibitors, noting that apoptotic cell death by vinblastine was AP-1-dependent, which death by paclitaxel

was through an AP-1-independent mechanism [37]. Over-expression of transcription factors such as AP-1 contribute to the enhanced survival, radioresistance, and chemoresistance of GBM [125]. Given the role of AP-1 activation by NK1R signaling, inhibition of AP-1 activation by NK1R antagonists could explain why cells are so sensitive to the AP-1-dependent cell death mechanism of vinca alkaloids but not paclitaxel [126, 127].

6.0 CONCLUSION

Despite the availability of 132 FDA-approved anticancer drugs, tumor recurrence within the treatment dosing range in a majority of GBM patients emphasizes the fact that we need better chemotherapeutic agents or strategies. To identify novel potential cancer chemotherapy combinations, I developed a synthetic lethal siRNA screen and used it to identify genes and networks that modulate tumor cell sensitivity to sub-lethal concentrations of two microtubule perturbing agents, vinblastine and disorazole C_1. I identified 34 genes whose silencing enhanced the cytotoxicity of both vinblastine and disorazole C_1 in T98G GBM cells. The protein products of these genes represent potential drug targets for sensitizing T98G cells to MDAs, with great potential for synergistic cytotoxicity.

The final aim of this dissertation was to determine if pharmacological inhibition of screening hits could potentiate MDA mediated cancer cytotoxicity. I anticipated that functional inhibitors of the biological functionality of the identified target proteins would enhance the cytoxic actions of either vinblastine or disorazole C_1 against human GBM. To this end, I selected several candidate compounds against identified hits for synergism study. Two candidate targets were selected from the list of siRNA hits based on the biology of the expressed protein and the commercial availability of compounds against that protein: MID2 and NK1R.

The candidate MID2 was selected in light of its role as a tether of the phosphatase PP2A to the microtubules. I was intrigued that silencing this tether sensitized cancer cells to MDAs, but MID2 has no known enzymatic activity that would be the target for pharmacologic inhibition. Although it is theoretically possible to seek direct inhibitors of the PP2A-α4-MID2-microtubule interaction, I decided to instead disrupt PP2A association with microtubules by targeting upstream PI3K/AKT pathway regulators of α4 phosphorylation, to prevent PP2A association with MID2 at the microtubules. A reasonable number of PI3K/AKT inhibitors are currently in early and advance stage clinical development. I confirmed that silencing MID2 induced tau hyperphosphorylation, a predictable result of microtubule destabilization. Moreover I demonstrated that the PI3K inhibitors wortmannin, LY-294,002, and PX866 sensitized T98G cells to both disorazole C_1 and vinblastine. The use of PX866 with vinblastine was also synergistic toxic in the bladder cancer cell line T24, which like T98G, has constitutively active PI3K, which I hypothesize was necessary for this combination. Thus, even molecular targets that are not immediately druggable can be addressed by focusing on proximal regulators.

siRNA against the tachykinin receptor NK1R sensitized T98G cells to both disorazole C_1 and vinblastine. This screening hit was selected for further study due to its expression in many cancer types, the antiproliferative properties of NK1R antagonists (Esteban, Munoz et al. 2006), and the availability of several commercially available compounds targeting NK1R. The NK1R antagonist L-733,060 was selected for synergy studies with MDAs because this compound has cytotoxic activity against human glioma, neuroblastoma, retinoblastoma, laryngeal, melanoma, and pancreas carcinoma cell lines [96, 97, 101, 103, 104]. I hypothesized that an antagonist of NK1R should emulate the sensitization seen with siRNA against NK1R. I confirmed this with

combination studies showing that the NK1R antagonist L-733,060 sensitized T98G cells to both disorazole C_1 and vinblastine. I demonstrated that L-733,060 combined with vinblastine was synergistic in T98G cells at multiple combination ratios and fraction levels. To confirm studies by other researchers that NK1R is located in non-neuronal cancer tissues [85, 86, 91, 95, 98, 100], I demonstrated NK1R protein levels in T98G, U87, MDA-MB-231, Hela, T24, and IMR-90 cell lines. I demonstrated that L-733,060 combined with vinblastine was synergistic for inhibition in all five of these NK1R-possessing cancer cell lines, but not in IMR-90 cells, suggesting that this combination may be more potent in NK1R-overexpressing cancer cells. The NK1R antagonist WIN-51,708 also sensitizes T98G cells to vinblastine. Further, I discovered that L-733,060 sensitizes cancer cells to other microtubule disrupting agents, including vincristine and vinorelbine, but not the microtubule stabilizer paclitaxel nor the DNA intercalating agent doxorubicin. These results reveal that it is the functional signaling associated with NK1R rather than the structural aspects of the protein that are important for the synergy. Moreover, the potent and novel interaction between two classes of small molecule inhibitors, the MDAs and the NK1R antagonists, might be clinically useful as NK1R antagonists have been approved by the FDA for chemotherapy induced emesis. My studies demonstrate the utility of this synthetic-lethal siRNA screening to predict novel collaborations between different classes of compounds for cancer chemotherapy.

7.0 BIBLIOGRAPHY

1. Strebhardt, K. and A. Ullrich, *Paul Ehrlich's magic bullet concept: 100 years of progress.* Nat Rev Cancer, 2008.

2. Papac, R.J., *Origins of cancer therapy.* Yale J Biol Med, 2001. **74**: p. 391-8.

3. Chabner, B.A. and T.G. Roberts, Jr., *Timeline: Chemotherapy and the war on cancer.* Nat Rev Cancer, 2005. **5**: p. 65-72.

4. Sporn, M.B., *The war on cancer.* Lancet, 1996. **347**: p. 1377-81.

5. Jemal, A., T. Murray, E. Ward, A. Samuels, R.C. Tiwari, A. Ghafoor, E.J. Feuer, and M.J. Thun, *Cancer statistics, 2005.* CA Cancer J Clin, 2005. **55**: p. 10-30.

6. Daumas-Duport, C., Scheithauer, B, O'Fallon, J, and Kelly, P, *Grading of astrocytomas: a simple and reproducible method.* Cancer, 1988. **62**: p. 2152–2165.

7. Miller, C.R. and A. Perry, *Glioblastoma.* Arch Pathol Lab Med, 2007. **131**: p. 397-406.

8. Debinski, W., *Drug cocktails for effective treatment of glioblastoma multiforme.* Expert Rev Neurother, 2008. **8**: p. 515-7.

9. Sharom, F.J., *ABC multidrug transporters: structure, function and role in chemoresistance.* Pharmacogenomics, 2008. **9**: p. 105-27.

10. Kamb, A., S. Wee, and C. Lengauer, *Why is cancer drug discovery so difficult?* Nat Rev Drug Discov, 2007. **6**: p. 115-20.

11. Lahaye, T., B. Riehm, U. Berger, P. Paschka, M.C. Muller, S. Kreil, K. Merx, U. Schwindel, C. Schoch, R. Hehlmann, and A. Hochhaus, *Response and resistance in 300 patients with BCR-ABL-positive leukemias treated with imatinib in a single center: a 4.5-year follow-up.* Cancer, 2005. **103**: p. 1659-69.

12. DiMasi, J.A. and H.G. Grabowski, *Economics of new oncology drug development.* J Clin Oncol, 2007. **25**: p. 209-16.

13. Kola, I. and J. Landis, *Can the pharmaceutical industry reduce attrition rates?* Nat Rev Drug Discov, 2004. **3**: p. 711-5.

14. Sakharkar, M.K., P. Li, Z. Zhong, and K.R. Sakharkar, *Quantitative analysis on the characteristics of targets with FDA approved drugs.* Int J Biol Sci, 2008. **4**: p. 15-22.

15. Hopkins, A.L. and C.R. Groom, *The druggable genome.* Nat Rev Drug Discov, 2002. **1**: p. 727-30.

16. Lipinski, C.A., F. Lombardo, B.W. Dominy, and P.J. Feeney, *Experimental and computational approaches to estimate solubility and permeability in drug discovery and development settings.* Adv Drug Deliv Rev, 2001. **46**: p. 3-26.

17. Russ, A.P. and S. Lampel, *The druggable genome: an update.* Drug Discov Today, 2005. **10**: p. 1607-10.

18. Lehar, J., G.R. Zimmermann, A.S. Krueger, R.A. Molnar, J.T. Ledell, A.M. Heilbut, G.F. Short, 3rd, L.C. Giusti, G.P. Nolan, O.A. Magid, M.S. Lee, A.A. Borisy, B.R. Stockwell, and C.T. Keith, *Chemical combination effects predict connectivity in biological systems.* Mol Syst Biol, 2007. **3**: p. 80.

19. Saltz, L.B., S. Clarke, E. Diaz-Rubio, W. Scheithauer, A. Figer, R. Wong, S. Koski, M. Lichinitser, T.S. Yang, F. Rivera, F. Couture, F. Sirzen, and J. Cassidy, *Bevacizumab in combination with oxaliplatin-based chemotherapy as first-line therapy in metastatic colorectal cancer: a randomized phase III study.* J Clin Oncol, 2008. **26**: p. 2013-9.

20. O'Shaughnessy, J.A. and J.L. Blum, *Capecitabine/Taxane combination therapy: evolving clinical utility in breast cancer.* Clin Breast Cancer, 2006. **7**: p. 42-50.

21. Cheong, K., J. Spicer, S. Chowdhury, and P. Harper, *Combination therapy versus single agent chemotherapy in non-small cell lung cancer.* Expert Opin Pharmacother, 2005. **6**: p. 1693-700.

22. Hu, J., G.B. Zhou, Z.Y. Wang, S.J. Chen, and Z. Chen, *Mutant transcription factors and tyrosine kinases as therapeutic targets for leukemias: from acute promyelocytic leukemia to chronic myeloid leukemia and beyond.* Adv Cancer Res, 2007. **98**: p. 191-220.

23. Kaelin, W.G., Jr., *The concept of synthetic lethality in the context of anticancer therapy.* Nat Rev Cancer, 2005. **5**: p. 689-98.

24. Sachse, C. and C.J. Echeverri, *Oncology studies using siRNA libraries: the dawn of RNAi-based genomics.* Oncogene, 2004. **23**: p. 8384-91.

25. Gonczy, P., C. Echeverri, K. Oegema, A. Coulson, S.J. Jones, R.R. Copley, J. Duperon, J. Oegema, M. Brehm, E. Cassin, E. Hannak, M. Kirkham, S. Pichler, K. Flohrs, A. Goessen, S. Leidel, A.M. Alleaume, C. Martin, N. Ozlu, P. Bork, and A.A. Hyman, *Functional genomic analysis of cell division in C. elegans using RNAi of genes on chromosome III.* Nature, 2000. **408**: p. 331-6.

26. Fraser, A.G., R.S. Kamath, P. Zipperlen, M. Martinez-Campos, M. Sohrmann, and J. Ahringer, *Functional genomic analysis of C. elegans chromosome I by systematic RNA interference.* Nature, 2000. **408**: p. 325-30.

27. Brown, E.D., *Screening in academe: a perspective on implementation of university-based small molecule screening.* J Biomol Screen, 2003. **8**: p. 377-9.

28. Sorger, P.K., M. Dobles, R. Tournebize, and A.A. Hyman, *Coupling cell division and cell death to microtubule dynamics.* Curr Opin Cell Biol, 1997. **9**: p. 807-14.

29. Woods, C.M., J. Zhu, P.A. McQueney, D. Bollag, and E. Lazarides, *Taxol-induced mitotic block triggers rapid onset of a p53-independent apoptotic pathway.* Mol Med, 1995. **1**: p. 506-26.

30. Jordan, M.A., K. Wendell, S. Gardiner, W.B. Derry, H. Copp, and L. Wilson, *Mitotic block induced in HeLa cells by low concentrations of paclitaxel (Taxol) results in abnormal mitotic exit and apoptotic cell death.* Cancer Res, 1996. **56**: p. 816-25.

31. Jordan, M.A. and L. Wilson, *Microtubules and actin filaments: dynamic targets for cancer chemotherapy.* Curr Opin Cell Biol, 1998. **10**: p. 123-30.

32. Hayflick, L., *Mortality and immortality at the cellular level. A review.* Biochemistry (Mosc), 1997. **62**: p. 1180-90.

33. Tozer, G.M., C. Kanthou, C.S. Parkins, and S.A. Hill, *The biology of the combretastatins as tumour vascular targeting agents.* Int J Exp Pathol, 2002. **83**: p. 21-38.

34. Jordan, M.A. and L. Wilson, *Microtubules as a target for anticancer drugs.* Nat Rev Cancer, 2004. **4**: p. 253-65.

35. Wang, L.G., X.M. Liu, W. Kreis, and D.R. Budman, *The effect of antimicrotubule agents on signal transduction pathways of apoptosis: a review.* Cancer Chemother Pharmacol, 1999. **44**: p. 355-61.

36. Brantley-Finley, C., C.S. Lyle, L. Du, M.E. Goodwin, T. Hall, D. Szwedo, G.P. Kaushal, and T.C. Chambers, *The JNK, ERK and p53 pathways play distinct roles in apoptosis mediated by the antitumor agents vinblastine, doxorubicin, and etoposide.* Biochem Pharmacol, 2003. **66**: p. 459-69.

37. Kolomeichuk, S.N., D.T. Terrano, C.S. Lyle, K. Sabapathy, and T.C. Chambers, *Distinct signaling pathways of microtubule inhibitors - vinblastine and Taxol induce JNK-dependent cell death but through AP-1-dependent and AP-1-independent mechanisms, respectively.* FEBS J, 2008. **275**: p. 1889-99.

38. Stadheim, T.A., H. Xiao, and A. Eastman, *Inhibition of extracellular signal-regulated kinase (ERK) mediates cell cycle phase independent apoptosis in vinblastine-treated ML-1 cells.* Cancer Res, 2001. **61**: p. 1533-40.

39. Judde, J.G., M. Rebucci, N. Vogt, P. de Cremoux, A. Livartowski, A. Chapelier, C. Tran-Perennou, K. Boye, R. Defrance, M.F. Poupon, and R.A. Bras-Goncalves, *Gefitinib and chemotherapy combination studies in five novel human non small cell lung cancer xenografts. Evidence linking EGFR signaling to gefitinib antitumor response.* Int J Cancer, 2007. **120**: p. 1579-90.

40. Holland, E.C., *Glioblastoma multiforme: the terminator.* Proc Natl Acad Sci U S A, 2000. **97**: p. 6242-4.

41. CBTRUS, *Statistical Report: Primary Brain Tumors in the United States, 1995–1999. Central Brain Tumor Registry of the United States.* 2002.

42. Raizer, J.J., *HER1/EGFR tyrosine kinase inhibitors for the treatment of glioblastoma multiforme.* J Neurooncol, 2005. **74**: p. 77-86.

43. Louis, D.N., H. Ohgaki, O.D. Wiestler, W.K. Cavenee, P.C. Burger, A. Jouvet, B.W. Scheithauer, and P. Kleihues, *The 2007 WHO classification of tumours of the central nervous system.* Acta Neuropathol, 2007. **114**: p. 97-109.

44. Stupp, R., Mason, W.P., Van Den Bent, M.J., Weller, M., Fisher, B., Taphoorn, M., Brandes, A.A., Cairncross, G.,Lacombe, D. and R.O. Mirimanoff : Concomitant and, *: Concomitant and adjuvant temozolomide (TMZ) and radiotherapy for newly diagnosed glioblastoma multiforme (GBM). Conclusive results of a randomized phase III trials by the EORTC brain and RT groups and NCIC clinical trials group. Proc Am Soc Clin Oncol 23: 1 (abstract 2).* 2004.

45. Burger, P.C. and P. Kleihues, *Cytologic composition of the untreated glioblastoma with implications for evaluation of needle biopsies.* Cancer, 1989. **63**: p. 2014-23.

46. Jendrossek, V., W. Kugler, B. Erdlenbruch, H. Eibl, F. Lang, and M. Lakomek, *Erucylphosphocholine-induced apoptosis in chemoresistant glioblastoma cell lines:*

involvement of caspase activation and mitochondrial alterations. Anticancer Res, 2001. **21**: p. 3389-96.

47. Chang, T.T. and T.C. Chou, *Rational approach to the clinical protocol design for drug combinations: a review.* Acta Paediatr Taiwan, 2000. **41**: p. 294-302.

48. Chou, T.C., *Drug combinations: from laboratory to practice.* J Lab Clin Med, 1998. **132**: p. 6-8.

49. Chou, T.C. and P. Talalay, *Quantitative analysis of dose-effect relationships: the combined effects of multiple drugs or enzyme inhibitors.* Adv Enzyme Regul, 1984. **22**: p. 27-55.

50. Chou, T.C., R.J. Motzer, Y. Tong, and G.J. Bosl, *Computerized quantitation of synergism and antagonism of taxol, topotecan, and cisplatin against human teratocarcinoma cell growth: a rational approach to clinical protocol design.* J Natl Cancer Inst, 1994. **86**: p. 1517-24.

51. Chou, J., *Dose-effect analysis with microcomputers: Quantitation of ED50, LD50, synergism, antagonism low-dose risk, receptor-ligand binding and enzyme kinetics.* 1987, Biosoft, Cambridge, U.K.

52. Chou, J., *Quantitation of synergism and antagonism of two or more drugs by computerized analysis (Synergism and antagonism in chemotherapy).* T. Chou-Rideout, Editor. 1991, Academic Press: San Diego, CA.

53. Fewell, G.D. and K. Schmitt, *Vector-based RNAi approaches for stable, inducible and genome-wide screens.* Drug Discov Today, 2006. **11**: p. 975-82.

54. Nagy, V., *FuGENE 6 transfection reagent: minimizing reagent-dependent side effects as analyzed by gene expression.* Nature Methods, 2006. **3**: p. 3-5.

55. Bartz, S.R., Z. Zhang, J. Burchard, M. Imakura, M. Martin, A. Palmieri, R. Needham, J. Guo, M. Gordon, N. Chung, P. Warrener, A.L. Jackson, M. Carleton, M. Oatley, L. Locco, F. Santini, T. Smith, P. Kunapuli, M. Ferrer, B. Strulovici, S.H. Friend, and P.S.

Linsley, *Small interfering RNA screens reveal enhanced cisplatin cytotoxicity in tumor cells having both BRCA network and TP53 disruptions.* Mol Cell Biol, 2006. **26**: p. 9377-86.

56. Overington, J.P., B. Al-Lazikani, and A.L. Hopkins, *How many drug targets are there?* Nat Rev Drug Discov, 2006. **5**: p. 993-6.

57. MacKeigan, J.P., L.O. Murphy, and J. Blenis, *Sensitized RNAi screen of human kinases and phosphatases identifies new regulators of apoptosis and chemoresistance.* Nat Cell Biol, 2005. **7**: p. 591-600.

58. Ciechanover, A., *The ubiquitin-proteasome pathway: on protein death and cell life.* EMBO J, 1998. **17**: p. 7151-60.

59. Glickman, M.H. and A. Ciechanover, *The ubiquitin-proteasome proteolytic pathway: destruction for the sake of construction.* Physiol Rev, 2002. **82**: p. 373-428.

60. Wilkinson, K.D., *Roles of ubiquitinylation in proteolysis and cellular regulation.* Annu Rev Nutr, 1995.

61. Wojcik, C., *Regulation of apoptosis by the ubiquitin and proteasome pathway.* J Cell Mol Med, 2002. **6**: p. 25-48.

62. Debigare, R. and S.R. Price, *Proteolysis, the ubiquitin-proteasome system, and renal diseases.* Am J Physiol Renal Physiol, 2003. **285**: p. F1-8.

63. Johnson, I.S., J.G. Armstrong, M. Gorman, and J.P. Burnett, Jr., *The vinca alkaloids: a new class of oncolytic agents.* Cancer Res, 1963. **23**: p. 1390-427.

64. Whitehurst, A.W., B.O. Bodemann, J. Cardenas, D. Ferguson, L. Girard, M. Peyton, J.D. Minna, C. Michnoff, W. Hao, M.G. Roth, X.J. Xie, and M.A. White, *Synthetic lethal screen identification of chemosensitizer loci in cancer cells.* Nature, 2007. **446**: p. 815-9.

65. Berns, K., E.M. Hijmans, J. Mullenders, T.R. Brummelkamp, A. Velds, M. Heimerikx, R.M. Kerkhoven, M. Madiredjo, W. Nijkamp, B. Weigelt, R. Agami, W. Ge, G. Cavet,

P.S. Linsley, R.L. Beijersbergen, and R. Bernards, *A large-scale RNAi screen in human cells identifies new components of the p53 pathway.* Nature, 2004. **428**: p. 431-7.

66. Iorns, E., C.J. Lord, N. Turner, and A. Ashworth, *Utilizing RNA interference to enhance cancer drug discovery.* Nat Rev Drug Discov, 2007. **6**: p. 556-68.

67. Sakharkar, M.K. and K.R. Sakharkar, *Targetability of human disease genes.* Curr Drug Discov Technol, 2007. **4**: p. 48-58.

68. Perry, J., K.M. Short, J.T. Romer, S. Swift, T.C. Cox, and A. Ashworth, *FXY2/MID2, a gene related to the X-linked Opitz syndrome gene FXY/MID1, maps to Xq22 and encodes a FNIII domain-containing protein that associates with microtubules.* Genomics, 1999. **62**: p. 385-94.

69. Short, K.M., B. Hopwood, Z. Yi, and T.C. Cox, *MID1 and MID2 homo- and heterodimerise to tether the rapamycin-sensitive PP2A regulatory subunit, alpha 4, to microtubules: implications for the clinical variability of X-linked Opitz GBBB syndrome and other developmental disorders.* BMC Cell Biol, 2002. **3**: p. 1.

70. Planel, E., K. Yasutake, S.C. Fujita, and K. Ishiguro, *Inhibition of protein phosphatase 2A overrides tau protein kinase I/glycogen synthase kinase 3 beta and cyclin-dependent kinase 5 inhibition and results in tau hyperphosphorylation in the hippocampus of starved mouse.* J Biol Chem, 2001. **276**: p. 34298-306.

71. Sayas, C.L., J. Avila, and F. Wandosell, *Regulation of neuronal cytoskeleton by lysophosphatidic acid: role of GSK-3.* Biochim Biophys Acta, 2002. **1582**: p. 144-53.

72. Fujiwara, Y., Y. Hosokawa, K. Watanabe, S. Tanimura, K. Ozaki, and M. Kohno, *Blockade of the phosphatidylinositol-3-kinase-Akt signaling pathway enhances the induction of apoptosis by microtubule-destabilizing agents in tumor cells in which the pathway is constitutively activated.* Mol Cancer Ther, 2007. **6**: p. 1133-42.

73. Schultz, R.M., R.L. Merriman, S.L. Andis, R. Bonjouklian, G.B. Grindey, P.G. Rutherford, A. Gallegos, K. Massey, and G. Powis, *In vitro and in vivo antitumor activity*

of the phosphatidylinositol-3-kinase inhibitor, wortmannin. Anticancer Res, 1995. **15**: p. 1135-9.

74. Ihle, N.T., R. Williams, S. Chow, W. Chew, M.I. Berggren, G. Paine-Murrieta, D.J. Minion, R.J. Halter, P. Wipf, R. Abraham, L. Kirkpatrick, and G. Powis, *Molecular pharmacology and antitumor activity of PX-866, a novel inhibitor of phosphoinositide-3-kinase signaling.* Mol Cancer Ther, 2004. **3**: p. 763-72.

75. Howes, A.L., G.G. Chiang, E.S. Lang, C.B. Ho, G. Powis, K. Vuori, and R.T. Abraham, *The phosphatidylinositol 3-kinase inhibitor, PX-866, is a potent inhibitor of cancer cell motility and growth in three-dimensional cultures.* Mol Cancer Ther, 2007. **6**: p. 2505-14.

76. Brognard, J., A.S. Clark, Y. Ni, and P.A. Dennis, *Akt/protein kinase B is constitutively active in non-small cell lung cancer cells and promotes cellular survival and resistance to chemotherapy and radiation.* Cancer Res, 2001. **61**: p. 3986-97.

77. Ermoian, R.P., C.S. Furniss, K.R. Lamborn, D. Basila, M.S. Berger, A.R. Gottschalk, M.K. Nicholas, D. Stokoe, and D.A. Haas-Kogan, *Dysregulation of PTEN and protein kinase B is associated with glioma histology and patient survival.* Clin Cancer Res, 2002. **8**: p. 1100-6.

78. Clark, A.S., K. West, S. Streicher, and P.A. Dennis, *Constitutive and inducible Akt activity promotes resistance to chemotherapy, trastuzumab, or tamoxifen in breast cancer cells.* Mol Cancer Ther, 2002. **1**: p. 707-17.

79. Cloughesy, T.F., K. Yoshimoto, P. Nghiemphu, K. Brown, J. Dang, S. Zhu, T. Hsueh, Y. Chen, W. Wang, D. Youngkin, L. Liau, N. Martin, D. Becker, M. Bergsneider, A. Lai, R. Green, T. Oglesby, M. Koleto, J. Trent, S. Horvath, P.S. Mischel, I.K. Mellinghoff, and C.L. Sawyers, *Antitumor activity of rapamycin in a Phase I trial for patients with recurrent PTEN-deficient glioblastoma.* PLoS Med, 2008. **5**: p. e8.

80. Fujiwara, Y., K. Kawada, D. Takano, S. Tanimura, K. Ozaki, and M. Kohno, *Inhibition of the PI3 kinase/Akt pathway enhances doxorubicin-induced apoptotic cell death in*

tumor cells in a p53-dependent manner. Biochem Biophys Res Commun, 2006. **340**: p. 560-6.

81. Meske, V., F. Albert, and T.G. Ohm, *Coupling of mammalian target of rapamycin with phosphoinositide 3-kinase signaling pathway regulates protein phosphatase 2A- and glycogen synthase kinase-3 -dependent phosphorylation of Tau.* J Biol Chem, 2008. **283**: p. 100-9.

82. Gundersen, G.G. and T.A. Cook, *Microtubules and signal transduction.* Curr Opin Cell Biol, 1999. **11**: p. 81-94.

83. Ruano, Y., M. Mollejo, F.I. Camacho, A. Rodriguez de Lope, C. Fiano, T. Ribalta, P. Martinez, J.L. Hernandez-Moneo, and B. Melendez, *Identification of survival-related genes of the phosphatidylinositol 3'-kinase signaling pathway in glioblastoma multiforme.* Cancer, 2008. **112**: p. 1575-84.

84. Pennefather, J.N., A. Lecci, M.L. Candenas, E. Patak, F.M. Pinto, and C.A. Maggi, *Tachykinins and tachykinin receptors: a growing family.* Life Sci, 2004. **74**: p. 1445-63.

85. Palma, C., F. Nardelli, S. Manzini, and C.A. Maggi, *Substance P activates responses correlated with tumour growth in human glioma cell lines bearing tachykinin NK1 receptors.* Br J Cancer, 1999. **79**: p. 236-43.

86. Patel, H.J., S.H. Ramkissoon, P.S. Patel, and P. Rameshwar, *Transformation of breast cells by truncated neurokinin-1 receptor is secondary to activation by preprotachykinin-A peptides.* Proc Natl Acad Sci U S A, 2005. **102**: p. 17436-41.

87. Johnson, C.L. and C.G. Johnson, *Characterization of receptors for substance P in human astrocytoma cells: radioligand binding and inositol phosphate formation.* J Neurochem, 1992. **58**: p. 471-7.

88. Sharif, T.R. and M. Sharif, *A novel approach for examining the anti-proliferative effect of protein kinase C inhibitors against human astrocytoma cells.* Int J Oncol, 1998. **13**: p. 685-92.

89. Ogo, H., N. Kuroyanagi, A. Inoue, H. Nishio, Y. Hirai, M. Akiyama, D.A. DiMaggio, J.E. Krause, and Y. Nakata, *Human astrocytoma cells (U-87 MG) exhibit a specific substance P binding site with the characteristics of an NK-1 receptor.* J Neurochem, 1996. **67**: p. 1813-20.

90. Palma, C. and C.A. Maggi, *The role of tachykinins via NK1 receptors in progression of human gliomas.* Life Sci, 2000. **67**: p. 985-1001.

91. Lazarczyk, M., E. Matyja, and A. Lipkowski, *Substance P and its receptors -- a potential target for novel medicines in malignant brain tumour therapies (mini-review).* Folia Neuropathol, 2007. **45**: p. 99-107.

92. Khawaja, A.M. and D.F. Rogers, *Tachykinins: receptor to effector.* Int J Biochem Cell Biol, 1996. **28**: p. 721-38.

93. Nelson, D.A. and K.L. Bost, *Non-neuronal mammalian tachykinin expression.* Front Biosci, 2004. **9**: p. 2166-76.

94. Maggi, C.A., R. Patacchini, P. Rovero, and A. Giachetti, *Tachykinin receptors and tachykinin receptor antagonists.* J Auton Pharmacol, 1993. **13**: p. 23-93.

95. Esteban, F., M. Munoz, M.A. Gonzalez-Moles, and M. Rosso, *A role for substance P in cancer promotion and progression: a mechanism to counteract intracellular death signals following oncogene activation or DNA damage.* Cancer Metastasis Rev, 2006. **25**: p. 137-45.

96. Munoz, M., A. Perez, R. Covenas, M. Rosso, and E. Castro, *Antitumoural action of L-733,060 on neuroblastoma and glioma cell lines.* Arch Ital Biol, 2004. **142**: p. 105-12.

97. Munoz, M., M. Rosso, A. Perez, R. Covenas, R. Rosso, C. Zamarriego, and J.I. Piruat, *The NK1 receptor is involved in the antitumoural action of L-733,060 and in the mitogenic action of substance P on neuroblastoma and glioma cell lines.* Neuropeptides, 2005. **39**: p. 427-32.

98. Friess, H., Z. Zhu, V. Liard, X. Shi, S.V. Shrikhande, L. Wang, K. Lieb, M. Korc, C. Palma, A. Zimmermann, J.C. Reubi, and M.W. Buchler, *Neurokinin-1 receptor expression and its potential effects on tumor growth in human pancreatic cancer.* Lab Invest, 2003. **83**: p. 731-42.

99. Goso, C., E. Potier, S. Manzini, and A. Szallasi, *Comparison of tachykinin NK1 receptors in human IM9 and U373 MG cells, using antagonist (FK888, (+/-)-CP-96,345, and RP 67580) binding.* Eur J Pharmacol, 1994. **254**: p. 221-7.

100. Monastyrskaya, K., A. Hostettler, S. Buergi, and A. Draeger, *The NK1 receptor localizes to the plasma membrane microdomains, and its activation is dependent on lipid raft integrity.* J Biol Chem, 2005. **280**: p. 7135-46.

101. Munoz, M., M. Rosso, F.J. Aguilar, M.A. Gonzalez-Moles, M. Redondo, and F. Esteban, *NK-1 receptor antagonists induce apoptosis and counteract substance P-related mitogenesis in human laryngeal cancer cell line Hep-2.* Invest New Drugs, 2008. **26**: p. 111-8.

102. Munoz, M.R., Marisa; Covenas, Rafael, *The NK-1 Receptor is Involved in the Antitumoural Action of L-733,060 and in the Mitogenic Action of Substance P on Human Pancreatic Cancer Cell Lines.* Letters in Drug Design & Discovery, 2006. **3**: p. 323-329.

103. Munoz, M., M. Rosso, A. Perez, R. Covenas, R. Rosso, C. Zamarriego, J.A. Soult, and I. Montero, *Antitumoral action of the neurokinin-1-receptor antagonist L-733,060 and mitogenic action of substance P on human retinoblastoma cell lines.* Invest Ophthalmol Vis Sci, 2005. **46**: p. 2567-70.

104. Munoz, M., A. Perez, M. Rosso, C. Zamarriego, and R. Rosso, *Antitumoral action of the neurokinin-1 receptor antagonist L-733 060 on human melanoma cell lines.* Melanoma Res, 2004. **14**: p. 183-8.

105. Ma, R., G. Song, W. You, L. Yu, W. Su, M. Liao, Y. Zhang, L. Huang, X. Zhang, and T. Yu, *Anti-microtubule activity of tubeimoside I and its colchicine binding site of tubulin.* Cancer Chemother Pharmacol, 2007. **21**: p. 21.

106. DeVane, C.L., *Substance P: a new era, a new role.* Pharmacotherapy, 2001. **21**: p. 1061-9.

107. Girish, C. and S. Manikandan, *Aprepitant: a substance P antagonist for chemotherapy induced nausea and vomiting.* Indian J Cancer, 2007. **44**: p. 25-30.

108. Navari, R.M., R.R. Reinhardt, R.J. Gralla, M.G. Kris, P.J. Hesketh, A. Khojasteh, H. Kindler, T.H. Grote, K. Pendergrass, S.M. Grunberg, A.D. Carides, and B.J. Gertz, *Reduction of cisplatin-induced emesis by a selective neurokinin-1-receptor antagonist. L-754,030 Antiemetic Trials Group.* N Engl J Med, 1999. **340**: p. 190-5.

109. Osorio-Sanchez, J.A., C. Karapetis, and B. Koczwara, *Efficacy of aprepitant in management of chemotherapy-induced nausea and vomiting.* Intern Med J, 2007. **37**: p. 247-50.

110. Guo, C.J., S.D. Douglas, Z. Gao, B.A. Wolf, J. Grinspan, J.P. Lai, E. Riedel, and W.Z. Ho, *Interleukin-1beta upregulates functional expression of neurokinin-1 receptor (NK-1R) via NF-kappaB in astrocytes.* Glia, 2004. **48**: p. 259-66.

111. Reinke, E.K., M.J. Johnson, C. Ling, J. Karman, J. Lee, J.V. Weinstock, M. Sandor, and Z. Fabry, *Substance P receptor mediated maintenance of chronic inflammation in EAE.* J Neuroimmunol, 2006. **180**: p. 117-25.

112. Dionne, R.A., M.B. Max, S.M. Gordon, S. Parada, C. Sang, R.H. Gracely, N.F. Sethna, and D.B. MacLean, *The substance P receptor antagonist CP-99,994 reduces acute postoperative pain.* Clin Pharmacol Ther, 1998. **64**: p. 562-8.

113. Ferreira, J., K.M. Triches, R. Medeiros, and J.B. Calixto, *Mechanisms involved in the nociception produced by peripheral protein kinase c activation in mice.* Pain, 2005. **117**: p. 171-81.

114. Luo, W., T.R. Sharif, and M. Sharif, *Substance P-induced mitogenesis in human astrocytoma cells correlates with activation of the mitogen-activated protein kinase signaling pathway.* Cancer Res, 1996. **56**: p. 4983-91.

115. DeFea, K.A., Z.D. Vaughn, E.M. O'Bryan, D. Nishijima, O. Dery, and N.W. Bunnett, *The proliferative and antiapoptotic effects of substance P are facilitated by formation of a beta -arrestin-dependent scaffolding complex.* Proc Natl Acad Sci U S A, 2000. **97**: p. 11086-91.

116. Koon, H.W., D. Zhao, Y. Zhan, M.P. Moyer, and C. Pothoulakis, *Substance P mediates antiapoptotic responses in human colonocytes by Akt activation.* Proc Natl Acad Sci U S A, 2007. **104**: p. 2013-8.

117. Amadoro, G., M. Pieri, M.T. Ciotti, I. Carunchio, N. Canu, P. Calissano, C. Zona, and C. Severini, *Substance P provides neuroprotection in cerebellar granule cells through Akt and MAPK/Erk activation: evidence for the involvement of the delayed rectifier potassium current.* Neuropharmacology, 2007. **52**: p. 1366-77.

118. Bigioni, M., A. Benzo, C. Irrissuto, C.A. Maggi, and C. Goso, *Role of NK-1 and NK-2 tachykinin receptor antagonism on the growth of human breast carcinoma cell line MDA-MB-231.* Anticancer Drugs, 2005. **16**: p. 1083-9.

119. Orosz, A., J. Schrett, J. Nagy, L. Bartha, I. Schon, and O. Nyeki, *New short-chain analogs of a substance-P antagonist inhibit proliferation of human small-cell lung-cancer cells in vitro and in vivo.* Int J Cancer, 1995. **60**: p. 82-7.

120. Fan, M., M.E. Goodwin, M.J. Birrer, and T.C. Chambers, *The c-Jun NH(2)-terminal protein kinase/AP-1 pathway is required for efficient apoptosis induced by vinblastine.* Cancer Res, 2001. **61**: p. 4450-8.

121. De Luca, A., A. Carotenuto, A. Rachiglio, M. Gallo, M.R. Maiello, D. Aldinucci, A. Pinto, and N. Normanno, *The role of the EGFR signaling in tumor microenvironment.* J Cell Physiol, 2008. **214**: p. 559-67.

122. Olayioye, M.A., R.M. Neve, H.A. Lane, and N.E. Hynes, *The ErbB signaling network: receptor heterodimerization in development and cancer.* EMBO J, 2000. **19**: p. 3159-67.

123. Yarden, Y., *The EGFR family and its ligands in human cancer. signalling mechanisms and therapeutic opportunities.* Eur J Cancer, 2001. **37 Suppl 4**: p. S3-8.

124. Yarden, Y. and M.X. Sliwkowski, *Untangling the ErbB signalling network.* Nat Rev Mol Cell Biol, 2001. **2**: p. 127-37.

125. Dhandapani, K.M., V.B. Mahesh, and D.W. Brann, *Curcumin suppresses growth and chemoresistance of human glioblastoma cells via AP-1 and NFkappaB transcription factors.* J Neurochem, 2007. **102**: p. 522-38.

126. Saban, R., C. Simpson, R. Vadigepalli, S. Memet, I. Dozmorov, and M.R. Saban, *Bladder inflammatory transcriptome in response to tachykinins: neurokinin 1 receptor-dependent genes and transcription regulatory elements.* BMC Urol, 2007. **7**: p. 7.

127. Springer, J., D. Pleimes, F.R. Scholz, and A. Fischer, *Substance P mediates AP-1 induction in A549 cells via reactive oxygen species.* Regul Pept, 2005. **124**: p. 99-103.